NASA CONTRACTOR REPORT

NASA CR-1534

NASA CR-1

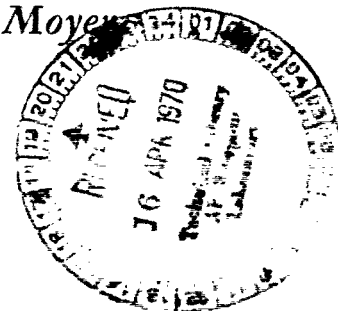*c.1*

AN INVESTIGATION OF SMALL-SCALE MOTIONS AND THE FORECASTING OF WIND PROFILES OVER SHORT PERIODS OF TIME AT CAPE KENNEDY, FLORIDA

by James R. Scoggins, M. M. Pendergast, and V. E. Moyer

Prepared by
TEXAS A & M UNIVERSITY
College Station, Texas
for George C. Marshall Space Flight Center

NATIONAL AERONAUTICS AND SPACE ADMINISTRATION • WASHINGTON, D. C. • APRIL 1970

1. REPORT NO. *call no.* ✓NASA CR-1534	2. GOVERNMENT ACCESSION NO.	3. RECIPIENT'S CATALOG NO.	
4. TITLE AND SUBTITLE AN INVESTIGATION OF SMALL-SCALE MOTIONS AND THE FORECASTING OF WIND PROFILES OVERS SHORT PERIODS OF TIME AT CAPE KENNEDY, FLORIDA *add e: T: Small-scale .. Florida .*		5. REPORT DATE April 1970	
		6. PERFORMING ORGANIZATION CODE	
7. AUTHOR(S) James R. Scoggins, M. M. Pendergast, and V. E. Moyer		8. PERFORMING ORGANIZATION REPORT #	
9. PERFORMING ORGANIZATION NAME AND ADDRESS ✓Texas A & M University College Station, Texas		10. WORK UNIT NO.	
		11. CONTRACT OR GRANT NO. NAS8-21257 *Smut*	
		13. TYPE OF REPORT & PERIOD COVERED Contractor Report	
12. SPONSORING AGENCY NAME AND ADDRESS NASA-George C. Marshall Space Flight Center Marshall Space Flight Center, Alabama 35812			
		14. SPONSORING AGENCY CODE	

15. SUPPLEMENTARY NOTES   This work was performed for the Aerospace Environment Division of the Aero-Astrodynamics Laboratory, MSFC, with Mr. William W. Vaughan as Contract Monitor.

note: app. B is thesis by James H. Blackburn, Jr.

16. ABSTRACT

Wind data provided by the FPS-16 radar/Jimsphere system (RJ) and thermodynamic data provided by the rawinsonde system (RW) were used to investigate relationships between motions of different scale. Small-scale motions were defined as the difference between a smooth profile defined to approximate the RW profile and the measured RJ profile. The statistics of these small-scale motions were related to a number of parameters including wind shear, the lapse rate of temperature, the Richardson number, and others. In addition, it was demonstrated that the small-scale motions influence greatly the Richardson number computed over layers of different thicknesses. Three of the terms representing the rate of mechanical production of turbulent kinetic energy were evaluated from the RJ data. The magnitude of the terms ranged from 10^{-7} to 10^{-4} m^2/sec^2. No significant relationship was found between these terms and the small-scale motions.

An attempt was made to relate small-scale motions to vorticity, divergence, curvature, and other parameters obtained from synoptic charts. The results show that no simple relationship exists between small-scale motions and any of the parameters investigated.

A simple model used to forecast the vertical wind profile at Cape Kennedy was developed and tested. Forecasts are made by assuming that the local rate-of-change of the mean virtual temperature of a layer, $\partial \bar{T}_v/\partial t$, is due to horizontal advection. Graphical and single-station methods were used to determine $\partial \bar{T}_v/\partial t$, with the graphical method providing the better results. The magnitude of the error in measurement is generally larger than: (1) changes that take place over short periods (less than 12 hr), (2) the
(continued on back)

17. KEY WORDS	18. DISTRIBUTION STATEMENT Unclassified – Unlimited

19. SECURITY CLASSIF. (of this report) ✓ Unclassified	20. SECURITY CLASSIF. (of this page) Unclassified	21. NO. OF PAGES 172	22. PRICE* $3.00

*For sale by the Clearinghouse for Federal Scientific and Technical Information
Springfield, Virginia 32151

magnitude of ageostrophic motions, and (3) the magnitude of the error expected because of vertical motion. It was found that the model is no better than persistence for periods less than 9 hours. It does seem that for periods greater than 9 hours, the model could be useful.

FOREWORD

This report is composed of nine sections and two appendices. The first seven sections deal with the statistical properties of the small-scale or turbulent motions and relationships between these motions and synoptic-scale parameters. Section VIII deals with the problem of forecasting the wind profile over short periods of time at Cape Kennedy from synoptic-scale data. It is essentially independent of Sections I-VII, thus making it possible for the reader to omit Section VIII if desired. Appendix B is a Master's Thesis prepared by Captain James H. Blackburn, Jr. Capt. Blackburn used data provided by NASA in the preparation of his thesis. The research conducted by Capt. Blackburn is essentially independent of, although somewhat related to, the research reported in this report. His thesis may be read independently of the remainder of the report although in many respects it complements the research reported in Sections I-VII.

ACKNOWLEDGMENTS

TABLE OF CONTENTS

LIST OF FIGURES

LIST OF TABLES

x

I. INTRODUCTION

Our knowledge of small-scale motions in the atmosphere above the immediate vicinity of Earth's surface has increased greatly within the last decade. The need for improved wind data in the design and operation of aerospace vehicles and, in particular, space vehicles necessitated the development of improved methods to measure the wind profile. However, once the improved wind data became available, it proved to be a formidable task to assimilate the information and to express the results in a form which could be used by design engineers. The task was complicated further by the lack of adequate detailed measurements of the wind profile over an extended area. Detailed wind profile data available from a few widely separated stations have been used effectively even though our knowledge of small-scale motions is quite incomplete. One of the principal aims of scientists has been to relate the statistics of small-scale motions to properties of large-scale flow since the latter are measured over much of Earth at regular intervals.

Since Leviton (1962) proposed the use of a superpressure balloon, tracked by a high-precision radar to measure the wind profile, considerable effort has gone into research and development of this system. Smooth, superpressure balloons with diameters of 2 m were found to be aerodynamically unstable (Scoggins, 1964, 1965 and 1967) and not suitable for use in the measurement of detailed wind profiles. The addition of roughness elements to the surface of the superpressure balloon (Scoggins, 1964) reduced the magnitude of

these aerodynamically-induced oscillations, and thereby provided a spherical balloon which was aerodynamically stable. This balloon configuration, now known as the "Jimsphere," has since been determined to be a suitable wind sensor for most purposes (Eckstrom, 1965; Zartarian and Thompson, 1968; Scoggins, 1967).

It has been shown (Eckstrom, op. cit.) that the response of the Jimsphere is adequate to measure wind shears over an altitude interval of a few meters, and also that the remaining self-induced motions are filtered out by the data reduction program (Rogers and Camnitz, 1965). Thus the RMS errors of approximately 0.6 m/sec and less found by Scoggins (1967) and Susko and Vaughan (1968) were due primarily to errors in radar data. A discussion of errors in the FPS-16 radar and their influence on the measurement of wind data is presented in a paper by Scoggins and Armendariz (1969). The altitude resolution of the wind data is believed to be approximately 50 m although this still is an unsettled question because of uncertainties in specifying radar error, editing the raw radar data, and processing the data. However, the wind profile data obtained by this method is at least one order of magnitude more accurate than those provided by the rawinsonde (RW)* system.

Sawyer (1961) performed a study of mesoscale motions associated with vertical wind profiles. From balloon data with a resolution

---

* RW and RJ will be used for rawinsonde and FPS-16 radar/Jimsphere, respectively.

2

considerably poorer than that provided by the FPS-16 radar/Jimsphere (RJ) system, he observed features which were persistent and maintained their identity over periods of several hours. Similar and even smaller features have been observed on the detailed profiles provided by the RJ system (Weinstein et al., 1966; DeMandel and Scoggins, 1967; and others). While a satisfactory theory has not been developed to explain all of the observed features, some exhibit the properties of wave motions characteristic of inertia, shear-gravity, gravity, and other types of waves. Some of the high frequency components whose character changes from observation to observation apparently are due to turbulent motions.

The improved wind profile data have been used in a number of studies relating to the design and operation of aerospace vehicles (see, for example, Ryan et al., 1967; Blackburn, 1968). Many of these studies dealt with the influence of small-scale motions on the vehicle, since they are important in terms of their contribution to vehicle response and loads caused by the wind. Scoggins and Vaughan (1964) discussed general aspects of the importance of atmospheric motions of different scale in the design of space vehicles. Vaughan (1968) described the use of the RJ system in monitoring wind conditions prior to the launch of space vehicles at Cape Kennedy.

In most studies relating to the design and operation of aerospace vehicles, assumptions must be made regarding the relationships between motions of different scale. The basic design criteria

3

developed for the Saturn vehicle (Daniels, et al., 1966) employs a number of assumptions regarding the relationships between quasi-steady-state wind speed, wind shears over various intervals of altitude, and gusts. The total response of the vehicle in terms of control system requirements as well as structural loading is a function of these relationships. For this reason this subject has received considerable attention during recent years.

The primary purposes of this research were to investigate the relationships between motions of different scale by use of data provided by the RW and RJ systems, and to ascertain to what extent the wind profile can be forecast over short periods of time at Cape Kennedy. The results of this research are reported in the following sections of this report.

II. DATA

A. Source and Extent

Wind profile data from the RW and RJ systems were provided by the Aerospace Environment Division, NASA Marshall Space Flight Center. The RW data were in a form of computer output while the RJ data were on magnetic tape and microfilm. The period covered by the data was 1965 to 1968; however, data were not available for each day and in some cases no data were available for a number of successive days.

The RW data consisting of pressure, temperature, humidity, and wind direction and speed were presented at 250-m intervals from near the surface to the lower stratosphere. The RJ data were presented at intervals of 25 m from near the surface to an altitude of approximately 18 km, although some of these profiles terminated at a somewhat lower altitude.

B. Matching of RW and RJ Profiles

Most of the RW runs were made at 00 or 12Z on a regular basis and were available for each day. These data appear to be remarkably consistent with very few questionable points. Also a very small percentage of these data were missing. The detailed wind profile data were not measured on a strict schedule, although many of the data corresponded to the 00 and 12Z RW data. In addition, there were a number of profile measurements made at times between the RW profiles as well as approximately 20 sets of serial ascents

5

containing between 8 and 15 profile measurements. In these series of profiles there was a time interval of approximately 1 to 2 hours between successive profiles with one or more RW measurements made during each series. Since thermodynamic data must be obtained from the RW runs for use with the detailed wind profiles, measurements made by the two systems had to be matched. If the time interval between the RW wind profile and the RJ wind profile was 2 hours or less, they were considered to be a matched pair. There were approximately 300 matched pairs in the data, but because of missing points in either the RW or RJ data, about 50 of the sets were not used in the analysis. The remaining 250 sets of profiles were nearly complete over the altitude of interest and were determined to be reasonable by a visual inspection.

C. Preparation of Data for Machine Processing

The RW data for the approximately 250 profiles were key-punched to permit machine processing. Data for each sounding included altitude, pressure, temperature, humidity, wind direction and speed, and date and time. It was not necessary to key-punch any of the RJ wind profile data since these were provided by NASA on magnetic tape.

III. DATA PROCESSING

A. Computations Performed at Texas A&M

Computer programs were prepared at Texas A&M to define small-scale motions from the RJ wind profiles, and to compute the lapse rate in temperature, vertical wind shear, the Richardson number, the Colson-Panofsky CAT index, the statistical properties of small-scale motions, and numerous statistical parameters describing the characteristics of the small-scale motions. In addition, a special program was required for the preparation of a magnetic tape containing the RW data.

B. Computations Performed at MSFC

The original radar data obtained at 0.1-sec intervals were processed at the MSFC Computation Laboratory to define small-scale motions as represented by variations in slant range. These computations were provided by MSFC since a computer program was in existence for performing the computations, and also since it was not feasible to provide the large number of magnetic tapes required to transmit the data to Texas A&M. The results were provided in the form of tabulated output as well as in graphical form. These computations were used in conjunction with those performed at Texas A&M to arrive at a suitable definition of small-scale motions (see Section IV).

IV. DEFINITION OF SMALL-SCALE MOTIONS

A. Smoothing of Wind Profiles

The RJ wind profiles contain much more detail than those provided by the RW method. The detailed wind profiles contain wave lengths of approximately 100 m and longer and represent variations in the horizontal wind field as a function of altitude. Small-scale motions were defined by use of a filter function which, when applied to the measured wind profile, defines a smooth or average wind profile which varies as a function of altitude. An illustration is given in Fig. 1. The smoothing weights and the associated transfer function are given by Scoggins (1967). This filter function provides a smooth profile containing wave lengths of approximately 1000 m and longer. Thus the profile of the differences between the smooth profile and the measured profile contain wavelengths of approximately 1000 m and less. In this study small-scale motion has been defined as the difference between the smoothed and measured wind profiles. It is apparent that the properties of small-scale motions defined in this manner are a function of the data processing methods employed. For this reason it was deemed desirable to define the small-scale motions by a second method and to compare the results. This second method will now be discussed.
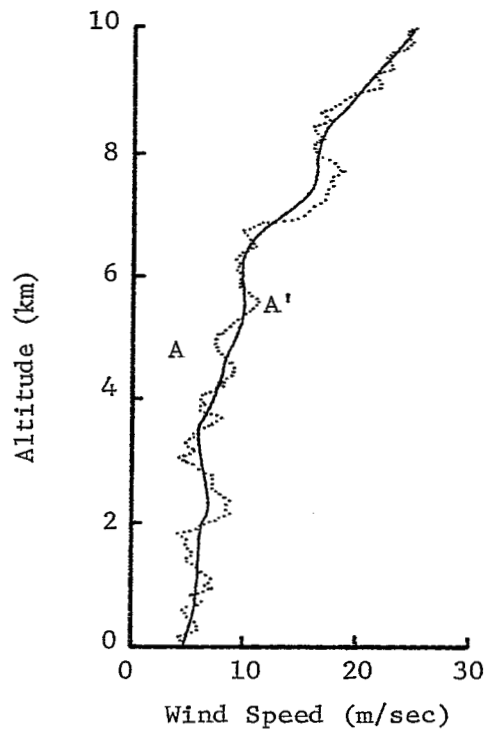
Fig. 1. An example of smoothing of a measured profile. Turbulent motions are defined as the difference between the smooth and measured profiles.

B. Smoothing of Slant Range

From the procedure developed by Endlich and Davies (1967), measurements of the slant range were averaged over a 1-min period; deviations from this mean were used to represent small-scale motions. Slant range was chosen as the variable to be smoothed because of its accuracy and also because it would be the best indicator of small-scale motions of the balloon. From these data the magnitude of the small-scale motions along the radar beam can be determined; these would approximate closely the horizontal component when the elevation angle is relatively small. It seems apparent that if the data-reduction method employed to compute the wind profiles smoothed so much that the small-scale motions were not adequately represented, the small-scale motions defined by smoothing the wind profiles and by smoothing the slant-range data would not show the same properties. Since it would be much more convenient to work with the wind profile data than with the slant-range data, relationships between small-scale data defined by the two methods were investigated.

C. Relationships Between Small-Scale Motions Defined by the Different Methods

The RMS of the turbulent fluctuations (small-scale motions)* was determined over layers of 250, 500, 1000, 2000, and 5000 m for

---

* In this report "small-scale motions" and "turbulence" are used interchangeably. They are not necessarily synonymous but no distinction is made here.

10

each method for 84 profiles. The top of each layer was at an altitude of 12 km. The linear correlation coefficients between the RMS values obtained from the two methods are shown in Table 1. In the table σ_u, σ_v, and σ_V refer to RMS turbulent fluctuations associated with the zonal, meridional, and scalar wind speed profiles, respectively; $\sigma_H = (\sigma_u^2 + \sigma_v^2)/2$ and σ_{SL} refers to RMS turbulent fluctuations determined from the slant range. The linear correlation coefficients given in the table all are rather large and increase in magnitude with layer thickness. All are statistically significant at the 1% level. These correlations indicate that either method for defining turbulence or small-scale motions is not preferable to the other. In subsequent sections of this report small-scale motions are defined as the difference between the smooth and original wind profiles.

Table 1. Correlation coefficients between RMS values of small-scale motions defined by different methods.

Variables Correlated	Layer Thickness (m)				
	250	500	1000	2000	5000
σ_u σ_{SL}	.47	.66	.67	.70	.79
σ_v σ_{SL}	.36	.44	.68	.67	.64
σ_V σ_{SL}	.54	.65	.83	.67	.75
σ_H σ_{SL}	.45	.50	.74	.74	.77

V.   THEORETICAL CONSIDERATIONS

A.   The Energy Equation

The basic energy equation for turbulence may be written as follows (Lumley and Panofsky, 1964):

$$\frac{D\overline{(KE')}}{Dt} = \frac{\tau_{ij}}{\overline{\rho}} \frac{\partial \overline{u}_j}{\partial x_i} + \sum \overline{F'_j u'_j} - \frac{1}{\overline{\rho}} \frac{\partial(\overline{\rho u'_i KE'})}{\partial x_i}$$

where:

KE' is the kinetic energy of the turbulent motions, i.e.,

$$KE' = \frac{u'^2 + v'^2 + w'^2}{2} \; ;$$

τ is the shearing stress tensor (i, j = 1, 2, 3);

ρ is the density of the air;

F   is force;   and

u   is wind speed.

Primes are used to denote turbulence parameters, and a bar is used to indicate an average. The first term on the right-hand side of the equation represents nine shear terms and involves Reynolds stresses. The second term represents the effects of eddy forces, the most important of which are believed to be buoyancy and friction. The last term in the equation represents the divergence of the flux of kinetic energy.

The first two terms on the right-hand side of the above equation are responsible for the production of turbulence, while the last term represents the redistribution of kinetic energy in space. The term

12

involving shearing stresses and wind shears often is reduced to
only one term involving stress along the mean wind and the vertical
wind shear. The reason for this simplification seems to be that
measurements near Earth's surface, where the frictional influence
is great, show that all other components of the shearing stress
and wind shear are small in comparison to that in the downwind
direction. In addition, suitable data usually are not available
to permit evaluation of all the terms even if they are important,
and investigators tend to follow precedent. In the free atmosphere
away from the influence of surface friction, less is known about
the magnitudes of the various terms in the stress tensor, although
a reasonable knowledge about the wind shears in all three spatial
directions exists. Fortunately the wind profile data provided by
the RJ system can be used to investigate the magnitude of several
terms.

B.   The Richardson Number

An investigation of the magnitude of the terms in the energy
equation when applied near Earth's surface indicate that, in the
shear term, only the vertical wind shear is of importance, and,
in the eddy force term, only the buoyancy is of importance. Richard-
son (see Sutton, 1953) defined a nondimensional number, which is
widely known as the Richardson number, as the ratio of buoyancy to
wind shear. He rationalized that in a laminar flow where turbu-
lent kinetic energy did not exist turbulence would begin when this

13

nondimensional number became less than unity. Thus a limiting value of unity for the Richardson number was believed to differentiate between turbulence and no turbulence. From the basic energy equation for turbulence, it is evident that once turbulence is present, the Richardson number should not be used in the same sense as a turbulence criterion. In addition, as shown above, other components of the term representing the rate of the production of mechanical energy may be large in the free atmosphere, thus casting doubt on the propriety of the Richardson number at altitudes where surface influences are negligible.

The gradient Richardson number is given by

$$Ri = \frac{g(\frac{\partial \overline{T}}{\partial z} + \Gamma_d)}{\overline{T}(\frac{\partial \overrightarrow{V_2}}{\partial z})^2}$$

where:

g is gravity,

$\partial \overline{T}/\partial z$ is the existing lapse rate of temperature,

Γ_d is the dry adiabatic lapse rate of temperature, and

$\partial \overrightarrow{V_2}/\partial z$ is the vertical shear of the horizontal wind.

Colson and Panofsky derived a clear-air turbulence (CAT) index from the Energy Equation based only on the vertical component of turbulent fluctuations. This relationship is given by

$$I = (\Delta \overrightarrow{V})^2 (1 - \frac{Ri}{Ri_{crit}})$$

14

where:

I   is the CAT index,

$\overrightarrow{\Delta V}$ is the vector change of wind within the layer over which the Richardson number is computed,

Ri is the Richardson number, and

Ri$_{crit}$ is the critical Richardson number, which Colson and Panofsky believe has a magnitude of about 0.5.

These authors found a reasonably good relationship between the CAT index and CAT as reported by aircraft. The Richardson number was evaluated using RW data from averaged values of wind shear and temperature profiles. The results obtained by Blackburn (1969) (see Appendix B) were not as good using turbulence defined from detailed wind profiles, although a reasonably good relationship was obtained between the CAT index and the lapse rate of temperature. Colson and Panofsky found an increase in the intensity of CAT with an increase in the CAT index. These conditions would result from a strong vertical wind shear and an unstable lapse rate. Blackburn's results showed the best correlation between CAT and stable layers, and were essentially independent of wind shear. For a more complete discussion of these relationships the reader is referred to Appendix B.

VI. EVALUATION OF STRESS/SHEAR TENSOR IN THE ENERGY EQUATION

The term involving the rate of mechanical production of turbulence in the equation on page 12 may be written

$$-\overline{u_i u_j} \ \frac{\partial \overline{u_j}}{\partial x_i} \ ,$$

which makes it clear that

$$\tau_{ij} = -\overline{\rho u_i' u_j'} \ .$$

The components of the stress tensor may be interpreted in terms of momentum transport which is assumed to be proportional to the mean wind shear in the appropriate direction. The justification of this assumption is that the flux of any quantity is observed to be proportional to the mean gradient of the quantity and in a direction opposite the mean gradient. Since it is observed that mean vertical wind shears are much larger than horizontal wind shears, even in the free atmosphere, it appears permissible to express the shear tensor as the sum of only three components which involve the vertical component of wind shear.

The covariances between fluctuations of the u, v, and w wind components, $\overline{u_i' u_j'}$, can be evaluated from the detailed wind profile data. If it is assumed that the deviations from the mean profile, u_i' and u_j', are composed of true wind fluctuations and error, we may write

$$u_i' = u_{i_T}' + e_i$$

and

$$u'_j = u'_{j_T} + \epsilon_j$$

where the subscript T represents true turbulent fluctuations and
ϵ denotes errors in the wind measurements. Thus the covariance
tensor may be written

$$\overline{u'_i u'_j} = \overline{(u'_{i_T} + \epsilon_i)(u'_{j_T} + \epsilon_j)} = \overline{u'_{i_T} u'_{j_T}} + \overline{u'_{i_T} \epsilon_j} + \overline{u'_{j_T} \epsilon_i} + \overline{\epsilon_i \epsilon_j}.$$

If it is assumed further that the errors in the measured wind data
are independent and not correlated with the true wind-speed fluctu-
ations, then we have

$$\overline{u'_i u'_j} = \overline{u'_{i_T} u'_{j_T}}.$$

Thus random errors would not contribute to the covariances between
the true wind fluctuations.

The covariances given by $\overline{u'v'}$, $\overline{u'w'}$, and $\overline{v'w'}$ were computed
for selected profiles over 1-km altitude intervals between 2 and
8 km. The profiles were not chosen for any particular reason
although they contained some low as well as high values of vector
wind shear. The turbulent fluctuations u', v', and w' were obtain-
ed by use of the filter function employed in defining the small-
scale motions from detailed wind profiles. The method is presented
in Section IV.

The covariances were multiplied by vector vertical wind shears
computed over the same 1-km layers over which the covariances were

17

computed; scatter diagrams were prepared. Turbulent kinetic energy
was defined as $(u'^2 + v'^2)/2$, which was computed for the same alti-
tude interval over which the other computations were performed.
The results of the computations are shown in Figs. 2, 3, and 4. A
significant correlation between the magnitude of the rate of mechan-
ical production and turbulent kinetic energy is not indicated in
any of these figures for this limited sample of data. Some of the
terms were negative and some positive with magnitudes generally
between 10^{-7} and 10^{-4} m^2/sec^2. The sign of the product of the
covariance and wind shear is indicated on the figures by each dot.

A negative wind shear results when the wind decreases with
height. There were no apparent differences in the covariances
for low- and high-shear profiles. In addition, there were no ap-
parent differences between the different terms for which different
computations could be made. From these preliminary data it appears
that the omission of terms in the stress/shear tensor, as is usual-
ly done for the region near Earth's surface, is not justified in
the free atmosphere.
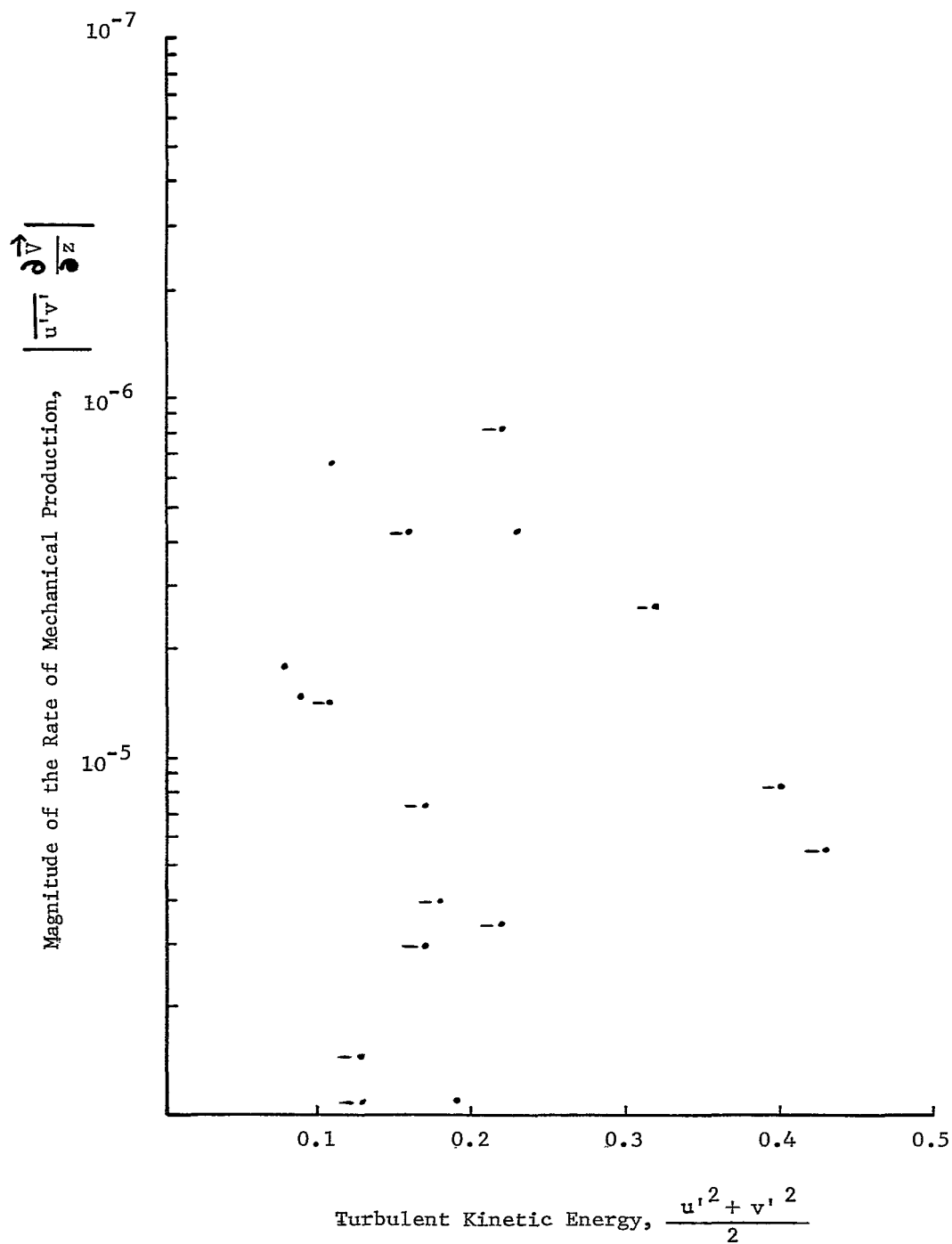
Fig. 2.   Magnitude of the rate of mechanical production of
turbulent kinetic energy vs the magnitude of tur-
bulent kinetic energy, u'v'.

19
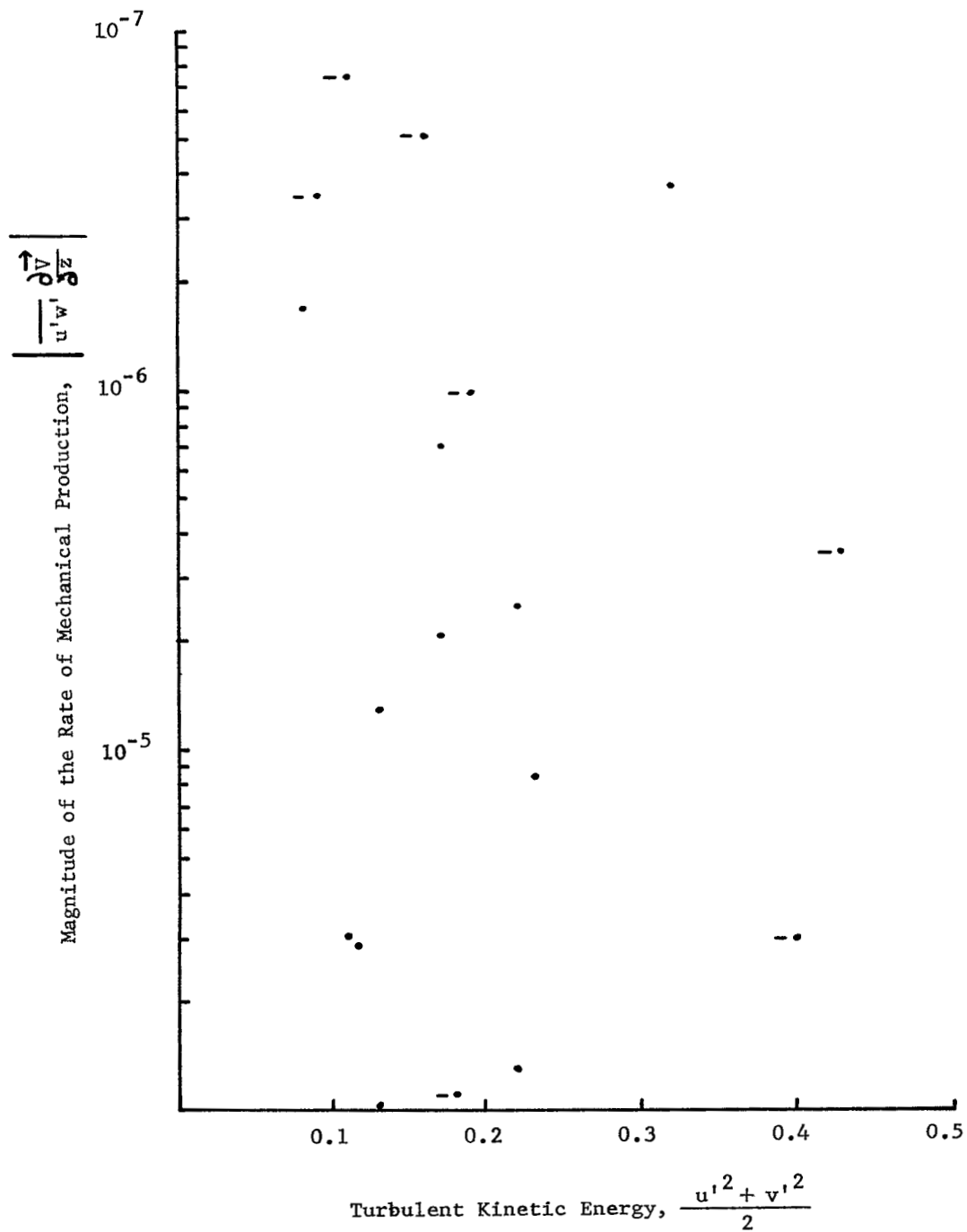
Fig. 3. Magnitude of the rate of mechanical production of turbulent kinetic energy vs the magnitude of turbulent kinetic energy, u'w'.

20
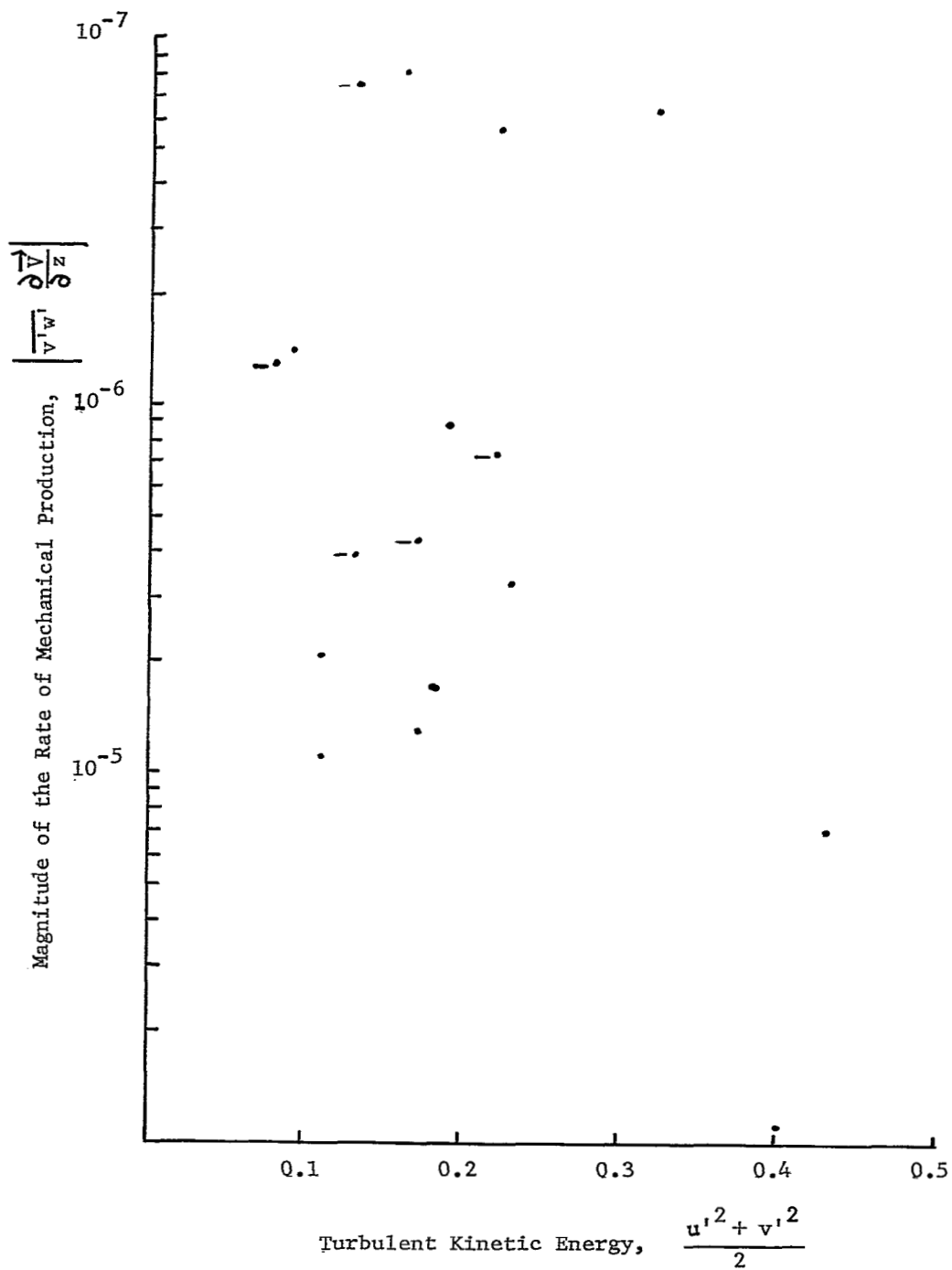
Fig. 4. Magnitude of the rate of mechanical production of turbulent kinetic energy vs the magnitude of turbulent kinetic energy, $\overline{v'w'}$.

21

VII. RELATIONSHIPS BETWEEN SMALL-SCALE MOTIONS ASSOCIATED WITH DETAILED WIND PROFILES AND SELECTED METEOROLOGICAL PARAMETERS

A. Lapse Rate of Temperature

Since the terms in the Energy Equation involve wind shear and lapse rate of temperature, and since these parameters are included in the definition of the Richardson number, it is logical to consider these parameters as predictors of turbulence. Various investigators have obtained varying degrees of success.

The lapse rate of temperature computed from the RW data was plotted against the RMS turbulence values associated with the zonal and meridional profiles for altitude layers of 250-, 500-, 1000-, and 2000-m thickness with the top of each layer at 6, 12, and 16 km. These altitudes were chosen to represent conditions in the mid-troposphere, in the troposphere near but below the tropopause, and in the lower stratosphere. A scatter diagram of $\partial T/\partial z$ versus RMS zonal turbulence is shown in Fig. 5 for an altitude interval of 1000 m at 12 km altitude. Diagrams involving RMS meridional turbulence were similar. There is no apparent correlation between the lapse rate of temperature and turbulence at altitudes of 6 and 16 km, but there is some suggestion of a slight correlation at 12 km. However, this relationship is so poor that it may be stated that a correlation between the lapse rate of temperature and turbulence does not exist.

Fig. 5. The lapse rate of temperature computed over a layer of 1000 m vs RMS zonal turbulence for the same layer. The top of the layer was at an altitude of 12 km.

B. Vertical Wind Shear

Vertical vector wind shear computed from the Jimsphere data was plotted against turbulence values obtained from the zonal, meridional, and scalar wind-speed profiles. A typical scatter diagram is shown in Fig. 6 for an altitude interval of 1000 m at 12 km altitude. Diagrams for other altitude intervals were similar. There is no significant correlation between vector wind shear and turbulence indicated in the figures. An interesting feature which appears in Fig. 6, as well as in similar figures not shown, is that there seems to be a limiting value of the vector wind shear for each altitude interval, and the magnitude of the turbulence appears to be essentially independent of the limiting shear value.

C. The Richardson Number

The Richardson number has been used by many investigators as an indicator of turbulence. A summary of some of the results obtained by different investigators and taken from a recent report by Reiter and Lester (1967) is presented in Table 2. The summary shows that the Richardson number has been used with varying degrees of success. The inconsistency in the results may be due in part to the omission of terms in the basic energy equation which may be important, as well as the improper application of the Richardson criterion. If turbulence is already present in the fluid, as is usually the case in the atmosphere, the Richardson number may no longer be used as a suitable turbulence criterion.

Fig. 6. The vector vertical wind shear computed over a layer of 1000 m vs RMS zonal turbulence for the same layer. The top of the layer was at an altitude of 12 km.

Table 2. Empirical Correlations between Ri and CAT
(taken from Reiter and Lester, 1967).

Investigator	Δz	Relationship between CAT and Ri
Anderson (1957)*	300 m	50% probability of CAT with Ri < 1.06, 82% with Ri < 6
Bannon (1951)		30% probability of CAT with Ri < 3. No relation between CAT and Ri in stratosphere
Berenger and Heissat (1959)		70% probability of CAT with Ri $\leq$ 1
Briggs (1961)		80% of CAT forecasts successful for Ri < 5 or horizontal shear > 0.3 hr^{-1}
Briggs and Roach (1963)		Significant increase in turbulence for a decrease in Ri. For Ri $\leq$ 5, 99 cases had no turbulence and 50 had slight to moderate turbulence
Colson (1963)	50-100 mb	Fair correlation between CAT and Ri for flights below 29,000'
Endlich (1964)		Ri_c=1 generally delineated regions that were larger than (but included) actual CAT regions
Endlich and McLean	2000'	50% increase in frequency of occurrence of all classes of turbulence with Ri $\leq$ 0.7

*See Reiter and Lester (1967) for the references cited in this table

26

Table 2 (continued).

Investigator	Δz	Relationship between CAT and Ri
Endlich and Mancuso (1964)	50, 25 mb	Ri = 0.6 correctly identified 28% of turbulent cases and 92% of non-turbulent cases. $Ri_c = 1$ "over forecasts" CAT
Jaffe (1963)		Ri criterion verified as CAT indicator with $Ri_c = 1.5$
Kao and Woods (1964)		Agreement between CAT and low Ri (≈ 1.0)
Klemin and Pinus (1953)*		80-90% probability of CAT with Ri $\leq$ 0.5. 50% probability of CAT with 0.5 < Ri < 4.0
Korilova (1958)**		79% probability of CAT with Ri < 10
Kroneback (1964)	between standard reporting levels	Ri useful for 12-hour CAT forecast ($Ri_c = 1.0$)
Lake (1956)		No clear relationship between CAT and Ri
Panofsky and McLean (1964)		All CAT reports occurred in regions of low Ri. Uncertainty of wind shears leads to overestimate of Ri
P'chelko (1960)**		31% probability of CAT with Ri < 10
Petterssen and Swinbank	50 mb	Found $Ri_c = 1.54$ for the free atmosphere
Pinus and Shmeter (1962)		85% probability of CAT with Ri $\leq$ 4

** Studies summarized by Pinus and Shmeter (1962)

Table 2 (continued).

Investigator	Δz	Relationship between CAT and Ri
Pinus and Shmeter (1965)		Concluded: Ri does not give a necessary and sufficient condition for the occurrence of turbulence but the smaller the value, the greater the probability of turbulence
Rustenbeck (1963)	2000'	In general; CAT frequency 64%, Ri ≤ 5, although in the region 4000' above to 10,000' below the level of maximum winds 79% of CAT with Ri ≤ 5. Poor correlation in the stratosphere
Scoggins (1963)		No correlation
Scorer (1957)		CAT probability approaches 100% with Ri ≤ 0.01
Stinson et al. (1964)	250 m	Layers with Ri < 1 were common and persisted for many hours
Weinstein et al. (1966)	250 m	Utilized Ri criterion (e.g., Ri < 0.5 turbulent, Ri > 1.0 non-turbulent) to show that the strong shears can be maintained in a stable stratosphere by quasi-inertial oscillations
Zavarina and Yudin (1960)	1000 m	Found good correlation with $Ri_c = 1$

An investigation was made of the relationships between the small-scale motions defined in Section IV and the Richardson number (see also Appendix B). Computations were performed of the Richardson number and the RMS value of turbulence computed over layers of various thicknesses with tops at 6, 12, and 16 km. The Richardson number plotted against turbulence is shown in Fig. 7 for a selected case with the top of the layer at 12 km altitude. The Richardson number was computed over an altitude interval of 1000 m for the case shown. Similar results were obtained for other altitude intervals and turbulence components. Even though the Richardson number has been used widely as a criterion for turbulence, a correlation does not exist in the data considered here. As pointed out in Section V, the Richardson number represents the ratio of only two terms in the energy equation under the assumption that all other terms may be neglected in comparison. Results of the present investigation, as well as those summarized in Table 2, suggest that this assumption may not be valid.

Relationships between CAT and the Richardson number often are inferred from tabular data rather than scatter diagrams as presented above. The relative frequency of balloon-measured turbulence versus the Richardson number, both computed over a layer 1000 m deep and with tops at 6, 12, and 16 km, are shown in Tables 3, 4, and 5.
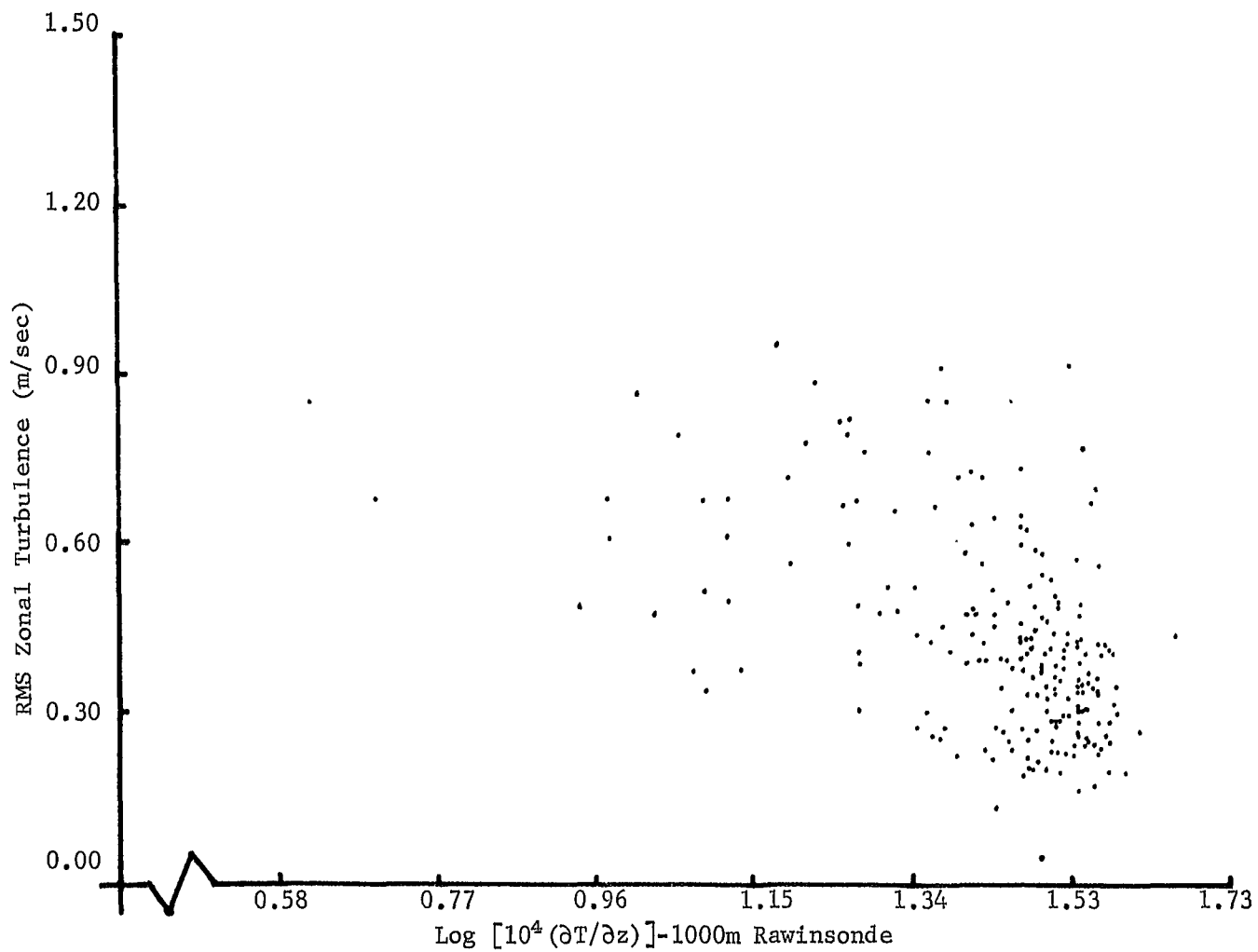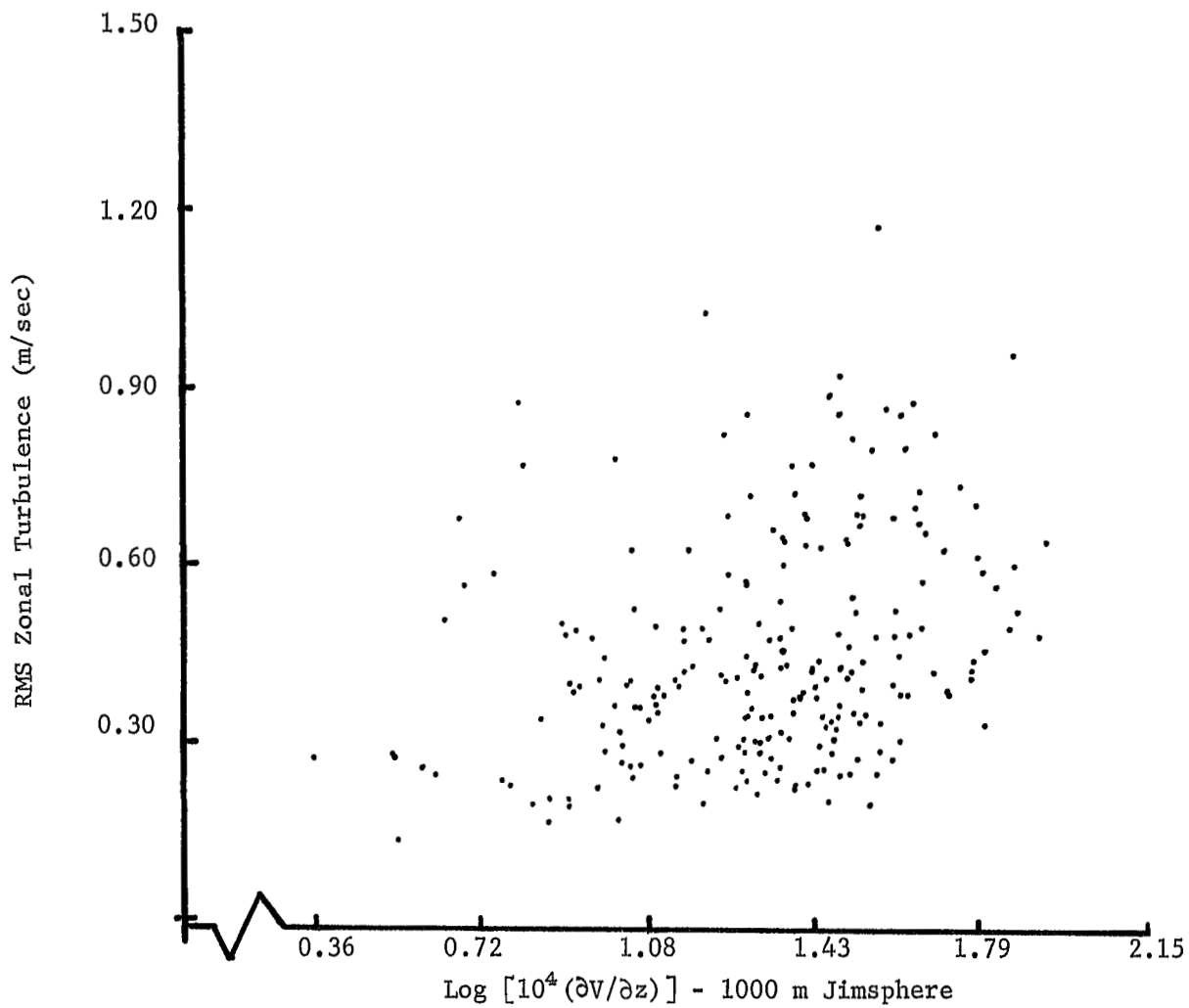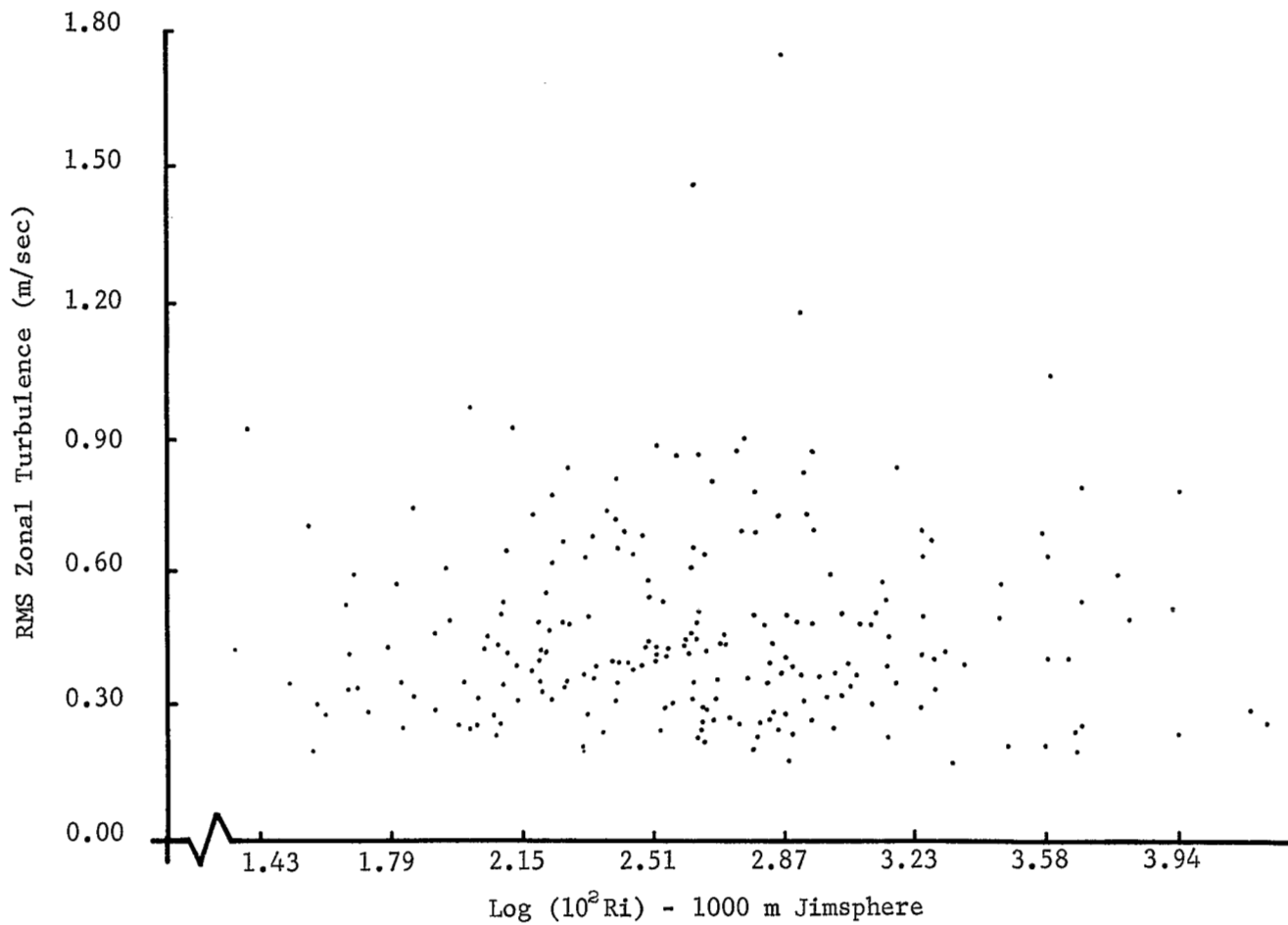
Fig. 7. The Richardson number computed over a layer of 1000 m vs the RMS of the zonal turbulence for the same layer. The top of the layer was at an altitude of 12 km. RJ winds and RW temperatures were used in the computations.

Table 3. The relative frequency of balloon-measured turbulence versus Richardson number with the top of the layer at 6 km. Computations were performed over a layer of 1000 m. Total number of data points - 240.

Intensity of u-component of turbulence (m/sec)

Richardson Number	RMS < 0.3		0.3 < RMS ≤ 0.6		0.6 < RMS ≤ 0.9		RMS > 0.9	
	%Total	%Sample	%Total	%Sample	%Total	%Sample	%Total	%Sample
Ri ≤ 2.5	2.5	12.8	13.5	18.7	3.0	36.8		
2.5 < Ri ≤ 5.0	4.2	21.3	11.4	15.8	2.1	26.3		
5.0 < Ri ≤ 10	3.4	17.0	13.9	19.3	.8	10.5		
10 < Ri ≤ 50	7.6	38.3	27.0	37.4	2.1	26.3		
Ri > 50	2.1	10.6	6.3	8.8	0	0		

Intensity of v-component of turbulence (m/sec)

Richardson Number	RMS < 0.3		0.3 < RMS ≤ 0.6		0.6 < RMS ≤ 0.9		RMS > 0.9	
	%Total	%Sample	%Total	%Sample	%Total	%Sample	%Total	%Sample
Ri ≤ 2.5	2.6	16.2	12.8	16.9	2.6	30		
2.5 < Ri ≤ 5.0	4.3	27.0	12.4	16.4	1.7	20		
5.0 < Ri ≤ 10	2.6	16.2	15.0	19.8	1.3	15		
10 < Ri ≤ 50	3.8	24.3	27.8	36.7	2.6	30		
Ri > 50	2.6	16.2	7.7	10.2	.4	5		

Intensity of scalar turbulence (m/sec)

Richardson Number	RMS < 0.3		0.3 < RMS ≤ 0.6		0.6 < RMS ≤ 0.9		RMS > 0.9	
	%Total	%Sample	%Total	%Sample	%Total	%Sample	%Total	%Sample
Ri ≤ 2.5	2.6	12	13.7	19.2	1.3	20	.4	50
2.5 < Ri ≤ 5.0	3.8	18	12.4	17.4	1.7	26.7	.4	50
5.0 < Ri ≤ 10	4.3	20	12.8	18.	.9	13.3		
10 < Ri ≤ 50	7.3	34	25.2	35.3	2.6	40		
Ri > 50	3.4	16	7.3	10.2	0	0		

Table 4. The relative frequency of balloon-measured turbulence versus Richardson number with the top of the layer at 12 km. Computations were performed over a layer of 1000 m. Total number of data points - 225.

Intensity of u-component of turbulence (m/sec)

Richardson Number	RMS <0.3		0.3 <RMS ≤0.6		0.6 <RMS ≤0.9		RMS >0.9	
	%Total	%Sample	%Total	%Sample	%Total	%Sample	%Total	%Sample
Ri ≤2.5	7.1	31.4	19.6	35.5	5.4	28.6	1.3	42.9
2.5 <Ri ≤5.0	4.5	19.6	15.6	28.2	5.4	28.6	0.4	14.3
5.0 <Ri ≤10	5.4	23.5	7.6	13.7	4.5	23.8	.9	28.6
10 <Ri ≤50	4.5	19.6	11.2	20.2	3.1	16.7	0.4	14.3
Ri >50	1.3	5.9	1.3	2.4	0.4	2.4	0	0

Intensity of v-component of turbulence (m/sec)

Richardson Number	RMS <0.3		0.3 <RMS ≤0.6		0.6 <RMS ≤0.9		RMS >0.9	
	%Total	%Sample	%Total	%Sample	%Total	%Sample	%Total	%Sample
Ri ≤2.5	8.9	31.7	16.1	35.3	5.4	27.3	2.2	33.3
2.5 <Ri ≤5.0	5.4	19.0	14.3	31.4	4.5	22.7	2.7	40
5.0 <Ri ≤10	3.6	12.7	7.1	15.7	6.3	31.8	0.9	13.3
10 <Ri ≤50	8.9	31.7	6.7	14.7	3.6	18.2	0.4	6.6
Ri >50	1.3	4.8	1.3	2.9	0	0	0.4	6.6

Intensity of scalar turbulence (m/sec)

Richardson Number	RMS <0.3		0.3 <RMS 0.6		0.6 <RMS ≤0.9		RMS >0.9	
	%Total	%Sample	%Total	%Sample	%Total	%Sample	%Total	%Sample
Ri ≤2.5	8.5	31.7	17.4	33.9	4.9	28.9	1.8	36.4
2.5 <Ri ≤5.0	6.3	23.3	13.8	27.0	5.8	34.2	.9	18.2
5.0 <Ri ≤10	4.9	18.3	8.9	17.4	2.2	13.2	2.2	45.5
10 <Ri ≤50	6.3	23.3	9.4	18.3	3.6	21.1	0	0
Ri >50	.9	3.3	1.8	3.5	0.4	2.6	0	0

32

Table 5. The relative frequency of balloon-measured turbulence versus Richardson number with the top of the layer at 16 km. Computations were performed over a layer of 1000 m. Total number of data points – 195.

Intensity of u-component of turbulence (m/sec)

Richardson Number	RMS <0.3		0.3 <RMS ≤0.6		0.6 <RMS ≤0.9		RMS >0.9	
	%Total	%Sample	%Total	%Sample	%Total	%Sample	%Total	%Sample
Ri ≤ 2.5	0	0	4.6	18.4	10.3	22.5	6.7	23.2
2.5 <Ri ≤ 5.0	0	0	6.2	24.5	9.7	21.3	8.7	30.4
5.0 <Ri ≤ 10	0	0	4.6	18.4	11.3	24.7	8.2	28.6
10 <Ri ≤ 50	.5	100	7.2	28.6	10.8	23.6	3.6	12.5
Ri > 50	0	0	2.6	10.2	3.6	7.9	1.5	5.4

Intensity of v-component of turbulence (m/sec)

Richardson Number	RMS <0.3		0.3 <RMS ≤0.6		0.6 <RMS ≤0.9		RMS >0.9	
	%Total	%Sample	%Total	%Sample	%Total	%Sample	%Total	%Sample
Ri ≤ 2.5	0	0	4.6	31.0	6.7	15.3	10.3	25
2.5 <Ri ≤ 5.0	0	0	3.1	20.1	10.3	23.5	11.3	27.5
5.0 <Ri ≤ 10	0	0	2.1	13.8	9.7	22.4	12.3	30
10 <Ri ≤ 50	.5	100	3.1	20.1	13.3	30.6	5.1	12.5
Ri > 50	0	0	2.1	13.8	3.6	8.2	2.1	5

Intensity of scalar turbulence (m/sec)

Richardson Number	RMS <0.3		0.3 <RMS ≤0.6		0.6 <RMS ≤0.9		RMS >0.9	
	%Total	%Sample	%Total	%Sample	%Total	%Sample	%Total	%Sample
Ri ≤ 2.5	0	0	5.1	18.9	10.8	22.6	5.1	21.3
2.5 <Ri ≤ 5.0	0	0	7.2	26.4	14.4	30.1	8.2	34.0
5.0 <Ri ≤ 10	1	100	3.1	11.3	9.2	19.4	6.2	25.5
10 <Ri ≤ 50	0	0	8.7	32.1	9.7	20.4	3.6	14.9
Ri > 50	0	0	3.1	11.3	3.6	7.5	1.0	4.3

Table 3 presents relationships between the frequency of occurrence of turbulence, magnitude of the turbulence, and the Richardson number for turbulence associated with the zonal (u), meridional (v), and scalar wind profiles. Table 3 refers to the layer 5-6 km, Table 4 to the layer 11-12 km, and Table 5 to the layer 15-16 km. The "% Total" column gives the percentage of the total number of observations in each category, while the "% Sample" column gives the percentage of observations in each category of Richardson number for the given intensity of turbulence. Thus the sum of all "% Total" columns in each table should be 100%, as should the sum of each "% Sample" column.

Based on data presented by Susko and Vaughan (op. cit.) and Scoggins (1967), it appears reasonable to assume that RMS turbulent fluctuations with a magnitude less than 0.6 m/sec are caused largely by errors in the measurement system. RMS values greater than 0.6 m/sec would then indicate the presence of turbulence.

In a study of clear air turbulence, Colson and Panofsky (op. cit.) present data which show that CAT occurs between approximately 3 to 18% of the time at pressure altitudes between 500 and 200 mb based on aircraft data. The percentage increases from 3 to 18% with an increase in wind shear which would be equivalent to a decrease in the Richardson number. This compares with the range of approximately 10-25% in Tables 3 and 4 when the turbulence intensity is between 0.6 and 0.9 m/sec. At higher altitudes (Table 5) the percentages are considerably larger, suggesting that errors may be larger

34

or there is a greater frequency of the occurrence of turbulence. Based on the appearance of the measured profiles, one is led to suspect that larger system errors are responsible for the indicated larger turbulence intensities at the higher altitudes.

It cannot be stated conclusively that turbulence can be detected and its intensity measured by the RJ system until simultaneous and quantitative aircraft or other independent data are available. However, the above results, which agree so closely with those presented by Colson and Panofsky and based on aircraft data, suggest that turbulence can be detected by the system.

The lapse rate of temperature and the vertical shear of the horizontal wind are important parameters in the definition of the Richardson number. Temperature lapse rate is not as critical as wind shear since it enters to the first power, whereas wind shear enters to the second power. In addition, the lapse rate of temperature computed by finite differences over layers of different thicknesses does not vary as much as the vertical wind shear measured over the same layers. Thus, the shape of the wind profile and the thickness of the layer over which the computations are performed may produce large variations in the computed Richardson number. For example, it is possible for the wind shear to be large over a layer of 500 m and small over a layer of 2000 m within the same profile and overlapping layers. The depth of the layer over which the computations should be performed is not known. Some aspects of this problem are presented below.

The influence of more accurate wind profile data in computations of the Richardson number is illustrated in Fig. 8 where Richardson numbers computed with RW and RJ winds are compared. As shown in the figure, wind shear has an important influence on the magnitude of the Richardson number. The dispersion of the points is due to the influence of small-scale motions present in the RJ wind profiles which are not present in the RW wind profiles. Fig. 9 is similar to Fig. 8 but with wind shears calculated over a layer 2000 m in depth. The agreement is much better, as might be expected, since both systems measure wind shears over deep layers with approximately the same accuracy. The influence of wind shears measured over different altitude intervals on the Richardson number is illustrated in Fig. 10, where Richardson numbers computed over 500 m are compared with those computed over a layer of 2000 m in depth. There is very little, if any, correlation between the Richardson number computed over the two layers even though the top of each layer was at the same altitude.

Figure 11 demonstrates that wind shear measured over different altitude layers is primarily responsible for variations in the Richardson numbers computed over the various layers. The dispersion of points in Figs. 10 and 11 is large, indicating the poor relationship between wind shears computed over different layers.
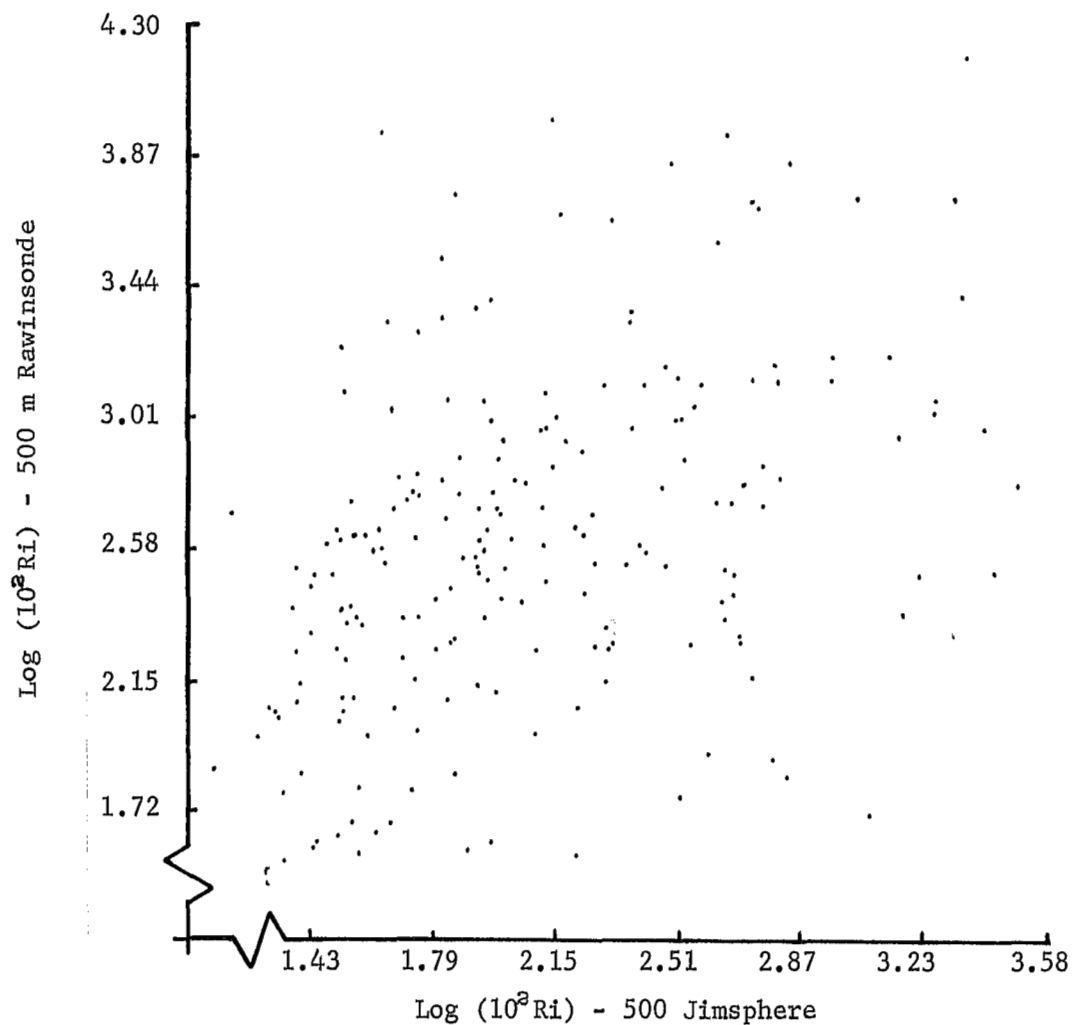
Fig. 8. The Richardson number computed over a layer of 500 m with RJ winds vs the Richardson number computed over the same layer with RW winds. The top of the layer was at an altitude of 12 km.
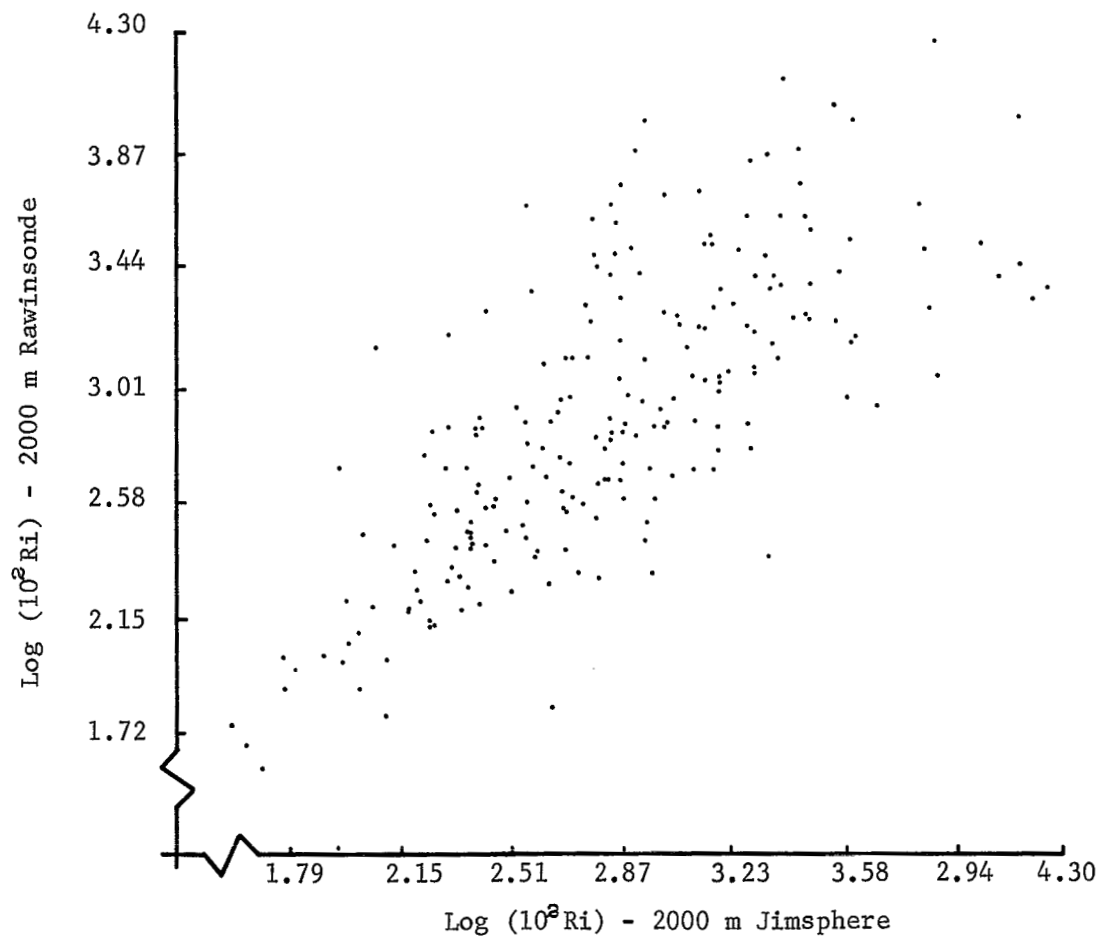
Fig. 9. The Richardson number computed from RJ winds and RW temperatures vs the Richardson number computed from RW winds and temperatures. The computations were performed over a layer of 1000 m with the top of the layer at 12 km.

38

D. Parameters Determined From Synoptic Charts

Temporal cross sections of the RMS value of turbulence determined over altitude intervals of 1 km for the meridional, zonal, and scalar wind-speed profiles, and changes in the corresponding wind speeds to an altitude of 12 km were prepared. In addition, synoptic charts were prepared from RW data for the 850-, 700-, 500-, 400-, 300-, and 200-mb levels with data measured at times corresponding to the temporal cross sections. For identification purposes these are called: Case 1 (April 5, 1966); Case 2 (April 8, 1966); Case 3 (July 5, 1966), and; Case 4 (September 16, 1966). The maps and cross sections are shown in Figs. 12-19, which are shown in the section in which each is discussed.

The temporal cross sections of changes in wind speed represent the change that took place between the first profile in the series and each profile thereafter. The change that took place between any two successive profiles is the difference between the values given for the profiles in the cross section. Care must be exercised in the interpretation of these figures. For example, the horizontal gradient of the isolines presented in the cross sections will be greatest when the change between successive profiles is greatest, but in the case where the wind speed did not change with time at a given altitude, the isolines will be horizontal. The temporal cross sections representing the small-scale motions present an analysis of the RMS value of the motions over 1-km altitude intervals for each profile at the time indicated. Thus large horizontal

41

gradients on these cross sections also represent a large change in the properties of the small-scale motions with time, and in this respect may be interpreted in a similar manner as the temporal cross sections of changes in the wind speed. This method of presentation was chosen because it was easy to visualize altitude regions with high persistence in the wind speeds as well as regions where changes take place in the observed intensity of small-scale motions. In the interpretations of the figures it should be kept in mind that the changes of wind speed can be measured quite accurately with the RJ system but that RMS values of leas than ca. 0.6 m/sec in the small-scale motions cannot be detected with certainty. Because of the large variations observed in the cases studied, each one will be considered separately.

Case 1 (Figs. 12 and 13). Strong cold advection is indicated at 12Z below an altitude of 400 mb, with weak cold advection at 400, 300, and 200 mb. Twelve hours later, cold advection still persisted at all levels from 300 mb and below, with warm advection at 200 mb. The wind backed with height at both times as it should when cold advection is occurring. When the winds back with height, and if the initial wind is from the west, one might expect the zonal component to decrease in magnitude with time. This was not observed. Whether or not the component wind speeds increased or decreased apparently depended upon the increase or decrease in the magnitude of the scalar wind speed. This of course is related to the magnitude of the pressure gradient force which, in turn, is related to

Fig. 12.   Synoptic maps for Case 1, April 5, 1966.

Fig. 13. Temporal cross sections of changes in wind speed
(m/sec) (A, B, and C) and RMS of small-scale motions
(hundreths of m/sec) (D, E, and F) computed over
1 km for Case 1, April 5, 1966.

the gradient of the mean virtual temperature below the level in question. An examination of the indicated advective change in temperature compared with the actual change in temperature for Tampa revealed that the sign of the measured change was the same as the sign for the advective change but of a smaller magnitude. Thus, in this case the slope of a given isobaric surface might differ considerably from that which would be calculated only on the basis of advective change in temperature. The observed changes in the magnitude of the component wind speeds were as high as 13 m/sec over a period of 12 hours but generally were between 2 and 6 m/sec.

Case 2 (Figs. 14 and 15). In this case the advection of temperature was not pronounced, however the observed changes between 00 and 12Z were greater than in Case 1 where the advective change was much greater. There was cold advection in Case 2 below 400 mb and the winds were observed to back with height. But again the behavior of the meridional and zonal components appeared to be influenced by the magnitude of the vector wind and thus did not change in a systematic manner. Between 00 and 12Z, the largest changes were observed below an altitude of 5 km (about 500 mb) and reached a magnitude for the meridional component of 11 m/sec. Between 12 and 00Z the largest changes occurred above an altitude of 8 km where the zonal component decreased as much as 10 m/sec. The changes observed in Case 2 would not have been predicted on
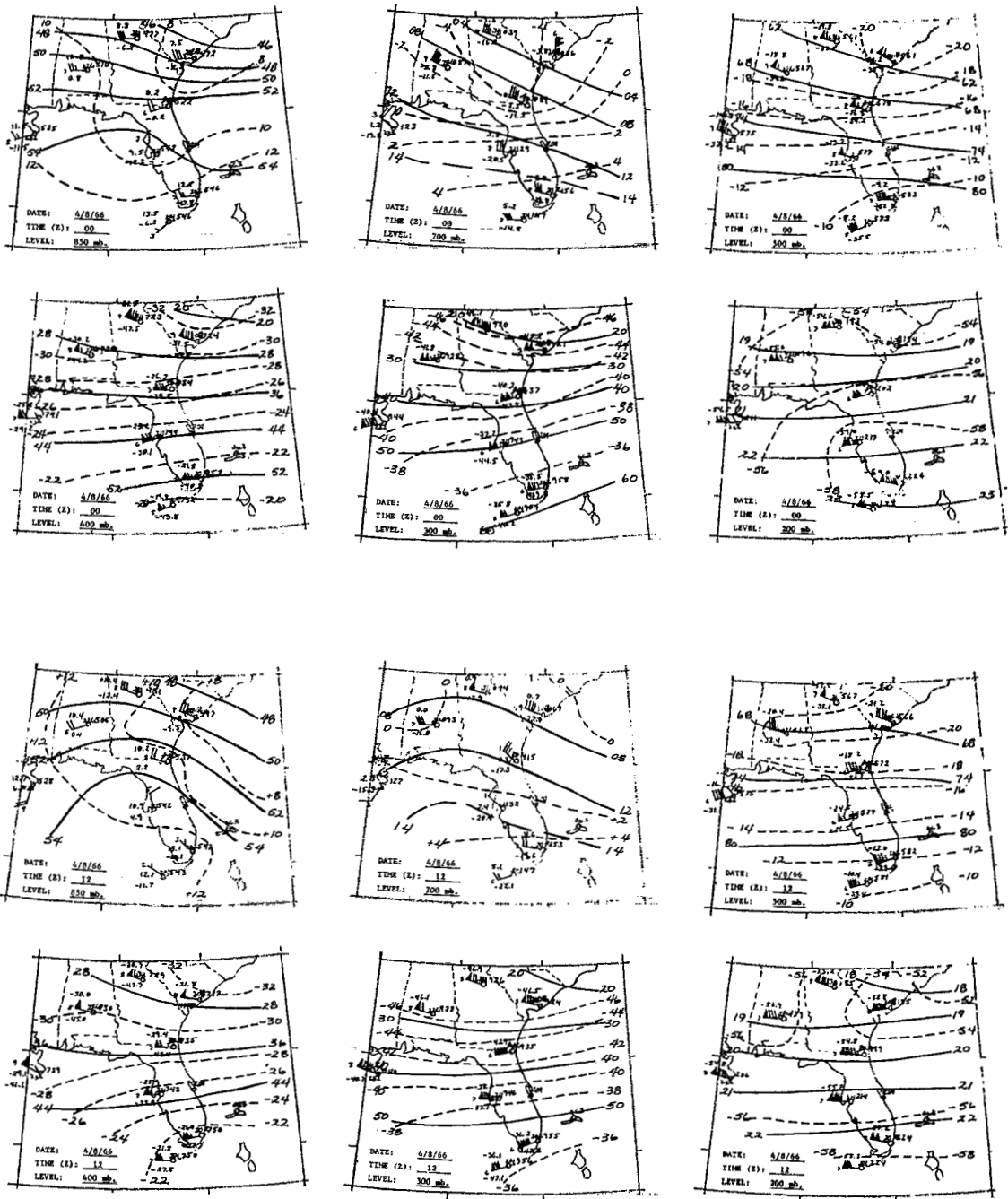
Fig. 14.   Synoptic maps for Case 2, April 8, 1966.

46
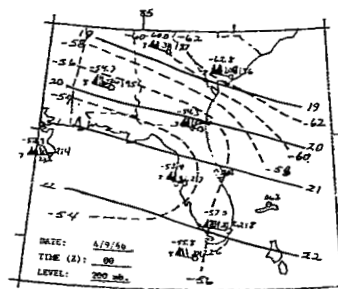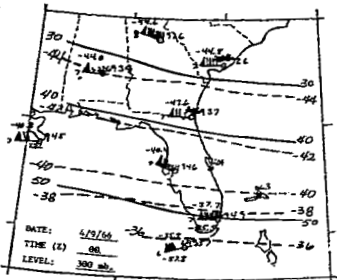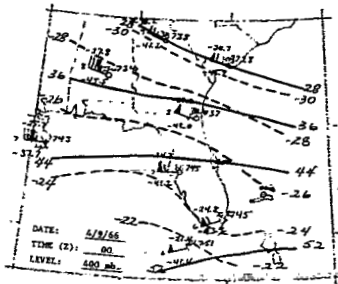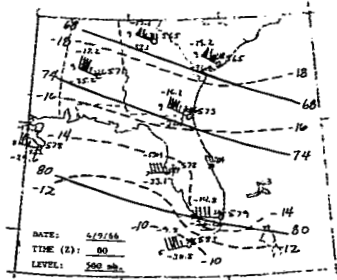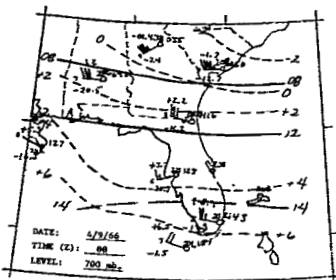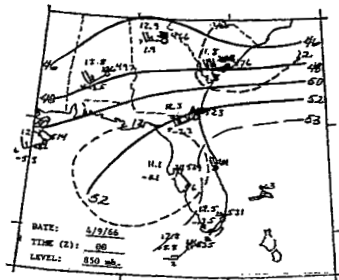
Fig. 14 (continued).
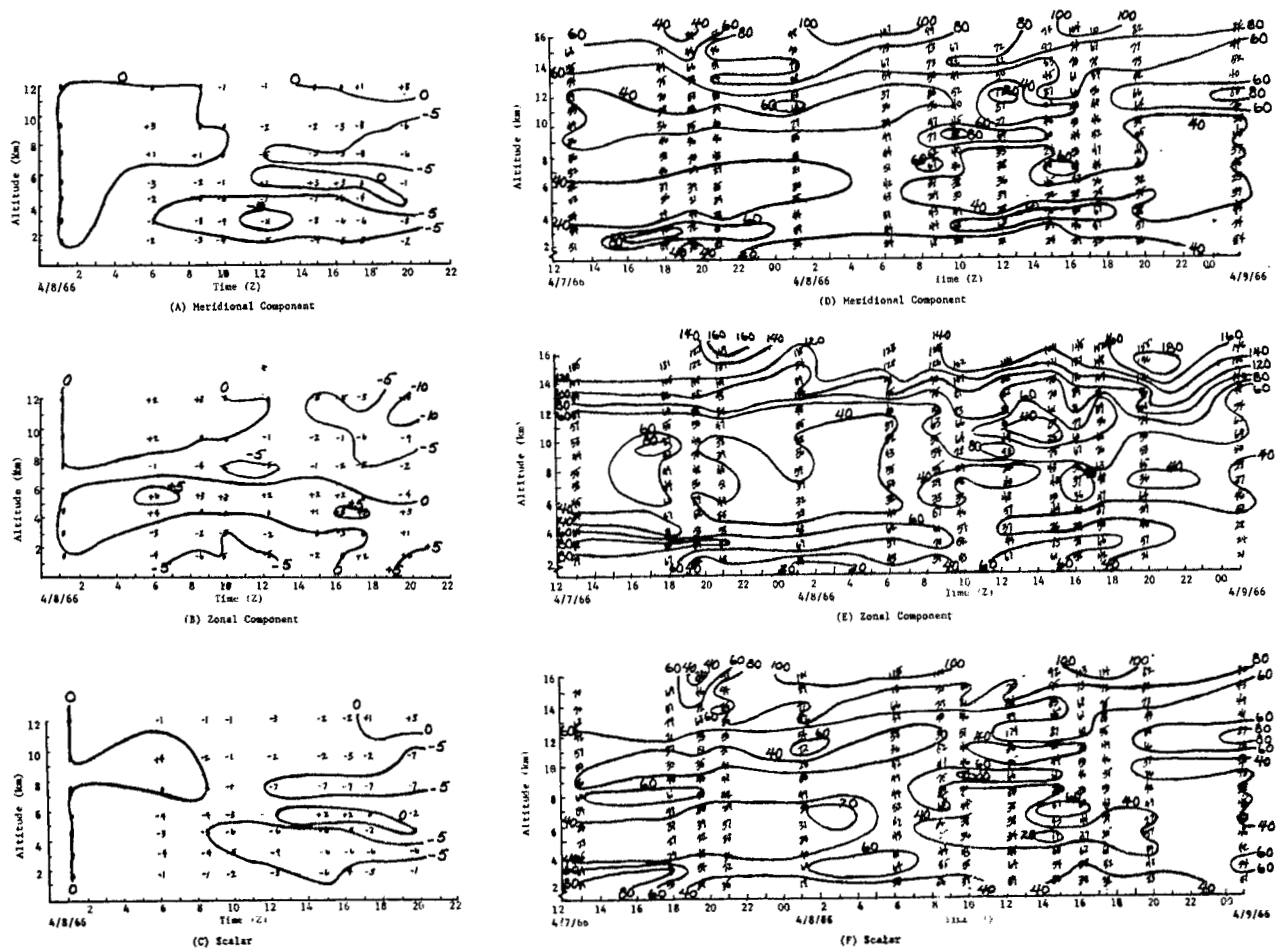
Fig. 15. Temporal cross sections of changes in wind speed (m/sec)
(A, B, and C) and RMS of small-scale motions (hundreths of
m/sec) (D, E, and F) computed over 1 km for Case 2, April 8,
1966.

48

the basis of a change in the mean virtual temperature of the air column as indicated by advection.

Case 3 (Figs. 16 and 17). The indicated advection at all levels in this case is small and might even be considered negligible. However, the observed changes in the temperature are as large or larger than those for Case 1 where the indicated advection was large. The temperatures were observed to decrease with height at almost all levels; this led to a backing of the wind with height. There was a definite decrease in both components as well as the scalar wind speed between 00 and 12Z. The magnitude of the change reached 15 m/sec at a height of 12 km (about 200 mb) for the meridional component and 13 m/sec for the scalar wind speed.

Case 4 (Figs. 18 and 19). The indicated advection of temperature in this case was very small; however the observed changes in temperature were of the same order of magnitude as in the other cases. In this case the overall change in temperature showed an increase which led to a veering of the wind with height. The magnitude of change in this case was much larger than in the others, reaching a value of 25 m/sec and greater in both the zonal component and the scalar wind speeds. These large changes occurred at altitudes above 6 km.

From the discussions of the four cases presented above, the following tentative conclusions may be drawn: 1) in order to forecast changes in the wind profile, good forecasts of temperature (at least) must be made over a large area surrounding the station;
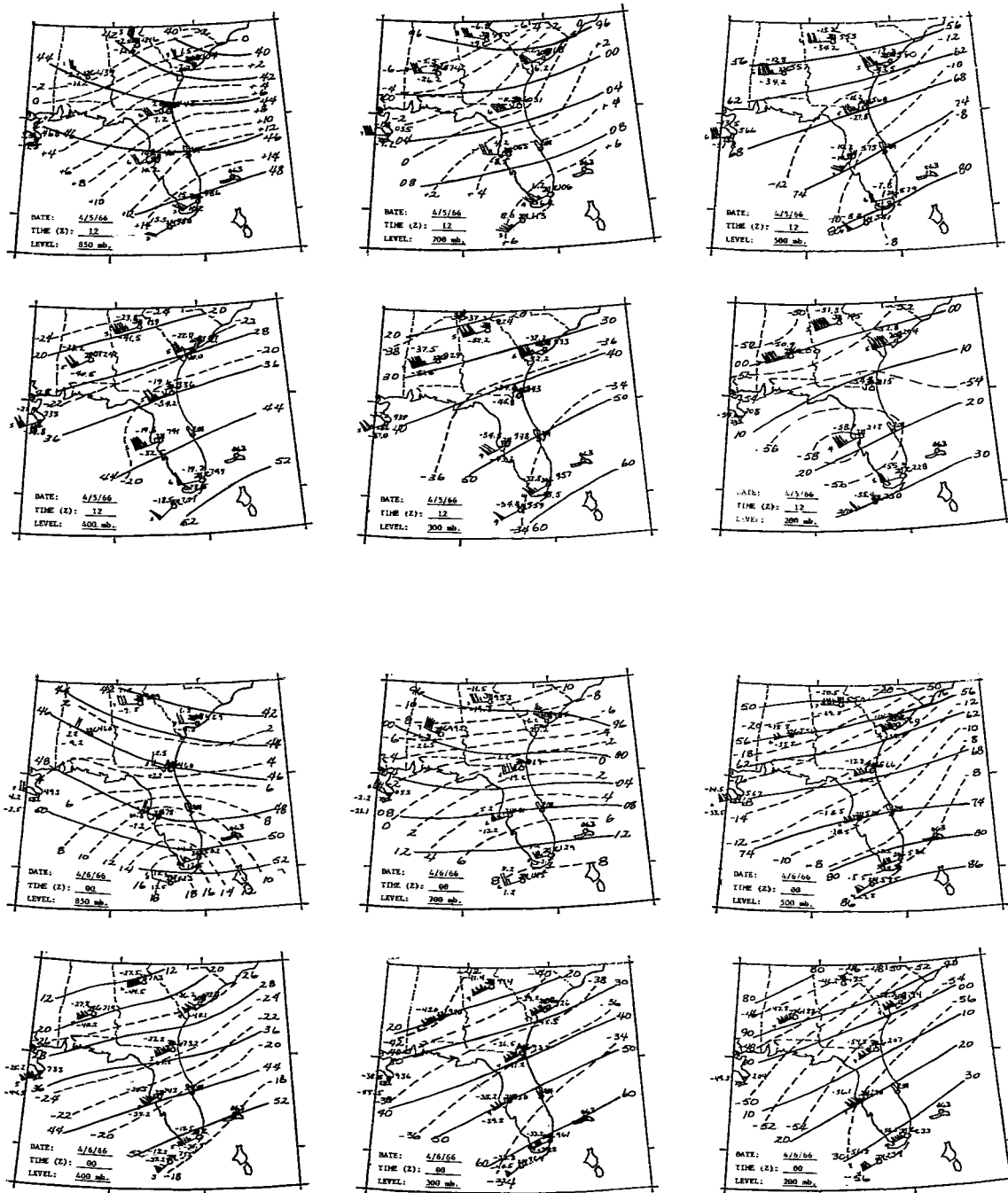
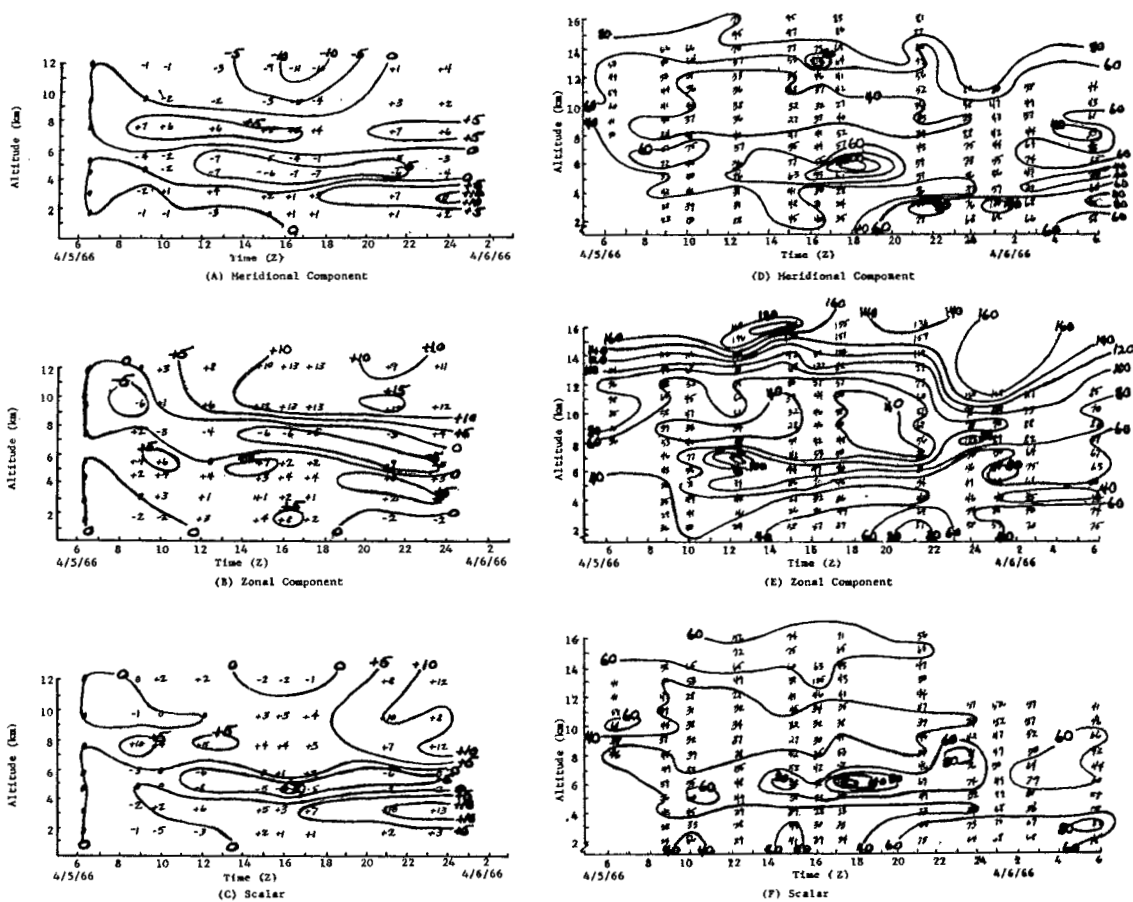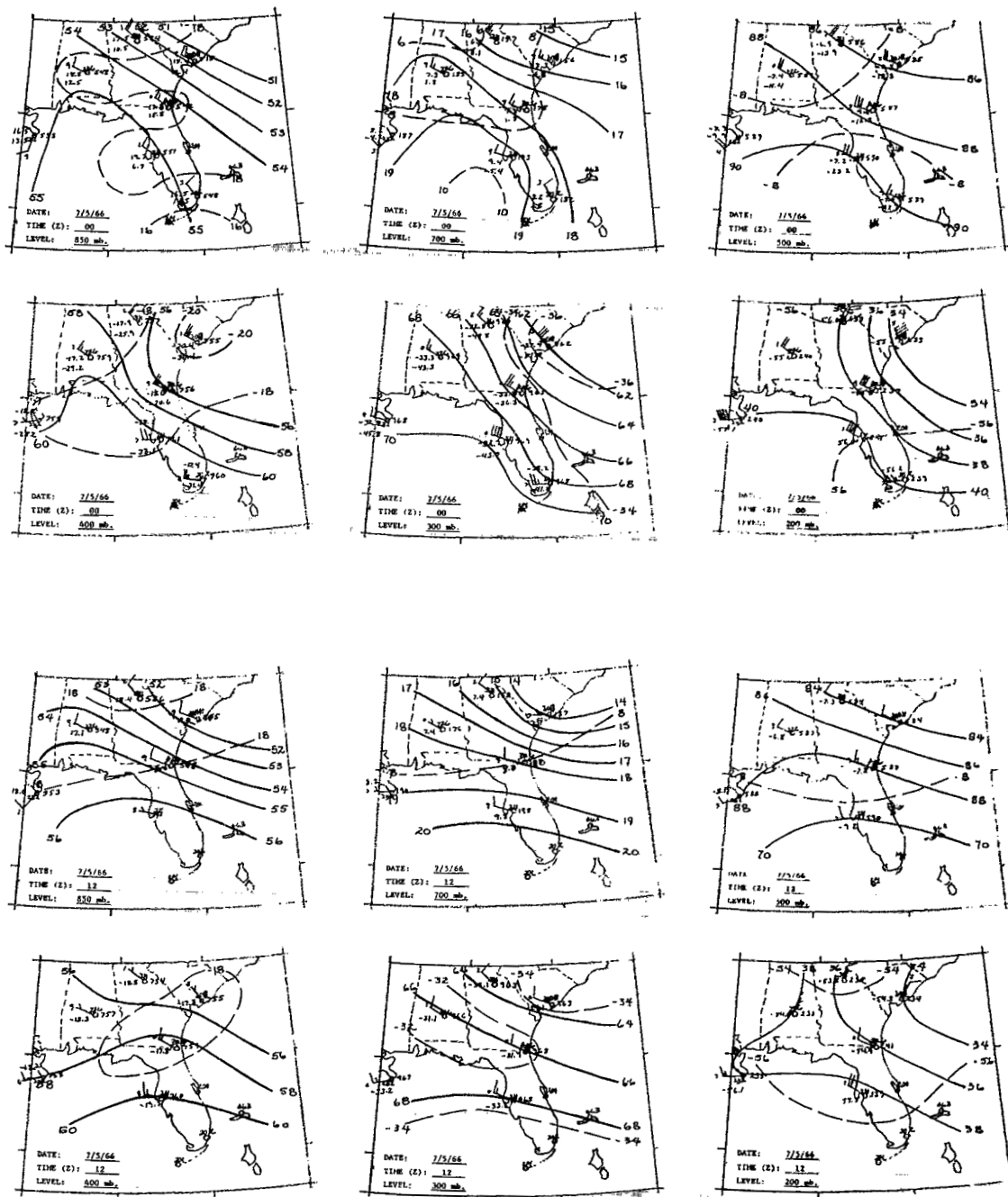Fig. 16.   Synoptic maps for Case 3, July 5, 1966.
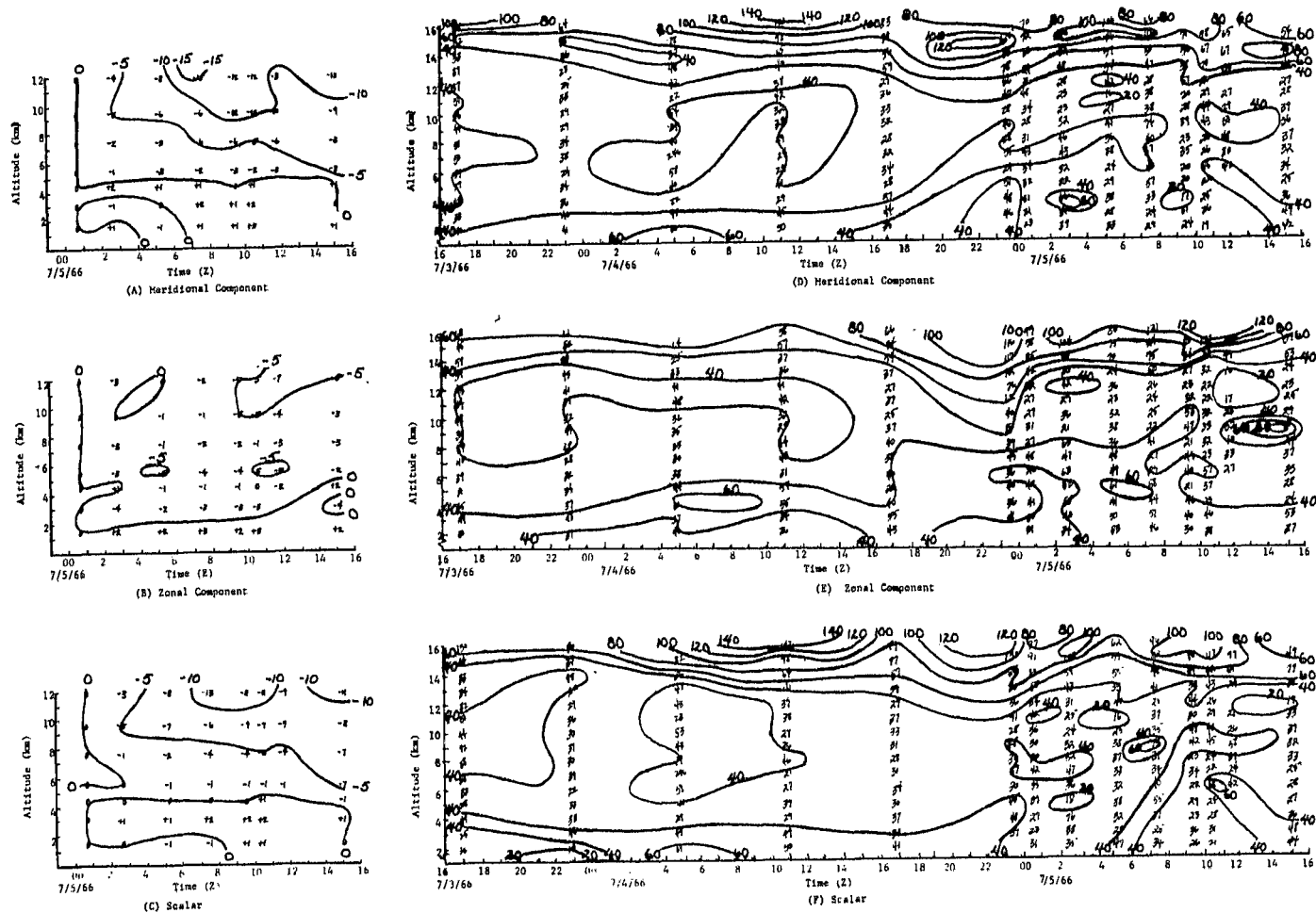
Fig. 17.   Temporal cross sections of changes in wind speed (m/sec)
(A, B, and C) and RMS of small-scale motions (hundreths of
(m/sec) (D, E, and F) computed over 1 km for Case 3,
July 5, 1966.
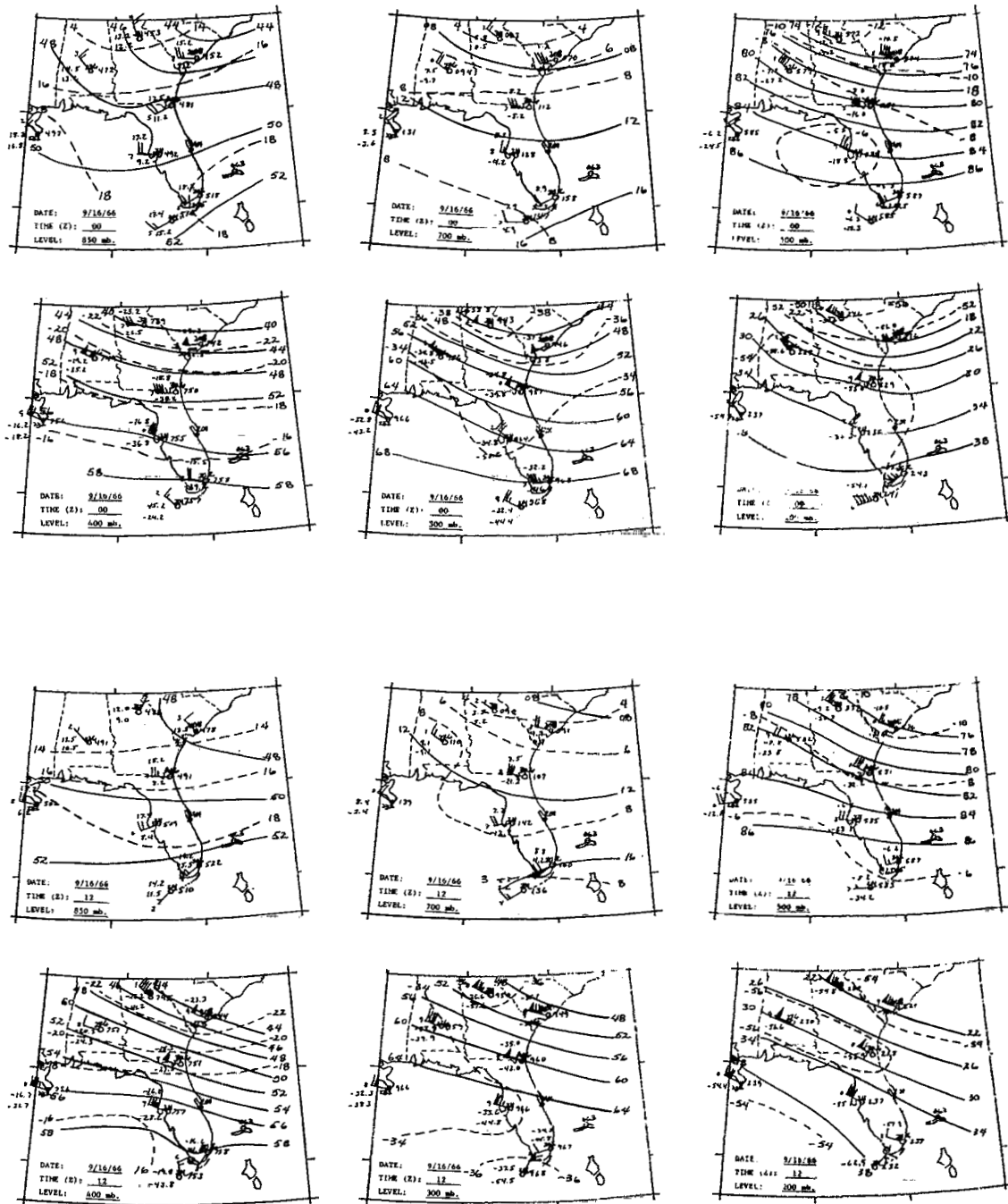
Fig. 18. Synoptic maps for Case 4, September 16, 1966.
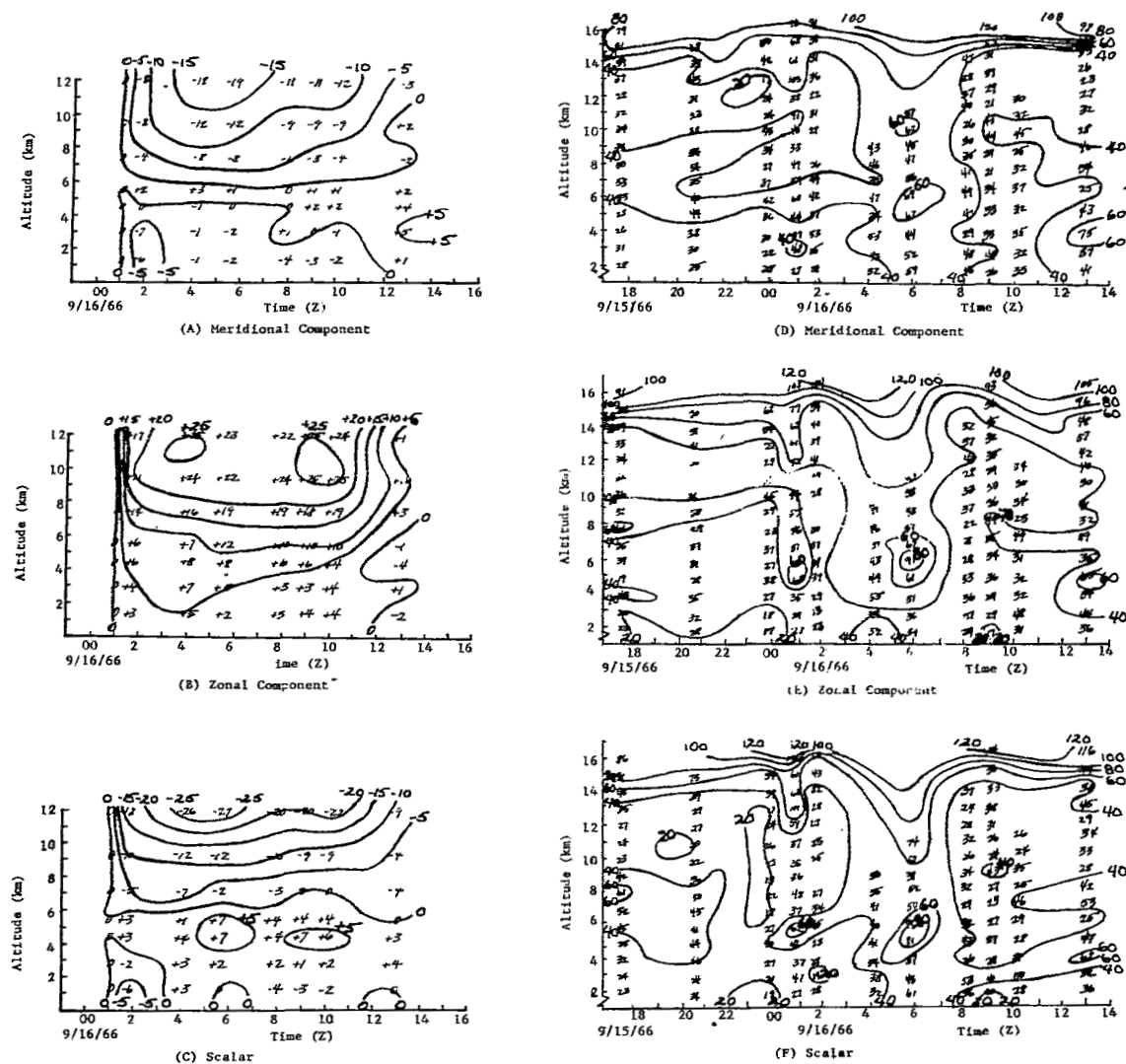
Fig. 19. Temporal cross sections of changes in wind speed
          (m/sec) (A, B, and C) and RMS of small-scale
          motions (hundreths of m/sec) (D, E, and F) computed
          over 1 km for Case 4, September 16, 1966.

2)   the correct sign of a change in the wind direction is determined

apparently by the sign of the observed change in temperature; back-

ing of the winds is associated with cold advection while veering

is associated with warm advection, and; 3)   the magnitude of the

observed change in the temperature over periods of 12 hours and

greater is not given by advection.   Advection of temperature over

shorter time periods and the influence of vertical motion on the

prediction of winds are treated in Section VIII.

An attempt was made to determine the relationships, if any,

between the RMS values of the small-scale motions and 1)   horizon-

tal wind shear, 2)   curvature of the flow (cyclonic or anti-cyclonic),

3)   advection of temperature, 4)   location and intensity of the

jet stream, 5)   vorticity, and 6) advection of vorticity.   The

first four of these parameters was calculated from the 700-, 500-,

and 300-mb charts in all cases and the last two parameters from

the 500-mb charts.   Large values of horizontal wind shear in cases

of both cyclonic and anti-cyclonic curvature were observed, as well

as large negative and positive values of both temperature and vorti-

city advection.   The magnitude of the vorticity at 500 mb varied

between 4 and 8 x 10^{-5} sec^{-1} with some values cyclonic and some

anti-cyclonic.   While some of the observed changes in the RMS

values of the small-scale motions were much larger than those ex-

pected from error, scatter diagrams did not reveal any systematic

relationships between the parameters investigated and the magni-

tude of the turbulent deviations. It appears that the relationships between synoptic-scale parameters and small-scale motions are so complex that it is not possible to relate the two by considering simple parameters obtained from individual constant-pressure charts. A much more complicated approach is required which considers the interaction between various layers. Additional research is required to establish these relationships.

VIII. A SIMPLE METHOD FOR FORECASTING THE WIND PROFILE

A. Introduction and Background of Problem

Forecasts of detailed wind profiles are of prime concern to both meteorologists and engineers. Wind shear and turbulence are important in the design and operation of space vehicles. Ryan, Scoggins, and King (1967) investigated the influence of small-scale (vertical wavelengths less than 1000 m) wind shears on the design of space vehicles. They demonstrated that small-scale wind shears influence significantly the control system as well as the bending moments experienced by the vehicle.

Spatial and temporal variations in small-scale winds are not known accurately. Thus, when a space vehicle is launched through the (partially) unknown wind field, a low risk must be accepted that the vehicle will be lost (Vaughan, 1968). This risk might be reduced singificantly if the wind profile could be forecast accurately.

In addition to the importance of wind profiles in the design and operation of space vehicles, consideration of them is significant in many meteorological problems (Panofsky, 1956; Hess, 1959). Vertical shears of the horizontal wind are related to clear-air turbulence and are important in exchange processes which relate directly to atmospheric diffusion and to the flux of quantities through the atmosphere (Lumley and Panofsky, 1964; Reiter, 1963).

In addition, wind shear is related to the thermal structure of the atmosphere which, in turn, is related to many dynamical and thermo-dynamical processes (Petterssen, 1956). Thus wind shear is an important consideration in many practical as well as theoretical problems.

Most wind profiles now available are "smooth" because the small-scale fluctuations have been filtered out due to the smooth-ing inherent in the calculations of the RW wind data.[1] A few stations now have an RJ system which provides "detailed" profiles with resolution sufficient to include the small-scale motions (wavelengths longer than about 100 m). Scoggins (1967) showed that the RJ data are at least an order of magnitude more accurate than the wind data obtained by the RW system.

Small-scale features of a vertical wind profile, which may amount to a few meters per second or less, cannot be obtained from the conventional RW data. The "detailed" wind profiles, measured by the RJ system, contain these features and are used for the veri-fication of the forecasts.

Little has been accomplished toward the development of a method to forecast wind profiles over short periods of time. At

---

[1] Circular O, 1959; Manual of Winds-Aloft Observations, U. S. Government Printing Office, Washington, D. C., 182 pp.

present the n-level baroclinic and primitive models used by the National Meteorological Center (NMC) have at most six to nine levels which could provide an abbreviated forecast of the wind profile. In particular, if a forecast of the wind profile is desired for a station on a routine basis, it seems logical that a provision could be made in the NMC program and a forecast provided. The wind profile obtained in this manner would be smooth because the input data are smooth, and the models also smooth the profile by filtering out small-scale motions such as gravity, inertia, and sound waves.

Hadeen (1966) formulated and tested a meteorological model which used four grid points to forecast the smooth wind profile. The model was based on horizontal advection of the geostrophic wind shear, and input was restricted to wind data only.

A 12-hr forecast of the vertical wind profile at a station was made as follows. First, a "forecast" of the wind at the 6-km level, called the base level, was obtained from NMC facsimile charts. Next, the vertical shear of the geostrophic wind was forecast for the 6 to 7-km layer using the mean wind of this layer to advect the vertical shears of the geostrophic wind at the grid points surrounding the station. The wind forecast at the 7-km level then was obtained from the forecast of the vertical wind shear for the 6 to 7-km layer and the wind at the 6-km level. In this manner (i.e., by applying this procedure to successive 1-km

layers) the wind both above and below the base level was calculated.

The forecast winds at the various levels were built from the base level and, for test purposes, the wind used for verification was used also as input for the base level. Satisfactory 12-hr forecasts were made after a one-fourth reduction of the advection terms had been applied. The model is very sensitive to input data, and when a "forecast" wind is used for the base level, results are quite variable. Hadeen concluded that the model by itself is not adequate. He recommended that in order to forecast a wind profile accurately, the model should include meteorological parameters other than the wind and should utilize a larger grid network.

Endlich et al. (1969) examined some prediction models which provide short-range (12- and 24-hr) forecasts of the vertical wind profile at Cape Kennedy, Florida. To forecast the smooth wind profile, a grid was used which covered the United States, Mexico, and the Caribbean, with grid points 2.5 deg apart (in their model it was necessary to choose a grid large enough to encompass all winds that could be advected to Cape Kennedy in less than 1 day under jet-stream conditions). An objective analysis of the wind components at each of the selected levels was done by a computer and displayed on a cathode ray tube. From these analyses, the divergence, vorticity, and wind gradients were computed.

The forecast was obtained by advection of the wind components, vorticity, and divergence, then at the end of each time step, the wind components were adjusted to fit the new fields of vorticity and divergence. This process was repeated for successive time steps until the desired forecast was achieved.

In an attempt to find a technique that could be used to forecast the perturbations on the smooth profile, Endlich et al. (op. cit.) examined deviation profiles and speed-difference profiles as computed from several sets of serial RJ ascents. The deviation profiles were obtained by computing the differences between the individual profiles and the mean profile (average of speeds at each height of all profiles in the series); the speed-difference profiles were obtained by computing the differences of wind speeds between successive pairs of speed profiles. The series examined indicated that the features on the deviation profiles were random and showed little persistence. Features on the speed-difference profiles showed also, in general, a lack of continuity that would be necessary for their direct utilization in a forecast model.

Endlich et al. concluded from an analysis of the power spectra of the individual, mean, and deviation profiles that no well-defined separation of the scales of motion existed in the series examined. This lack of natural separation of the scales of motion leads to much difficulty in forecasting these minor but significant perturbations on the smooth profile.

Due to the limited success of present methods to forecast accurately the wind profile, the RJ system is used to monitor wind conditions prior to the launch of space vehicles at Cape Kennedy (Vaughan, 1968). This system provides detailed wind profiles (data are presented at 25-m intervals of altitude) to an altitude of 18 km, as input to the vehicle's flight simulation program in approximately 1 hr after launch of the Jimsphere. Thus, it is possible to have knowledge of the winds aloft before the launch of the vehicle, but not at the time of the launch.

Changes in speed and direction as indicated by successive profiles are very complex (Vaughan, op. cit.; DeMandel and Scoggins, 1967; Weinstein et al., 1965). Frequently, these deviations about the mean wind profile change rapidly in a few hours while at other times (or levels) fluctuations of more than 5 m/sec can persist for several hours (Weinstein et al., op. cit.). Thus, over short periods of time, the small-scale features associated with vertical wind profiles may or may not be persistent.

The goal of this research was to develop a model (using input data obtained from routine synoptic charts and RW and RJ measurements) that would provide forecasts of the vertical wind profile at Cape Kennedy, Florida, and to determine to what degree of detail wind profiles could be forecast. The accuracy of short-range forecasts (less than 12 hr) of zonal[*] wind speed between 2 and 12 km provided by the model was examined.

---

[*] E-W component of horizontal wind

61

B. Wind Measurements and Data

Most wind measurements throughout the United States are made using the RW system. This system consists of a radio-direction finder and an instrument package called a radiosonde attached to a free-rising balloon. Winds are measured by tracking the signal transmitted from the radiosonde as it is carried aloft by the balloon. From changes in the positions of the radiosonde, wind data are obtained which represents an average over about 600 m of altitude (for altitudes between 2 and 12 km). Due to this averaging in the computations, wind details of a short time duration are lost and a smooth wind profile results. Approximate rms errors in the measurement of wind speed vary between 2 and 15 m/sec, depending upon wind conditions and tracking geometry. The corresponding rms error in wind direction ranges between 5 and 20 deg.[2]

In the RJ system, wind measurements are made by tracking a superpressure sphere, called a Jimsphere, with the FPS-16 radar. As the Jimsphere rises, its position is recorded at intervals of 0.1 sec, from which wind data averaged over about 50 m in altitude and presented at 25 m intervals are obtained. The light-weight and high-drag characteristics of the Jimsphere, coupled with the precision of the FPS-16 radar, provide an rms error in wind speed measurements of approximately 0.6 m/sec, and 1 deg or less in wind

---

[2] AMR, 1963: Meteorological Handbook, Headquarters, Air Force Missile Test Center, Patrick AFB, Florida, 12 pp.

direction (Scoggins, op. cit.).

RW measurements for approximately 70 stations located throughout the United States are made at 12-hr intervals, at 00 and 12 GMT. RJ measurements are taken at only a few selected stations, the principal locations being Vandenberg AFB, Calif., Cape Kennedy, Fla., and White Sands Missile Range, New Mexico. At Cape Kennedy, RJ measurements are made frequently at 00 and 12 GMT, but more useful data, in the form of series of RJ measurements, are available. The time interval between successive runs varies usually between 1 and 2 hr and a series usually consists of up to ten such runs.

Figure 1 shows a comparison between a vertical wind profile constructed from RJ data and a profile simulated to represent the RW data. Wind speed is plotted along the abscissa and altitude along the ordinate. Rapid changes or deviations of wind speed with height, such as from A to A', exist at most altitudes on the RJ profile. Notice that these features are not observed on the corresponding RW profile. It is easy to see that many differences exist between the two profiles and the names "detailed" and "smooth" describe their appearance.

C. The Forecast Model

The equation of motion for the meridional[*]component of the horizontal wind is given by

$$\frac{dv}{dt} = - fu - 980 \left[\frac{\partial h}{\partial y}\right]_p \tag{1}$$

where terms involving friction and the curvature of the co-ordinate system are omitted, and the subscript p refers to constant pressure. This equation states that the horizontal acceleration of the meridional component is given by two terms, the coriolis force (-fu) and the pressure gradient force $(-980(\partial h/\partial y)_p)$.

If the acceleration is assumed to be zero, then a balance exists between the pressure gradient and coriolis forces. The wind defined by such a balance is called geostrophic and the zonal component, u_g, is given by

$$u_g = - \frac{980}{f} \left[\frac{\partial h}{\partial y}\right]_p . \tag{2}$$

Since the acceleration term in Eq. 1 is normally small, Panofsky (1956) has estimated that above the friction layer and away from jet streams, the geostrophic wind is in error from the true wind by approximately 10 per cent of its magnitude.

Differentiation of Eq. 2 with respect to time, gives

$$\frac{\partial u_g}{\partial t} = - \frac{980}{f} \frac{\partial}{\partial t}\left[\frac{\partial h}{\partial y}\right]_p \tag{3}$$

---

[*] N-S component of horizontal wind

which is a prognostic equation for u_g. Thus, local changes of the geostrophic wind may be obtained from changes in the slope of the constant-pressure surface. A similar equation may be written for the v_g component.

A frequently used relationship in meteorology is the hypsometric equation given by

$$\Delta h = \frac{R_d \overline{T}_v}{980} \ln\left[\frac{p}{p_t}\right] \tag{4}$$

where:

Δh is the thickness of a layer defined by two pressure surfaces, p and p_t, where $p_t < p$,

R_d is the gas constant for dry air, and

$\overline{T}_v$ is the mean virtual temperature of the layer.

Therefore, for a layer defined by two constant-pressure surfaces, the thickness and mean virtual temperature of the layer can be used interchangeably since they differ only by a constant.

The height, h, of any pressure surface is given by

$$h = h_o + \Delta h \tag{5}$$

where h_o is the height of the lower pressure surface (p). Combining Eqs. 3 and 5 gives

$$\frac{\partial u_g}{\partial t} = -\frac{980}{f}\frac{\partial}{\partial t}\left[\frac{\partial h}{\partial y}\right]_p - \frac{980}{f}\frac{\partial}{\partial t}\left[\frac{\partial \Delta h}{\partial y}\right]_p . \tag{6}$$

Substitution of Eq. 3 for the first term on the right-hand side of Eq. 6 and changing the order of differentiation of the second term gives

$$\frac{\partial u_g}{\partial t} = \frac{\partial u_{go}}{\partial t} - \frac{980}{f}\frac{\partial}{\partial y}\left[\frac{\partial \Delta h}{\partial t}\right]_p \tag{7}$$

which is the desired basic forecast equation.

This equation states that the rate-of-change of the zonal geostrophic wind at the top of a layer is given by the sum of two terms. The first term is the rate-on-change of the zonal geostrophic wind at the bottom of the layer, and the second is a term involving the y-component of the gradient of the rate-of-change of thickness of the layer. The last term also could be written in terms of the rate-of-change of the mean virtual temperature of the layer by use of Eq. 4.

In summary, in order to make a forecast of the vertical profile of the zonal wind, it is necessary to know the rate-of-change of the zonal wind at the lower pressure surface (called the base surface) and the gradient of the rate-of-change of thickness (or $\overline{T}_v$) for the layer above. The top of the first layer becomes the base of the next layer.

In this study the atmosphere was separated into five layers defined by the 850-, 700-, 500-, 400-, 300-, and 200-mb surfaces.

The base surface was chosen to be 850 mb and the rate-of-change of the zonal wind determined by interpolation of measured data. The second term on the right-hand side of Eq. 7 was evaluated by assuming that the local rate-of-change of thickness is given by horizontal advection since thickness or mean virtual temperature is approximately conservative. The wind forecast for the 700-mb surface then was obtained as the sum of the two terms. By use of this forecast for the 700-mb surface and the gradient of the rate-of-change of thickness between 700 and 500 mb, the wind at the 500-mb surface was predicted. This procedure may be repeated for as many layers as necessary to forecast the complete zonal wind profile.

Operationally, the base surface could be chosen to be at any altitude, the only restriction being that the forecast rate-of-change of wind speed be accurate. For example, picking the base surface at 500 mb, the forecast rate-of-change of wind speed could be obtained from the NMC baroclinic prognosis. Forecasts for the other surfaces then are obtained by building up and down from this base surface in the manner described above.

D. Discussion of Factors Related to the Forecast Model

1. Location of Data. In order to test the model, a grid network made up of RJ and RW data would be desirable. In such a grid, as depicted in Fig. 20 for the Cape Kennedy area, the central point would have measurements available from the RJ system at 1-hr intervals, and the outer grid points would have available measurements taken with the conventional RW system. With such a grid network, the RW data would provide the input for the forecast and the RJ data would be used for verification of the forecast. The grid in Fig. 20 shows the absolute minimum number of stations even if single-station techniques are employed to determine the local rate-of-change of thickness. Obviously a more extensive grid network is desirable.

The forecast model is to be used at Cape Kennedy. This location, on the eastern shore of Florida, presents problems for calculation of the gradient of quantities, especially in the east-west direction. Figure 20 shows that data from Jacksonville and Miami would be a good approximation to data at the northern and southern grid points. Therefore, changes in the north-south direction can be obtained from available RW data, but east-west changes would have to be obtained from computations made from analyzed maps. In addition, data are not available over the Gulf of Mexico, so that it often is difficult to determine advection especially over Miami and Tampa.
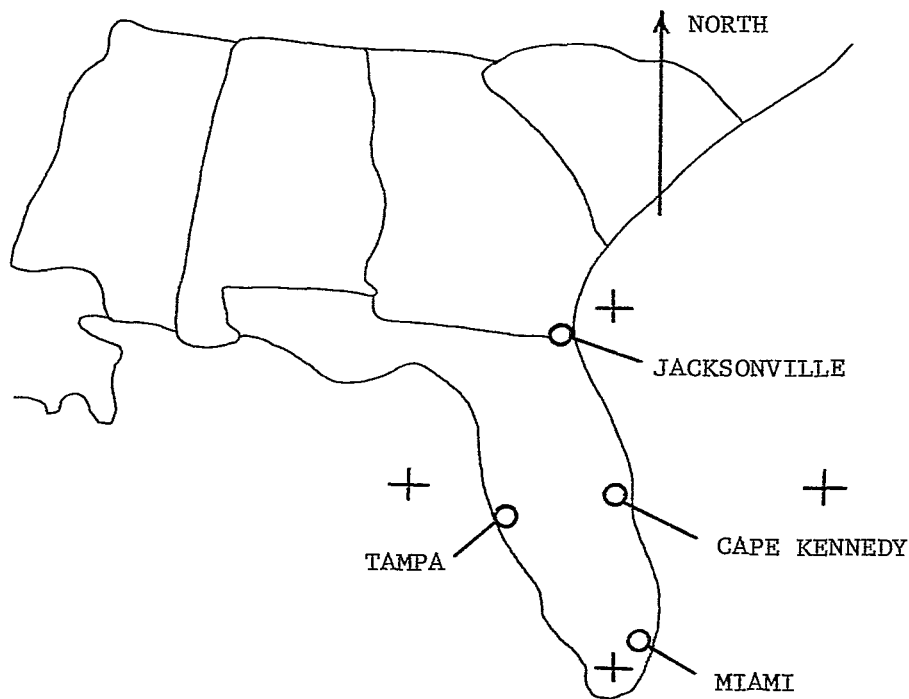
Fig.20. A map of the rawinsonde stations in the Cape Kennedy
area (circles) and locations of stations forming the desired
4-point grid (plus signs).

2. <u>Forecasting Mean Virtual Temperature ($\overline{T}_V$) or Thickness (Δh).</u>

Equations 2 and 4 can be used to illustrate the importance of a change in the gradient of the mean virtual temperature ($\overline{T}_V$) on the geostrophic wind. Consider the case where the 1000-mb surface has the same height over both Jacksonville and Miami. If the height of the 700-mb surface at Jacksonville is 3100 m and $\overline{T}_V$ between the 1000- and 700-mb surfaces is 4°C, and the corresponding values at Miami are 3125 m and 6°C, the zonal component of the geostrophic wind would be approximately 6 m/sec. If $\overline{T}_V$ at Jacksonville is decreased by only 2°C, a very nominal change which could be realized and the height of the 1000-mb surface remains unchanged, the resulting change in the height of the 700-mb surface would be approximately 25 m. This increases the slope of the 700-mb surface (also the magnitude of the pressure gradient force) by a factor of approximately 2 from its original value and, hence, increases the wind speed by the same factor, or to about 12 m/sec.

A change in $\overline{T}_V$ of this magnitude easily could result from the advection of temperature or from vertical motion over a short period of time. If we consider a vertical velocity of only 1 cm/sec at all altitudes below the level in question and in the absence of condensation, approximately a 2°C drop in temperature would result due to expansion over a period of 6 hr. Vertical motions of a few centimeters per second over a large area are not uncommon, and thus changes in $\overline{T}_V$ due to vertical motion could result in a significant

70

change in the geostrophic wind over relatively short periods of time.

The total derivative of $\overline{T}_v$ in the x, y, p, t system may be written

$$\frac{d\overline{T}_v}{dt} = \frac{\partial \overline{T}_v}{\partial t} + \vec{V} \cdot \vec{\nabla}\overline{T}_v + \omega \frac{\partial \overline{T}_v}{\partial p} . \qquad (8)$$

The first term on the right-hand side is the local rate-of-change of $\overline{T}_v$. The second term represents advection of $\overline{T}_v$ where $\vec{V}$ is the average wind vector in the layer. The last term represents vertical advection of $\overline{T}_v$.

As noted by Panofsky (op. cit.), if $\overline{T}_v$ were a conservative quantity, and vertical advection could be neglected, Eq. 8 becomes

$$\frac{\partial \overline{T}_v}{\partial t} = - \vec{V} \cdot \vec{\nabla}_p \overline{T}_v \qquad (9)$$

which states that the local rate-of-change of $\overline{T}_v$ is the result of advection of $\overline{T}_v$. Normally, when there is warm (cold) advection, the air is rising (falling) and this motion produces adiabatic cooling (warming) and thus reduces the temperature change. Although the error caused by neglecting vertical motion and changes in temperature following the air varies in individual cases, the long-term average is that the change in $\overline{T}_v$ is less than that expected from advection alone (Panofsky, op. cit.).

The local time rate-of-change of thickness as given by horizontal advection only was investigated. The isobaric advection of

thickness, $-\vec{V} \cdot \vec{\nabla}_p(\Delta h)$, is numerically equal to $-\overline{V} \, \partial(\Delta h)/\partial s$, where $\overline{V}$ is the mean speed of the wind and $\partial(\Delta h)/\partial s$ is the change of thickness along the streamlines (Panofsky, op. cit.). This relationship was used to evaluate the isobaric advection of thickness from constant-pressure maps.

NMC facsimile maps were re-analyzed as deemed appropriate and used to compute graphically the thickness patterns and the mean wind through and upstream from each station. The mean wind speed, $\overline{V}$, for the station, was computed by averaging the wind speed both along the streamline and between the two pressure surfaces. The product of wind speed and the forecast period gives the approximate distance traveled by a parcel during the forecast period. The forecast of the thickness for the station is made by reading the thickness value from the analyzed map at a point this distance upstream along the contours.

The advection of thickness at Cape Kennedy, Jacksonville, and Miami between 500 and 700 mb, and between 500 and 300 mb, was computed for a 12-hr period without respect to synoptic conditions. Figure 21 shows the results of a comparison between the forecast and measured change in thickness for all three stations and for both layers. The grouping of all the points in one figure was justified because the distribution of points for each station and layer showed no significant difference from that of the composite. The measured change is plotted along the abscissa and the forecast change along the ordinate. The solid diagonal line is where

72
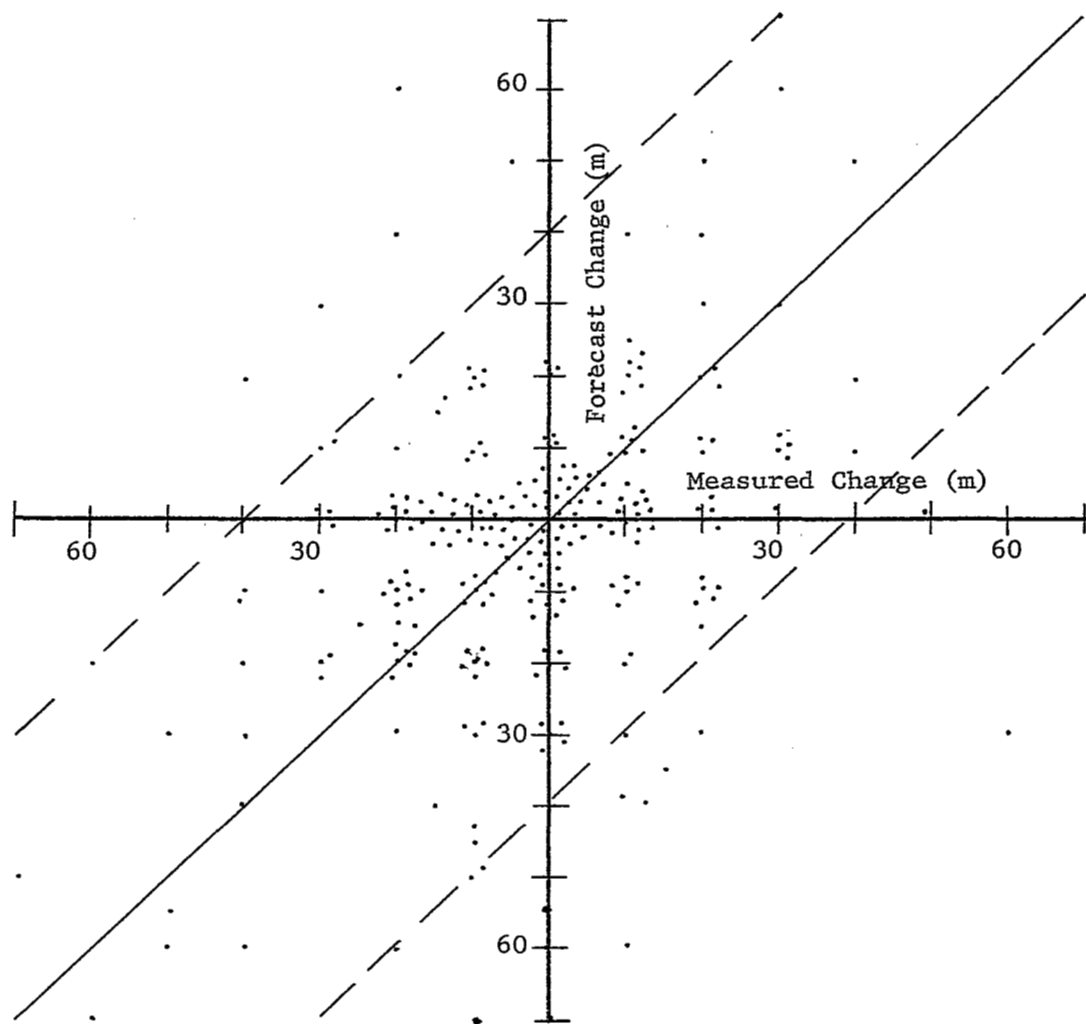
Fig. 21. A comparison of the forecast change of thickness for
the 700-500-mb and the 500-300-mb layer over a 12-hr period, and
the measured change of thickness at Jacksonville, Miami, and Cape
Kennedy. Points falling within the dashed lines represent within
measurable accuracy (±28 m) an acceptable forecast.

the points would fall if a one-to-one relationship existed between the measured and forecast change. For orientation purposes, from Eq. 4 a change of 60 m in thickness of the 500- to 700-mb layer corresponds to a 6°C change in the $\bar{T}_v$. For the 500- to 300-mb layer, a change of 60 m in thickness corresponds to a 4°C change in $\bar{T}_v$.

Below 13 km, the RMS error in pressure measurements by the RW system is 1.50 mb.[3] This means that 67% of the measured data are either higher or lower than the true value by an amount equal to or less than 1.50 mb. With this in mind, and using the hypsometric relationship, we can calculate a corresponding RMS error of height measurement. Since pressure decreases exponentially upwards from the surface, a 1.50-mb error in pressure corresponds to larger errors in height measurement at the higher altitudes. For example, at 700 mb it is 18 m and at 200 mb it is 48 m. For our purposes, an average RMS error of 20 m was chosen and assumed to apply at all levels.

Since the thickness between two surfaces is the difference in their heights, this thickness value also has a certain RMS error. This RMS error of the thickness (σ_{th}) is related to the RMS error of the height of the upper surface (σ_u) and the RMS error of the

---

[3] AMR, 1963: <u>Meteorological Handbook</u>, Headquarters, Air Force Missile Test Center, Patrick AFB, Florida, 12 pp.

lower surface (σ_1) by

$$\sigma_{th} = \sqrt{\sigma_u^2 + \sigma_1^2} \qquad (10)$$

(Deming, 1943). If there are errors of 20 m at each of the two surfaces, the RMS error in the thickness would be about 28 m.

The dashed lines in Fig. 21 bracket the RMS error in measurement (± 28 m) of thickness, so that any point that falls within these limits represents an acceptable forecast. Of the 280 points plotted in Fig. 21, 93% fall within these limits.

As noted previously, the wind speed depends upon the gradient of the thickness and not the thickness itself. Therefore, forecasts of the gradient of the thickness of a layer were examined. A measure of the gradient (north-south) of thickness is obtained by taking the difference in the thickness of a layer between Jacksonville and Miami, hereafter referred to as the "gradient".

On the assumption that the local rate-of-change of thickness is a result of horizontal advection alone, the forecast gradients were computed for both the 500-700-mb and the 500-300-mb layers and their measured and forecast changes compared. Figure 22 is a scatter diagram of the results of this comparison. The measured change of the gradient is plotted along the abscissa and the forecast change of the gradient along the ordinate. The diagonal lines in the figure have meanings similar to those in Fig. 21. Equation 10 was used to compute these limits using RMS errors obtained for the measurement of thickness for Jacksonville and Miami of 28 m, giving for the RMS
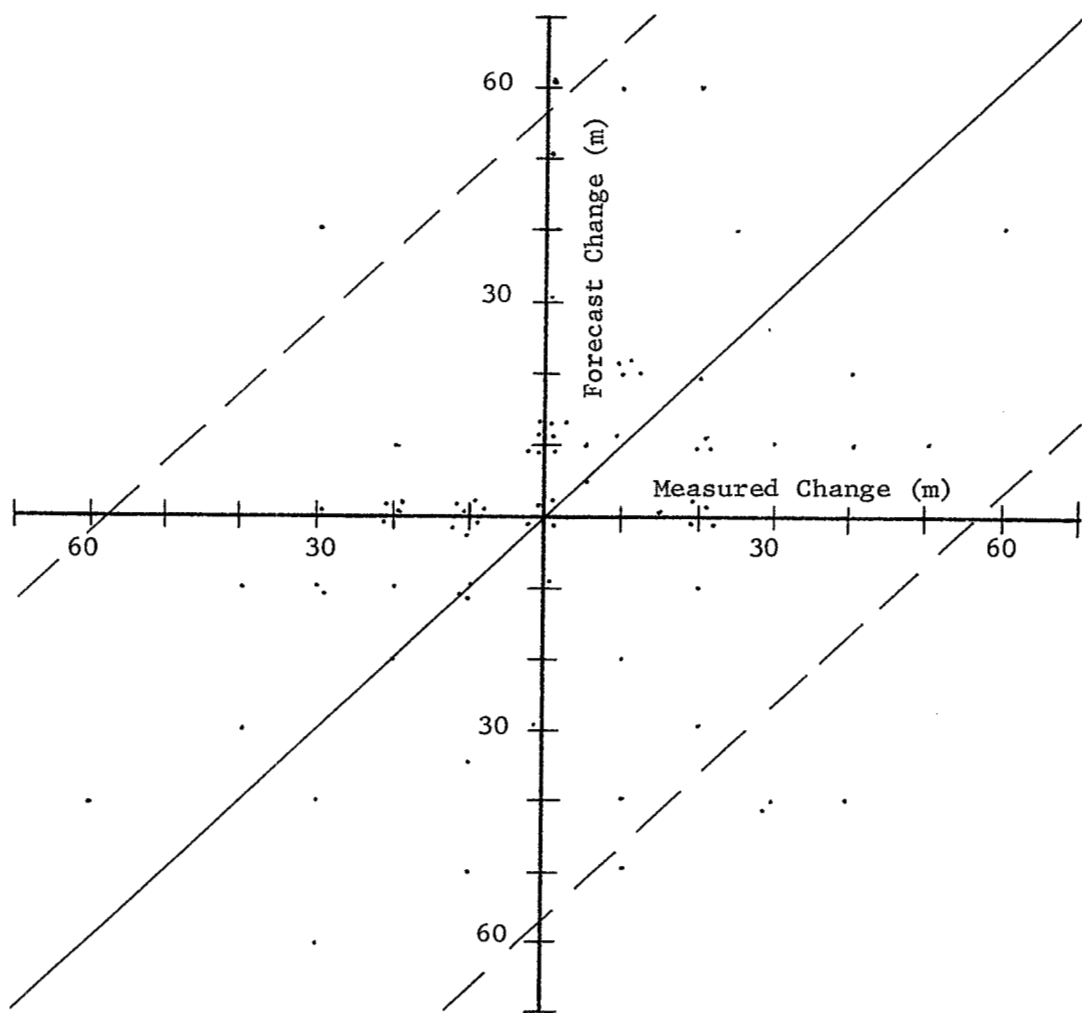
Fig. 22. A comparison of the forecast and measured change in the gradient of thickness between Jacksonville and Miami over a 12-hr period for the 700-500-mb and 500-300-mb layers. Points falling within the dashed lines represent within measurable accuracy (± 40 m) an acceptable forecast.

of the gradient a value of 40 m.

The results shown in Fig. 22 are similar to the results of the thickness forecast shown in Fig. 21. It is thus reasonable to conclude that, for forecasts of 12 hr and less, most of the local changes in thickness or gradients of thickness are smaller than the precision with which they are measured.

Another method used to forecast $\overline{T}_v$ was based upon data from a single station (Panofsky, op. cit.). The forecast equation is

$$\frac{\partial \overline{T}_v}{\partial t} = f\overline{V}^2 \frac{\partial \alpha}{\partial h} \frac{\overline{T}_v}{(980)(180)} \pi \tag{11}$$

where: $\overline{V}$ is the mean wind speed of the layer,

$\partial \alpha / \partial h$ is the rate-of-change of wind direction with height through the layer,

$\overline{T}_v$ is the mean virtual temperature of the layer, and

f is the coriolis parameter.

This equation provides a different approach to the problem of forecasting $\overline{T}_v$ of a layer using the relation between advection of temperature and changes of wind direction in the vertical. It is known that a counterclockwise change in the wind direction (backing) with altitude indicates cold advection and a clockwise change (veering) indicates warm advection. The amount of backing or veering that takes place, as well as the speed of the wind, is a measure of the strength of the advection. Certainly the magnitude of the errors in the measurement of wind direction and speed affect greatly the usefulness of such a method (results of forecasts of $\overline{T}_v$ by use of Eq. 11 are given indirectly in paragraph VIII E).

77

3. Vertical Motion. Errors in the forecast of $\bar{T}_v$ or Δh caused by vertical motion may be significant. Therefore, an attempt was made to relate the RMS error of the forecast results with an indicator of the expected error due to vertical motion.

From the "omega" equation, the sign of the vertical motion can be estimated by use of the following relationship (derived in Appendix A),

$$ w \propto -\vec{V} \cdot \vec{\nabla}_p T - \vec{V} \cdot \vec{\nabla}_p \eta \qquad (12) $$

where w is vertical motion (positive up and negative down), $-\vec{V} \cdot \vec{\nabla}_p T$ is the isobaric advection of temperature, and $-\vec{V} \cdot \vec{\nabla}_p \eta$ is the isobaric advection of vorticity. Analyses of temperature and vorticity were made for each of the 850-, 700-, 500-, 400-, 300-, and 200-mb pressure surfaces and the signs of the vorticity and temperature advection terms determined. If strong positive or negative advection occurred, a plus or minus sign was assigned to the term. If weak or no advection occurred, a zero was assigned to the term. Thus, for each surface, Eq. 12 was represented by two symbols, one for each term.

Table 6 shows all possible combinations of the symbols and breaks them into three main groups according to the relative magnitude of the vertical motion indicated, or, more exactly, according to our relative confidence that vertical motion is taking place. The notation used for the direction and magnitude of the indicated

78

vertical motion is + for upward and - for downward, N^+ for weak

upward, N^- for weak downward, and N for neutral.

Table 6. An estimate of the magnitude and direction of vertical
motion based on the sign of isobaric advection of tem-
perature and vorticity.

$-\vec{V} \cdot \vec{\nabla}_p T$	$-\vec{V} \cdot \vec{\nabla}_p \eta$	w	magnitude and direction
+	+	+	upward
-	-	-	downward
+	0	N^+	weak upward
0	+	N^+	weak upward
-	0	N^-	weak downward
0	-	N^-	weak downward
+	-	N	neutral
-	+	N	neutral
0	0	N	neutral

The effect that vertical motion has on the height of a pres-
sure surface was estimated by examining its effect on the mean
virtual temperature of the layer defined by the pressure surface
and the ground. If the surface pressure remains constant the
hypsometric equation indicates that an increase (decrease) of the
mean virtual temperature of the layer leads to an increase (de-
crease) of the height of the pressure surface. Since vertical
motions within the layer may have different magnitudes and/or di-
rections, some of the effects of the motions (warming or cooling)

may offset one another. Therefore, the height of the pressure surface will be affected by the integrated vertical motion below the pressure surface.

The integrated vertical motion was estimated using the relative magnitudes of the vertical motion indicated at each of the 850-, 700-, 500-, 400-, 300-, and 200-mb surfaces. For example, the integrated vertical motion below 850 mb was assumed to be represented by the motion indicated at the 850-mb surface; the integrated motion at 500 mb was assumed to be a combination of the motions indicated at the 500-, 700-, and 850-mb surfaces. Further, if the indicated motions at 850 and 700 mb are + and -, respectively, the integrated motion below 700 mb was assumed to be represented by N. Similarly, if the indicated vertical motions at 500, 700, and 850 mb are +, N^+, and N, respectively, the integrated vertical motion below 500 mb was assumed to be represented by N^+. In this manner, an indicator of the integrated vertical motion, hereafter referred to as vertical motion, below each surface for each case was obtained using the same notation as described in Table 6.

In order to determine the effect of vertical motion on the zonal wind speed at Cape Kennedy, the effects of vertical motion on the heights of the pressure surfaces at Jacksonville and Miami were examined. If the direction and magnitude of the vertical motion are identical at Jacksonville and Miami, then the slope of

the pressure surface in the N-S direction would not change as a result of vertical motion. On the other hand, if the directions and/or magnitudes of the vertical motions are different, the slope of the pressure surface and hence, the zonal wind speed, will be changed. The magnitude of the change, of course, depends upon this difference in the magnitude of the vertical motion.

Consider a normal situation in which the height of the pressure surface at Miami is higher than that at Jacksonville. An indication of how the different magnitudes and directions of the indicated vertical motion at Jacksonville and Miami affect the zonal wind speed at Cape Kennedy is given in Table 7 in the absence of condensation.

The forecasts were grouped according to the magnitude of the change expected in wind speed as a result of vertical motion as indicated in Table 7. Table 8 shows the RMS errors of forecasts made for surfaces that had similar magnitudes and distributions of indicated vertical motions. If the indications of vertical motion are correct, it would be expected that the RMS error of Group III would be smallest, Group II next largest, and Group I, largest. (The reasoning, of course, is that with increasing magnitudes of differential vertical motions, the effects on the zonal wind speed would be greatest.) This distribution of the RMS error was not observed in Group I but the error may be due to the fact that the sample for this group consisted of only 18 points. Group I and

81

Table 7. Relative magnitude of the effect of vertical motion at Miami and Jacksonville on the zonal wind speed at Cape Kennedy.

Indicated Vertical Motion		Effects on zonal wind speed at Cape Kennedy	Relative magnitude of effects on zonal-wind speed
Jacksonville	Miami		
+	-		
+	N^-		
N^+	N^-		
-	+	large change	I
-	N^+		
N^-	N^+		
N	-		
+	N		
N^+	N		
N	N^-	small change	II
-	N		
N	+		
N	N^+		
N^-	N		
+	+		
-	-		
N^+	N^+	no appreciable change	III
N^-	N^-		
N	N		

Group II were combined and the RMS error was found to be 6.90 m/sec which quite interestingly differs little from the RMS error of Group III. These results, if accurate, indicate that the errors in making the forecasts are approximately the same for all cases, irrespective of the magnitudes of the vertical motion as indicated

by the advection of temperature and vorticity. Thus, an indication of the magnitude and sign of vertical motions does not seem to explain the short-period changes in wind speed. Errors due to measurement far exceed those due to vertical motions.

Table 8. The RMS errors of forecasts of zonal wind speed at Cape Kennedy categorized according to the indicators of vertical motion.

Group	I	II	III	I&II
rms error	2.91	7.49	6.70	6.90
no. fcsts.	18	87	44	62

4. <u>Ageostrophic Motion</u>. The RMS error in the calculation of the zonal component of the geostrophic wind at Cape Kennedy was estimated on the assumption that the smoothed RJ profiles represent the geostrophic wind. The zonal wind was computed using Eq. 2, and the heights of the 850-, 700-, 500-, 400-, 300-, and 200-mb surfaces obtained from RW data (checked for validity using analyzed maps) at Jacksonville and Miami. The wind speed thus computed was compared with that obtained from smoothed RJ data and the RMS of the difference calculated. Table 9 shows that the RMS error in the computation, although representing quite small samples, becomes larger as the wind speed increases.

The RMS of the difference between the measured wind and the computed geostrophic wind, as shown in Table 9, easily could be caused by errors in measurement of the heights of constant-pressure

83

Table 9. The RMS of the difference between the zonal wind computed from the geostrophic wind equation, and that obtained from RJ data at Cape Kennedy, Florida.

	Zonal Wind Speed (m/sec)			
	0-14	15-30	> 30	all speeds
RMS of difference	5.85	6.24	7.92	7.19
no. of samples	13	14	13	40

surfaces used in the calculations of the geostrophic winds. For example an RMS error of 20 m in the reported height at Jacksonville and Miami corresponds to about a 28-m RMS error in the height gradient as given by Eq. 10. This RMS error corresponds to an RMS error of 7 m/sec in the zonal wind speed calculated at Cape Kennedy.

A similar comparison between the computed and measured winds was made for Oklahoma City. In this case the computed winds were compared with winds measured with the RW system. The RMS of the difference for the u-component and the v-component was 6.07 and 4.62 m/sec, respectively. The average magnitude of the u-component was 18.1 m/sec and that of the v-component was 9.0 m/sec. The larger RMS value for the u-component is associated with the higher wind speeds. Notice that the RMS error of the u-component for all speeds at Cape Kennedy (7.19 m/sec) is slightly larger than that at Oklahoma City (6.07 m/sec).

The approximate magnitude of ageostrophic motions has been shown to be a function of changes occurring in the geostrophic wind (Haltiner and Martin, 1957), and is given by

$$\vec{V} - \vec{V}_g \doteq \frac{1}{f} \left[\vec{k} \times \frac{\partial \vec{V}_g}{\partial t} + |\vec{V}_g| \, \vec{k} \times \frac{\partial \vec{V}_g}{\partial s} + w\vec{k} \times \frac{\partial \vec{V}_g}{\partial z} \right]. \qquad (13)$$

The use of $\vec{V}_g$ in the terms on the right-hand side "filters out" small-scale motions caused by sound, gravity, and inertial waves, but not any of the large-scale features of the wind field.

With the use of normal mid-tropospheric values measured at Cape Kennedy for the terms in Eq. 13, an order of magnitude of the ageostrophic motions can be computed. For this sample computation, a situation was chosen in which the jet-stream was located far to the north. The values and explanation of the terms are:

$\partial \vec{V}_g / \partial t$ – the local change of geostrophic wind with time (5 m/sec/6 hr),

$\partial \vec{V}_g / \partial s$ – down-stream change of geostrophic wind (2 m/sec/200 km),

$|\vec{V}_g|$ – absolute value of vector wind speed (15 m/sec),

w   – vertical motion (2 cm/sec),

$\partial \vec{V}_g / \partial z$ – vertical shear of geostrophic wind (6 m/sec/km), and

f   – Coriolis parameter at Cape Kennedy (0.6957×10^{-4} sec^{-1}).

These values would lead to a magnitude of the ageostrophic wind of about 7 m/sec, if the signs of all three terms were positive.

DeMandel and Scoggins (op. cit.) examined the small-scale
fluctuations below 16 km as measured by the RJ system. They ob-
served fluctuations in wind speeds, at times, in excess of 5 m/sec,
some of which persisted for several hours. Quite probably, many
of these fluctuations consisted of noise and turbulence caused by
random oscillations which were of the type filtered out because
of the assumption that the real wind can be replaced by the geo-
strophic wind. Thus, the RMS error in computing the geostrophic
wind is equal to or greater than the expected magnitude of the
ageostrophic motions. For this reason, these motions cannot be
forecast by the model.

E. Use of the Model

Forecasts of the zonal wind were made for several cases in which the initial RJ profile of a series coincided with the time of the RW data, 00 or 12 GMT. From this initial time, several short-range forecasts were made for times that coincided with measured RJ profiles. The forecasts provided by the model were compared with persistence.* Forecasts for the zonal wind speed were made by use of the forecast model presented in paragraph VIII C with 850 mb as the base surface. Heights of this surface for the forecast times were interpolated between the 00 and 12 GMT data. For example, if RJ profiles were measured at 0010, 0215, 0345, and 0800 GMT, the initial time would be assumed to be 00 GMT and the maps analyzed for this time used to make the forecasts. The 850-mb heights at Jacksonville at 00 and 12 GMT might be 1480 m and 1492 m, respectively. The height was assumed to increase linearly during this period. The corresponding heights at the three forecast times would be 1482, 1484, and 1488 m, respectively. This interpolation is not exact, but is believed to be better than a forecast based on information obtained at and prior to 00 GMT.

With the graphical technique for advecting the thickness patterns, a forecast was made for each of the 700-, 500-, 400-, 300-, and 200-mb pressure surfaces. These forecasts of the zonal wind were separated into three groups according to the length of their forecast period, P. The groups are $P \leq 3$ hr, $3 < P \leq 6$ hr, and

---

*A forecast of no change.

87

$6 < P \leq 9$ hr. Forecasts of all five surfaces within each group were combined to form a sample for each time period, and the rms errors of the forecasts provided by the model were computed.

Forecasts also were made using Eq. 11 to advect the thickness patterns. This is called the single-station method, since the local rate-of-change of thickness (or $\overline{T}_v$) was evaluated with data obtained from a single station. The forecasts were separated into groups in the same manner as the forecasts made using the graphical method, and the RMS errors were computed.

Figure 23 represents a comparison of the RMS errors of persistence (solid line), the graphical method (broken line), and the single-station method (dashed line). The horizontal line at 13.2 m/sec represents the annual RMS of the zonal wind speed (Vaughan, 1960). This value is for the 7-km height which is approximately in the middle of the region for which the model was tested.

Thompson (1961) presented some interesting results concerning the relative accuracy of numerical wind forecasts. He found that, in general, numerical techniques provide 24-hr forecasts with an rms error 1/4 that of climatology and 1/2 that of persistence. The points plotted to the right in Fig. 23 were calculated from this relationship and represent the RMS error of numerical forecasts (N) and persistence (P) based on the annual RMS error of the zonal wind at Cape Kennedy (13.2 m/sec). The points plotted at 3, 6, and 9 hr were computed from forecasts made with the model.
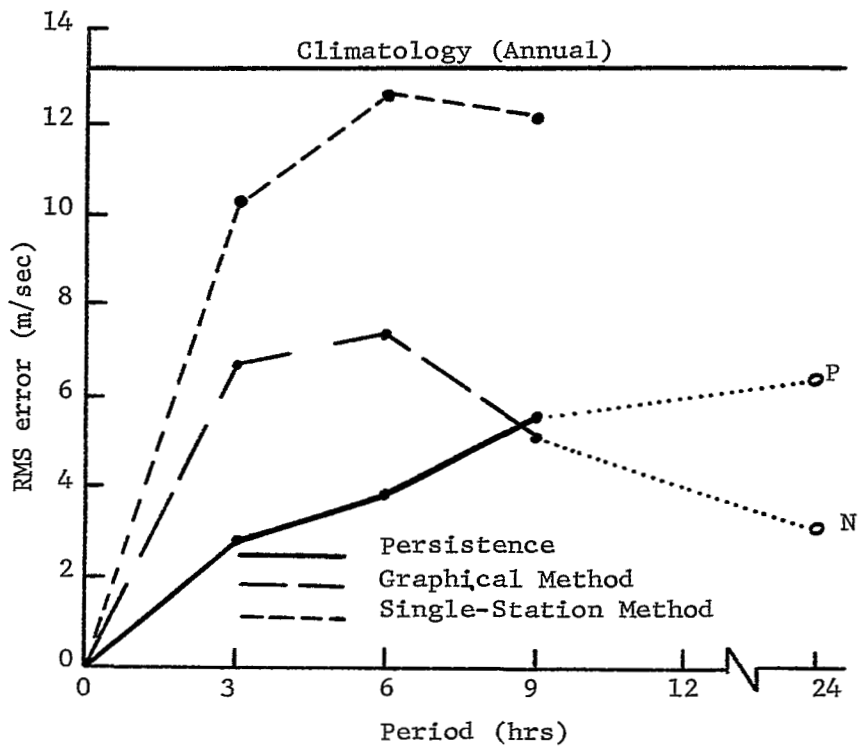
88

Fig. 23. Comparison of the RMS error in wind forecasts by the advection of mean virtual temperature or thickness with persistence and climatology at Cape Kennedy.

The RMS error of persistence increases throughout the 9-hr period. The RMS error of the forecast using the graphical method increases quite rapidly for short periods and then decreases, becoming smaller that the RMS error of persistence at a point corresponding to a period of 9 hr. The dotted lines connecting points P and N with the solid and broken lines, respectively, represent a logical continuation of the trend of the changes of the RMS errors out to a period of 24 hr. In other words, the values of the RMS errors for a 24-hr period are assumed to be approximately equal to the values obtained by use of Thompson's relationship. The RMS error of the forecast using the single-station method increases very rapidly becoming almost as large as the RMS of climatology at 6 hr.

The annual RMS error of climatology (13.2 m/sec) is much greater than the RMS errors of persistence and forecasts using the graphical method provided by the model. Although some months have an RMS error of climatology much smaller (4.9 m/sec for July), climatology is of little use as a forecast method.

Therefore, it would appear logical to assume from the information presented in Fig. 23 that short-period forecasts provided by the model are less accurate than persistence. For the cases examined, results indicate that for a period longer than 6-9 hr, the model using the graphical method for advection would provide forecasts with an RMS error less than that of persistence. Furthermore, the large RMS errors in the forecasts using the single-

station method indicate that this method is not practical at least when RW data are used as input.

The model was tested at Oklahoma City, Oklahoma for a forecast period of 6 hr. This was possible because RW measurements are made every 6 hr instead of the regular 12-hr interval. The forecasts were verified by use of RW data.

Forecasts were made in the same manner as those made for Cape Kennedy by use of the single-station method to forecast the rates-of-change of $\overline{T}_v$ at the surrounding stations. Figure 24 shows the location of the RW stations used to compute the wind from the forecast gradients of the rate-of-change of $\overline{T}_v$. Notice that since RW data are available to the east and west it also is possible to forecast the v-component as well as the u-component of the wind.

The RMS errors of the forecasts and of persistence were computed and are presented in Table 10.

Table 10. Comparison of the RMS error of forecasts using the single-station method and the RMS error of persistence for a period of 6 hr at Oklahoma City. The number of cases is 65.

	u-component (m/sec)	v-component (m/sec)
Persistence	5.7	7.1
Forecast	12.5	9.2

Notice that for the u-component, the RMS error of the forecasts (12.5 m/sec) is about twice the RMS error of persistence (5.7 m/sec). This result is similar to the comparison of the RMS errors obtained for the 6-hr forecasts of the u-component at Cape Kennedy using the graphical method. Figure 23 shows that the RMS error of the
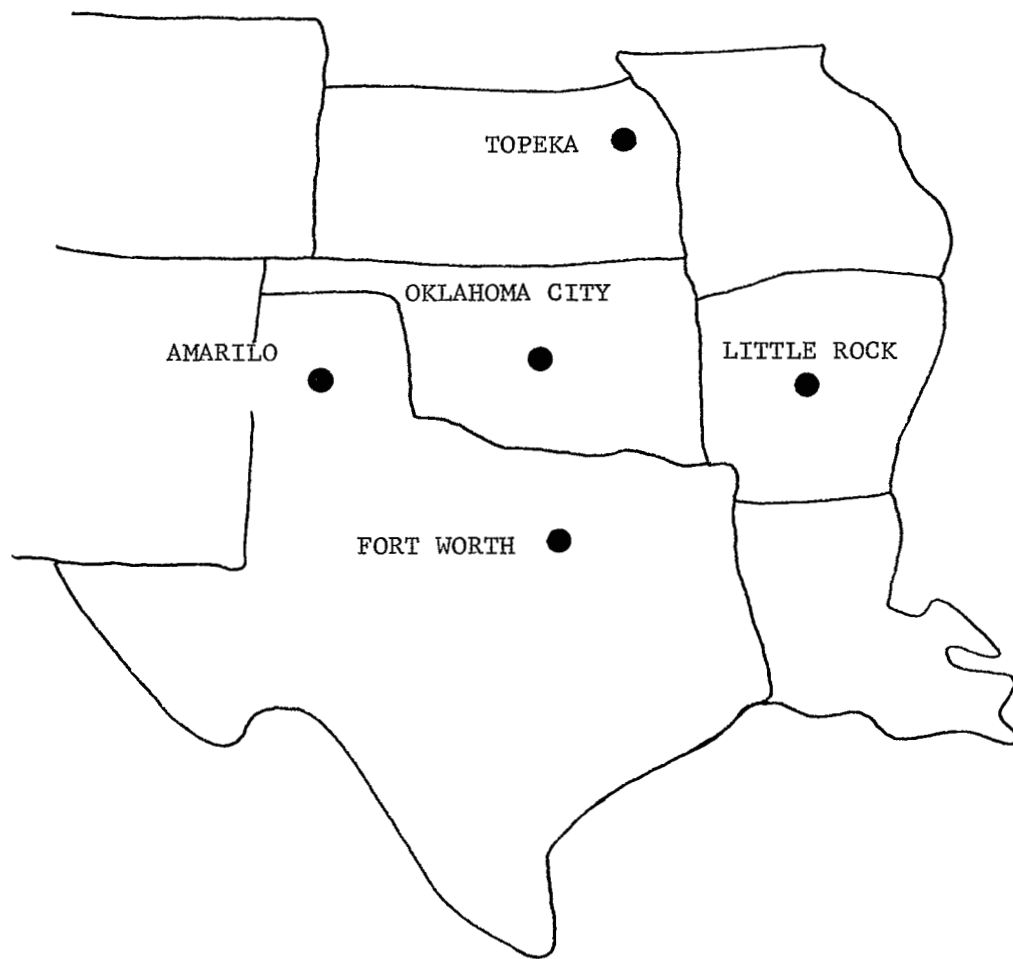
Fig.24. Relative location of rawinsonde stations used to compute wind forecasts for Oklahoma City.

92

forecast for Cape Kennedy (7.5) m/sec) also is about twice the RMS error due to persistence (3.9 m/sec). Therefore, the relative comparisons between the two sets of data are similar but the magnitudes of the RMS errors are not the same.

The increased magnitude of the RMS error for the forecast at Oklahoma City may be attributed to the fact that the single-station method is much more dependent upon input data, especially the error in wind-direction measurements. Quite probably, the analyzed maps used in the other method did eliminate some of the errors because of smoothing, hence the RMS error of the forecasts using the graphical method is much smaller than those using the single-station method.

IX. SUMMARY

Wind data provided by the RJ system and thermodynamic data provided by the RW system were used to investigate relationships between motions of different scale, and to test a simple model for forecasting the wind profile at Cape Kennedy.

Small-scale or turbulent motions were defined as the difference between a smoothed profile and the original profile measured by the RJ system, and also as the difference between the smoothed slant range and the original slant range. Linear correlation coefficients between the small-scale motions defined by the different methods were large in magnitude and statistically significant at the 1% level. This was interpreted to mean that there was no significant difference between the small-scale motions defined by the different methods. For convenience, small-scale motions were defined as the difference between a smooth profile which approximates the RW sounding and the original profile measured by the RJ system.

The RJ data were used to compute three of the terms representing the rate of mechanical production of turbulent kinetic energy. Only the terms involving the vertical wind shear could be computed since horizontal wind shears were not available. Of the three computed, which involved the covariance between u, v, and w, multiplied by the vertical wind shear, there did not appear to be any significant differences. The magnitude of the terms were approximately the same with some being negative and some positive.

Scatter diagrams were prepared with the RMS of the turbulent motions plotted against vertical wind shear, the lapse rate of temperature, and the Richardson number. A satisfactory relationship was not found between turbulence and any of the parameters investigated. In addition, scatter diagrams were prepared showing relationships between the Richardson number computed over different altitude intervals within the same profile. It was shown that wind shears over smaller intervals in particular influence the value of the Richardson number greatly, and that there was scarcely any relationship between Richardson numbers computed over thin layers and those over thick layers.

From the statistics of the small-scale motions, and considering only those motions whose RMS value exceeds that due to error, the frequency of measured turbulence agreed closely with the frequencies given by Colson and Panofsky (1965) which were computed from aircraft data. Thus it appears likely that the Jimsphere is a good turbulence sensor although this remains to be proven by independent measurements.

An attempt was made to establish relationships between parameters determined from large-scale flow and thermodynamic data taken from constant pressure maps, and the measured small-scale motions at Cape Kennedy, Florida. Parameters taken from the maps included vorticity, divergence, curvature, the advection of temperature and vorticity, and others. No significant relationships could be found. In addition to data taken from maps, temporal cross-sections of changes in

mean wind speed and small-scale motions taken from serial ascents were analyzed. An attempt was made to explain the observed changes from synoptic-scale data. Again there were no clear-cut relationships found except that, generally, when cold-air advection was taking place, the winds backed with height and when warm-air advection was taking place, the winds veered with height. Changes in wind speed, as well as the RMS of the turbulent motions, did not appear to be related to the differential advection of temperature or to the mean vertical wind shear.

In summary, this investigation has shown that there are no simple relationships between a number of synoptic-scale parameters and small-scale or turbulent motions. The processes involved are so complicated that a more sophisticated approach is required.

A model used to forecast the vertical wind profile was developed and tested. It was found that the accuracy of the forecast model was dependent upon how well the gradient of $\overline{T}_v$ was forecast. Two methods were tried to forecast $\overline{T}_v$, one using methods of single-station analysis, and the other a graphical technique that, if applied to a numerical scheme, would require a large grid network. Both methods assumed changes in $\overline{T}_v$ to take place through horizontal advection alone. The graphical method proved to be superior, although neither provided short-period forecasts more accurate than persistence for periods less than 9 hr.

It was found that the error in measurement was, in most cases, larger than the changes that took place. Also, the magnitude of the errors precluded the use of vertical motion in the model, since the effects of the errors were larger than the effects of vertical motion itself. It also was concluded that the magnitude of ageostrophic motions for the zonal wind speed is of the same magnitude as the errors in computing the wind speed. Therefore, even if optimum height data could be obtained, similar errors in the forecast would occur as a result of these random motions.

Although no attempt was made to estimate the error due to the finite-difference approximation used, it is assumed to be small in comparison to the other errors. This is substantiated partially by the fact that the rms error of the difference between the computed (using finite-difference approximation for slope of pressure surface) and measured wind speeds is similar to the values given for the magnitude of ageostrophic motion and the magnitude due to errors in height measurement.

It seems that forecasts for periods less than 9 hr cannot be made by the model with an accuracy better than persistence. However, it does seem that for periods greater than 9 hr, the forecast model could prove to be useful.

REFERENCES

Blackburn, James H., Jr., 1969: "A Study of Clear-Air Turbulence From Detailed Wind Profiles Over Cape Kennedy, Florida", M.S. Thesis, Department of Meteorology, Texas A&M University, 42 pp.

Blackburn, Robert R., 1968: "Responses of the Saturn V Space Vehicle to Inflight Wind Profiles", Proceedings of the Third National Conference on Aerospace Meteorology, American Meteorological Society, 327-336.

Colson, D., and H. A. Panofsky, 1965: "An Index of Clear Air Turbulence", Quart. Jour. Roy. Met. Soc., 91, 507-513.

Daniels, Glenn E., James R. Scoggins, and Orvel E. Smith, 1966: "Terrestrial Environment (Climatic) Criteria Guidelines for Use in Space Vehicle Development, 1966 Revision", NASA Technical Memorandum, TM X-53328.

DeMandel, R. E., and James R. Scoggins, 1967: "Mesoscale Wave Motions as Revealed by Improved Wind Profile Measurements", Jour. Appl. Met., 6(4), 617-620.

Deming, Edward W., 1943: Statistical Adjustment of Data, John Wiley and Sons, Inc., New York.

Eckstrom, Clinton V., 1965: "Theoretical Study and Engineering Development of Jimsphere Wind Sensor", Final Report, NASA Contract No. NAS8-11158, 78 pp.

Endlich, R. M., and J. W. Davies, 1967: "The Feasibility of Measuring Turbulence in the Free Atmosphere from Rising Balloons Tracked by FPS-16 Radar", Jour. Appl. Met., 6(1), 43-47.

Endlich, R. M., R. C. Singleton, K. A. Drexhage, and R. L. Mancuso, 1969: "Studies of Vertical Wind Profiles at Cape Kennedy, Florida", NASA CR-61263, Contract NAS8-21148, Stanford Research Institute, Menlo Park, California, 88 pp.

Hadeen, K. D., 1966: "A Meteorological Model for Forecasting the Wind-Profile Between 1.0 and 18.0 Kilometers". Ph.D. Dissertation, Texas A&M University, 85 pp.

Haltiner, G. J. and F. L. Martin, 1957: Dynamical and Physical Meteorology, McGraw-Hill Book Company, Inc., New York, 470 pp.

Hess, S. L. 1959: <u>Introduction to Theoretical Meteorology</u>, Henry Holt and Company, New York, 362 pp.

Leviton, Robert, 1962: "A Detailed Wind Profile Sounding Technique", <u>Air Force Surveys in Geophysics</u>, (140), AFCRL, Bedford, Mass., 187-195.

Lumley, J. L., and H. A. Panofsky, 1964: <u>Structure of Atmospheric Turbulence</u>, John Wiley and Sons, New York.

Panofsky, H. A., 1965: <u>Introduction to Dynamic Meteorology</u>, The Pennsylvania State University, University Park, Pennsylvania, 243 pp.

Petterssen, S., 1956: <u>Weather Analysis and Forecasting</u>, McGraw-Hill Book Company, Inc., New York, 428 pp.

Reiter, E. R., 1963: "Nature and Observation of High Level Turbulence Especially in Clear Air", Technical Paper No. 41, Department of Atmospheric Science, Colorado State University, Fort Collins, 39 pp.

Reiter, E. R., and P. F. Lester, 1967: "The Dependence of the Richardson Number on Scale Length", Atmospheric Sciences Paper No. 111, Colorado State University, Fort Collins, Colorado, 39 pp.

Rogers, R. R., and H. G. Camnitz, 1965: "Project Baldy -- An Investigation of Aerodynamically-Induced Balloon Motions", Final Report, NASA Contract No. NAS8-11140, 80 pp.

Ryan, R. S., J. R. Scoggins, and A. King, 1967: "Use of Wind Shears in the Design of Aerospace Vehicles", <u>Jour. Spacecraft and Rockets</u>, 4(11), 1526-1532.

Sawyer, J. S., 1961: "Quasi-Periodic Wind Variations with Height in the Lower Stratosphere", <u>Quar. Jour. Roy. Met. Soc.</u>, 87(371), 24 pp.

Scoggins, James R., and William W. Vaughan, 1964: "Problems of Atmospheric Wind Inputs for Missile and Space Vehicle Design", <u>J. Spacecraft</u>, 1(2), 181-184.

Scoggins, James R. 1964: "Aerodynamics of Spherical Balloon Wind Sensors", <u>Journal of Geop. Res.</u>, 69(4), 591-598.

Scoggins, James R., 1965: "Spherical Balloon Wind Sensor Behavior", Jour. of Appl. Met., 4(1), 139-145.

_____, 1967: "Sphere Behavior and the Measurement of Wind Profiles", NASA Technical Note TN D-3994, 53 pp.

Scoggins, James R. and Manuel Armendariz, 1969: "On the Measurement of Winds by the AN/FPS-16 Radar/Spherical Balloon Method", Jour. Appl. Met., 8(3), 449-452.

Susko, Michael and William W. Vaughan, 1968: "Accuracy of Wind Data Obtained by Tracking a Jimsphere Wind Sensor Simultaneously With Two FPS-16 Radars", NASA Technical Memorandum, TM X-53752, 43 pp.

Sutton, O. G., 1953: Micrometeorology, McGraw-Hill Book Company, 152-153.

Thompson, P. D., 1961: Numerical Weather Analysis and Prediction. MacMillan Company, New York, 170 pp.

Vaughan, W. W., 1960: "Interlevel and Intralevel Correlations of Wind Components for Six Geographical Locations", NASA TN D-561, 92 pp.

_____, 1968: "New Wind-Monitoring System Protects R&D Launches", Astronautics and Aeronautics, 6(12), 49-57.

Weinstein, A. I., E. R. Reiter and J. R. Scoggins: "Meso-scale Structure of 11-20 km Winds", Jour. Appl. Met., 5(1), 49-57.

Zartarian, Garabed and John H. Thompson, 1968: "Validity of Detailed Balloon Soundings in Booster Vehicle Design", Scientific Report No. 1, Contract No. F19-628-C-0205, AFCRL-68-0606.

APPENDIX A

DERIVATION OF A METHOD FOR FORECASTING THE SIGN OF VERTICAL MOTION

Djuric* has derived a method used to estimate the direction of large-scale vertical motion from constant-pressure maps. Explanations of the terms used are as follows:

θ - potential temperature,

ρ - density,

g - acceleration due to gravity,

f - Coriolis parameter,

T - temperature,

p - pressure,

R - gas constant,

C_p - specific heat at constant pressure,

ξ - relative vorticity,

η - absolute vorticity ($\xi + f$),

ω - omega (dp/dt), and

w - vertical motion (dz/dt).

The adiabatic equation,

$$\frac{d\theta}{dt} = \frac{\partial \theta}{\partial t} + \vec{V} \cdot \vec{\nabla}\theta + \omega \frac{\partial \theta}{\partial p} = 0, \qquad \text{(A-1)}$$

would be suitable for evaluation of vertical motion if it did not contain the term $\partial\theta/\partial t$ which is difficult to evaluate from constant-pressure maps with sufficient accuracy. This term can be rewritten

---

*Personal correspondence

and eliminated by use of the vorticity equation.

From the definition of θ,

$$\theta = T \left[\frac{1000}{p} \right]^K, \quad \text{where } K = \frac{R}{C_p},$$

and the equation of state,

$$p = R \rho T,$$

we can write

$$\theta = \frac{p}{R \rho} \left[\frac{1000}{p} \right]^K. \tag{A-2}$$

Using the hydrostatic equation,

$$- \frac{1}{\rho g} = \frac{\partial z}{\partial p},$$

and Eq. A-2, we can write

$$\theta = - \frac{1}{c} \frac{\partial z}{\partial p}, \tag{A-3}$$

where

$$c = \frac{R}{pg} \left[\frac{1000}{p} \right]^K.$$

Differentiating Eq. A-3 with respect to time gives

$$\frac{\partial \theta}{\partial t} = - \frac{1}{c} \frac{\partial}{\partial t} \left[\frac{\partial z}{\partial p} \right],$$

which, when substituted into Eq. A-1, gives

$$\frac{\partial}{\partial t} \left[\frac{\partial z}{\partial p} \right] - c \vec{V} \cdot \vec{\nabla} \theta + \sigma \omega = 0, \tag{A-4}$$

A-3

where

$$\sigma = -c\,\frac{\partial\theta}{\partial p}$$

is a measure of the stability, positive in a stable atmosphere.

An approximate form of the vorticity equation may be written (Thompson, 1961)

$$\vec{\nabla}^2\frac{\partial z}{\partial t} + \frac{f}{g}\,\vec{V}\cdot\vec{\nabla}\eta - \frac{f^2}{g}\,\frac{\partial\omega}{\partial p} = 0\,, \tag{A-5}$$

which neglects small-magnitude terms such as vertical advection of vorticity.

Taking the partial derivative of Eq. A-5 with respect to p and the Laplacian of Eq. A-4, we can eliminate the time derivative term ($\vec{\nabla}^2\partial^2 z/\partial t\partial p$) by subtracting one equation from the other. Rearranging terms gives the omega equation,

$$-\left[\vec{\nabla}^2\sigma\omega + \frac{f^2}{g}\,\frac{\partial^2\omega}{\partial p^2}\right] = \frac{f}{g}\,\frac{\partial}{\partial p}\left[-\vec{V}\cdot\vec{\nabla}\eta\right] + c\,\vec{\nabla}^2\left[-\vec{V}\cdot\vec{\nabla}\theta\right]. \tag{A-6}$$

Under ordinary conditions σ and f^2/g are positive. Then Eq. A-6 is an elliptical equation and has solutions if boundary conditions are provided on all boundaries of the region considered. The simplest condition, $\omega = 0$, on the boundaries is satisfactory if the boundaries are far from the area of interest.

The left side of Eq. A-6 behaves like a three-dimensional Laplacian of omega (ω). Also, the constants on the right-hand side are irrelevant in the process of a qualitative estimation of omega.

Therefore, the proportionality may be written

$$- \vec{\nabla}_3^2 \omega \; \propto \; \frac{\partial}{\partial p} \left[- \vec{V} \cdot \vec{\nabla} \eta \right] \; + \; \vec{\nabla}^2 \left[- \vec{V} \cdot \vec{\nabla} \theta \right]. \qquad \text{(A-7)}$$

For many meteorological functions which vary around zero, the proportionality holds that the sign of the two- or three-dimensional Laplacian of a quantity evaluated at a point is opposite that of the quantity at that point; thus,

$$- \vec{\nabla}_3^2 \omega \; \propto \; \omega \quad \text{and} \quad \vec{\nabla}^2 \left[- \vec{V} \cdot \vec{\nabla} \theta \right] \; \propto \; \vec{V} \cdot \vec{\nabla} \theta.$$

Since vorticity advection usually increases with height, we can write

$$\frac{\partial}{\partial p} \left[- \vec{V} \cdot \vec{\nabla} \eta \right] \; \propto \; \vec{V} \cdot \vec{\nabla} \eta .$$

Thus, Eq. A-7 can be rewritten

$$\omega \; \propto \; \vec{V} \cdot \vec{\nabla} \eta \; + \; \vec{V} \cdot \vec{\nabla} \theta ,$$

or, since $\omega \propto -w$,

$$w \; \propto \; - \vec{V} \cdot \vec{\nabla} \eta \; - \vec{V} \cdot \vec{\nabla} \theta .$$

Thus upward (downward) motion is followed by two main circumstances: (1) positive (negative) vorticity advection and (2) warm (cold) air advection. In most cases, if both terms are positive, upward motion would result. Conversely, if both terms are negative, downward motion would usually take place. When the terms

are of opposite sign, this method does not give the direction of motion but does indicate that the probability of vertical motion is lessened.

REFERENCE FOR APPENDIX A

Thompson, P. D., 1961: Numerical Weather Analysis and Prediction, MacMillan Company, New York, 170 pp.

APPENDIX B

A STUDY OF CLEAR-AIR-TURBULENCE
FROM DETAILED WIND PROFILES
OVER CAPE KENNEDY, FLORIDA

A Thesis

by

James Harvey Blackburn, Jr.

Captain

United States Air Force

Submitted to the Graduate College of the

Texas A&M University in
partial fulfillment of the requirements for the degree of

MASTER OF SCIENCE

May 1969

Major Subject: Meteorology

ABSTRACT

A Study of Clear-Air Turbulence from Detailed Wind Profiles Over

Cape Kennedy, Florida.

James H. Blackburn, Jr., B.S., Texas A&M University

Directed by: Dr. James R. Scoggins

Clear-air turbulence (CAT) is investigated by the analysis of detailed wind profiles from FPS-16 radar/Jimsphere balloons and of measurements of temperature from rawinsondes. Relationships were established between CAT, defined from the detailed wind profiles, and mean meteorological parameters. The results of this investigation show that large vertical wind shear is necessary, but not sufficient, for the occurrence of CAT. CAT occurred in relatively stable and shallow ($\leq$ 1000 m) vertical layers of the atmosphere from 5 to 14 km in the presence of large wind shear. These conditions are favorable for the existence of unstable shear-gravity waves. To predict CAT, these stable layers with large wind shear must be forecast.

The statistics relative to the frequency of occurrence of CAT agree well with previous data obtained by other methods. CAT was observed approximately 2 to 5% of the total number of observations, depending on thickness of the layer. The FPS-16 radar/Jimsphere balloon system, because of its over-all cost advantage, accuracy, and flexibility, provides what appears to be the best system available for the collection of CAT data.

ACKNOWLEDGMENTS

TABLE OF CONTENTS

LIST OF FIGURES

LIST OF TABLES

1. INTRODUCTION

a. <u>Background</u>. Clear-air turbulence (CAT) is defined as any turbulence above 6 km MSL not associated with clouds (Clem, 1957). CAT usually is associated with strong horizontal and vertical wind shears and/or temperature gradients. The intensity and probability of occurrence of CAT are higher over land than over water, and much higher over mountains than over plains (Reiter, 1963). Winter is the most favorable season for the occurrence of CAT. In winter, moderate and stronger CAT occurs less than 5% of flight-time (Endlich and Mancuso, 1965).

CAT is of considerable importance to the entire aviation establishment. Aircraft manufacturers must design airframes strong enough to withstand near extreme conditions of atmospheric turbulence. The airlines and the military agencies are interested in CAT because it affects the safety and comfort of passengers and crews. The government agencies responsible for the direction, control, and safety of aircraft must consider CAT. Scientists supporting the aviation establishment have an interest in CAT for all the previously mentioned reasons, and also because CAT is a phenomenon of our environment that is not clearly understood. Because of the increased range and speed of newer aircraft, CAT has become a problem of pronounced significance in relation to aircraft operations on a

---

The citations on the following pages follow the style of the <u>Journal</u> of <u>Applied</u> <u>Meteorology</u>.

world-wide basis.

CAT is found to be less intense than turbulence encountered in thunderstorms (Foltz, 1967), but CAT has been known to cause passenger injuries and loss of aircraft control. In rare instances, CAT has been found to be the prime cause of airframe damage (Reiter, op.cit.). CAT must be considered as dangerous as turbulence encountered in a thunderstorm because, in most cases, it occurs with no visible warning.

The present techniques of forecasting CAT for aircraft operations are based on the use of synoptic-scale data (> 500 km horizontal distance). This scale is inadequate because CAT is observed to occur more on a mesoscale (2- to 100 km horizontal distance). It is important to gain knowledge of the synoptic microscale (< 2 km horizontal distance) details of flow patterns in the free atmosphere in an attempt to identify the causes of CAT (Reiter, op.cit.). In this respect, Reiter suggests three possible causes of turbulence experiences by aircraft: (1) convective currents, (2) gravity waves, and (3) temperature discontinuities. Moore and Krishnamurti (1966) suggest that CAT is formed in regions of the atmosphere where wind shear is generated rapidly and reaches a critical value. The turbulence which results is advected away from the source region by the mean wind and gradually decays.

Composite results of recent studies indicate that CAT is generated in stable regions in the stratosphere above the jet stream,

as well as in the troposphere, by an excess of shearing stress over thermal stability (Reiter, op.cit.; Foltz, op.cit.; and others). The local imbalance between shear and stability may be controlled by mesoscale eddies, which may or may not be correlated strongly with the roughness of terrain. The existence of CAT in a stable layer of the atmosphere indicates that the shearing stresses have over-compensated for the buoyant effects of thermal stability.

The principal regions which must be considered in the analysis of CAT include: (1) atmospheric layers where wind speed and temperature change abruptly (such as upper fronts and gravity waves), (2) the immediate vicinity of a migratory jet stream maximum (particularly the cyclonic side), (3) below and south of the jet stream core, and (4) where wind shears appear to be strong horizontally or vertically or both (Foltz, op.cit.; Hardy and Ottersten, 1968; and others).

Wave perturbations in the atmosphere can be studied using detailed wind profiles (DeMandel and Scoggins, 1967). The wind measurements must be an order of magnitude more accurate than the measurements currently provided by the synoptic rawinsonde network. Data provided by the FPS-16 radar/Jimsphere balloon system are at least an order of magnitude more accurate than measurements provided by the rawinsonde system (Scoggins, 1967). The analyses of detailed wind profiles measured by the FPS-16 radar/Jimsphere system have revealed mesoscale motions at levels of the atmosphere below 20 km. These motions have periods of one-half pendulum day and

shorter, and vertical dimensions of approximately 2 km or less. These mesoscale motions have a considerable effect on vector wind shears over small intervals of altitude.

A balloon rising through an atmospheric layer containing eddies will follow an erratic path through this layer (Endlich and Davies, 1967). Endlich and Davies used data from ten FPS-16 radar/Jimsphere balloon tracks to investigate the possibility of detecting CAT from balloon motions. Turbulent motions were defined by smoothing slant range measurements, and then computing the deviations from the smoothed curve. These authors concluded that the properties of turbulence are determined with greater confidence from these data than from any turbulence measurements currently available.

The Richardson number (Ri) has been used repeatedly in associating the occurrence of CAT with atmospheric stability and vertical wind shear (Reiter and Lester, 1967; and others). The Ri can be used only qualitatively as a criterion for the separation of turbulence and no turbulence (Colson and Panofsky, 1965). Reiter and Lester summarized the broad discrepancies found in an attempt to associate CAT with Ri. They conclude that some of these discrepancies are due to inadequacies inherent in the synoptic rawinsonde network. Some of these inadequacies are: lack of resolution, lack of synchronization, and poor choice of scale length. Lumley and Panofsky (1964) conclude that the more detail provided by a sounding, the better the relation between Ri and CAT.

Colson and Panofsky (op.cit.) derived a CAT Index (I) which is proportional to the energy of the vertical component of turbulence. This expression is given by

$$I = \left(\Delta \vec{V}\right)^2 \left(1 - Ri/Ri_{crit}\right) \tag{1}$$

where $\Delta \vec{V}$ is the magnitude of the vector difference in wind velocity over a specified vertical distance, and Ri_{crit} is the critical Richardson number which is assumed to be approximately equal to 0.5. The authors used data from the synoptic rawinsonde network to compute the CAT Index, and obtained relevant aircraft reports of CAT to compare with their CAT Index values. They concluded that their CAT Index values were directly related to vertical wind shear, and that the probability of CAT occurrence increased with an increase in CAT Index values.

It has been stated that there exists no unique association between Ri and the occurrence of CAT (Reiter, op.cit.; Foltz, op.cit.; and others). Reiter and Lester (op.cit.) expect that a shearing layer would have to attain a certain minimum thickness before eddies of a size and energy to be felt as CAT could be generated. They analyzed 17 FPS-16 radar/Jimsphere wind profiles under conditions of weak anticyclonic flow. From their analysis, they estimated a functional relationship between Ri and the thickness, L, of the layer over which Ri was computed. Their relationship was of the form

$$Ri = AL^P \tag{2}$$

where A is a constant of proportionality, and $0 \leq p \leq 4/3$. They found no relevant association between Ri, L, and CAT.

Mesoscale perturbations which seem to be responsible for CAT exist in thin discrete horizontal layers of the atmosphere. These layers are found to move relative to each other without appreciable interchange, and persistant psuedo-inertial fluctuations occur within these layers (Axford, 1968; Weinstein, Reiter, and Scoggins 1966; Sawyer, 1961).

The magnitude of the turbulent fluctuations measured in time or space is of prime concern in practical problems as well as in research. Since turbulence must be inferred from mean meteorological parameters, a practical problem is to relate the statistics of the magnitudes of the fluctuations to the mean parameters (Lumley and Panofsky, op.cit.). The magnitude of the turbulent fluctuations, as well as relevant meteorological parameters, depends on the resolution of the data from which the parameters are computed (Colson and Panofsky, op.cit.).

b. Purpose and method of this study. The principal aim of this investigation is to relate the magnitudes of turbulent fluctuations obtained from detailed wind profiles to mean meteorological parameters. Detailed wind profiles, measured by the FPS-16 radar/Jimsphere system, and rawinsonde profiles are the main sources of data.

The Jimsphere balloon was developed to furnish a wind sensor that would give accurate response to small-scale changes in the

wind field (Scoggins, op.cit.). Scoggins defines small-scale motions (turbulence) as those which are not included in rawinsonde measured profiles. This same definition of turbulence is used in this investigation. With this definition, wavelengths of approximately 1000 m and shorter are included, thereby extending well beyond the wavelengths of all spurious motions of the balloon.

The radar/Jimsphere wind profiles furnish a form of data that has not been investigated to any great extent as a source of actual observations of CAT. Turbulence is defined from these profiles by application of a numerical filter. The filter function, which is shown in Fig. 1, is designed to provide a smooth profile with wavelengths of approximately 1 km and longer. Turbulent motions are defined in this study as the difference between the smooth and original profiles. The process is illustrated in Fig. 2.

In this study, the following items are investigated:

(1) The association between Ri, L, and CAT as defined from the detailed wind profiles.

(2) The relationships between the Colson and Panofsky CAT Index and turbulence defined from the detailed wind profiles.

(3) The relationships between turbulence defined from the detailed wind profiles and vertical wind shears and temperature gradients.

(4) The degree to which CAT can be forecast from mean meteorological parameters.
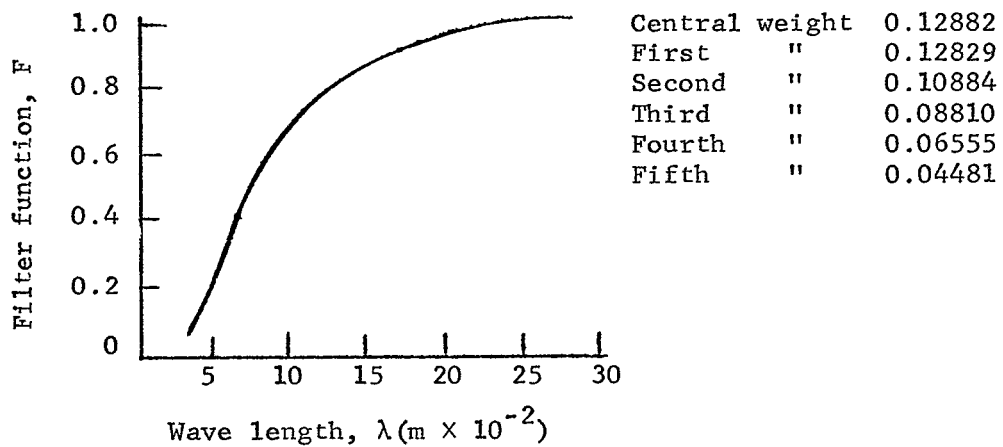
Fig. 1. Filter function used for defining small-scale motions (turbulence) from detailed FPS-16 radar/Jimsphere wind profiles (after Scoggins, 1967).
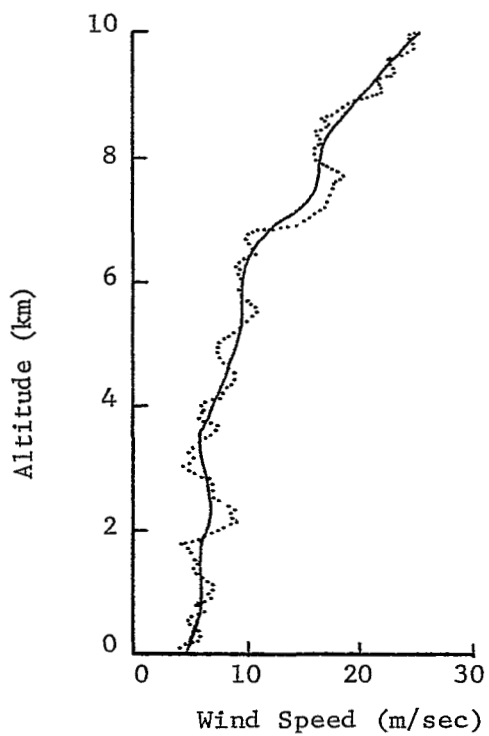
Fig. 2. Illustration of a smooth and an original scalar wind speed profiles. The solid line indicates the smoothed profile.

2. MEASUREMENT SYSTEMS AND DESCRIPTION OF THE DATA

The primary source of data for this study was 252 detailed wind profiles from the FPS-16 radar/Jimsphere system and an associated number of rawinsonde soundings. The data were selected on a random basis for the period September 1963 through March 1968. The criteria for selecting pairs of wind and temperature profiles for investigation were that the detailed wind profile be complete between 5 and 14 km, and that the time interval between a detailed wind profile and the associated rawinsonde sounding not exceed 3 hr.

a. The FPS-16 radar/Jimsphere system. The FPS-16 radar/Jimsphere system consists of a 2-m diameter, superpressure, aluminized, mylar balloon with conical roughness elements molded into its surface. The purpose of the roughness elements is to control vortex formation and separation in order to reduce aerodynamic or self-induced motions of the balloon. The sphere is tracked by the FPS-16 high-precision radar (DeMandel and Scoggins, op.cit.).

The response of the Jimsphere to vertical wind shears is sufficient to measure motions on a scale of only a few meters (Eckstrom, 1965). The method of data reduction developed by Scoggins essentially eliminates any spurious motions (Rogers and Camitz, 1965). In this procedure, the x, y, z position coordinates provided at 0.1-sec intervals are averaged over a period of 4 sec, centered on 25-m intervals of altitude. Component wind speeds are computed by finite differences over layers of 50-m

depth at each 25-m increment of altitude. It has been shown that
wind speeds measured by this method have an rms tracking error
generally less than 0.5 mps (Scoggins, op.cit.; Susko and Vaughan,
1968). Wind direction is measured with an rms tracking error of no
more than 1 or 2 deg to an altitude of 18 km (Scoggins, op.cit.).

   b. Rawinsonde system. A complete set of measurements available
from the rawinsonde (GMD-1) system includes pressure, temperature,
relative humidity, azimuth angle, elevation angle, and time. The
only data provided by this system that are used in this study are
temperatures. Temperature measurements are accurate to the nearest
0.5°C (Danielsen and Duquet, 1967).

3. MEASUREMENTS AND OBSERVATIONS OF CAT

   Measurements of turbulence are not included in routine meteor-
ological observations. These measurements are made by the use of
aircraft, balloons, instrumented towers, and wind tunnels. The
observations are made under both real and simulated atmospheric
environments.

   The primary source of CAT data has been measurements obtained
from aircraft flying in the troposphere and lower stratosphere. The
measurement of the intensity of CAT is determined largely by the
type, speed, and heading of the aircraft, and the relative flying
experience of the aircraft crew (Press, Meadows, and Hadlock, 1956).

   Observations from routine rawinsonde ascents, which normally are

made twice daily, are used in synoptic analyses of mean meteorological parameters which are assumed to be related to CAT. These measurements are valid on a large scale, but they are smoothed over several hundred meters in depth. Thus, these observations do not provide direct measurements of CAT. Aircraft measurements have been used extensively in turbulence studies, but again the details of the vertical structure of the atmosphere are smoothed owing to large time differences between traverses through the turbulent regimes (Axford, op.cit.; Reiter, op.cit.).

A study using radars of different wavelengths revealed a number of atmospheric structures with braided appearance. These structures were compared with meteorological data and it was concluded that breaking gravity waves were being observed in relatively stable layers of the atmosphere (Hicks and Angell, 1967). Wave motions such as these are thought to be a prime source of CAT.

Errors in the measured, detailed, wind-profile data due to errors in the radar data were investigated by Scoggins (op.cit.); and Vaughan and Susko (op.cit.). These authors found rms errors in the wind data ranging from approximately 0.3 to 0.6 mps each for the zonal (W-E) and meridional (S-N) components of the wind profiles. These rms errors also were found to be essentially independent of altitude. Since CAT in the horizontal plane is composed of both components of the wind, the rms error in the resultant (rms-r) is given by

$$rms\text{-}r = \sqrt{\sigma_u^2 + \sigma_v^2} \tag{3}$$

B-12

where σ_u and σ_v refer to rms errors in the zonal and meridional components of the wind, respectively. If it is assumed that both components have minimum or maximum error simultaneously, then rms-r will vary between about 0.4 and 0.85 mps. If the value of rms-r is less than 0.4 mps, it is assumed that no turbulence exists. If the rms-r value is greater than 0.85 mps, it is assumed that turbulence is present. In the range between these two values, turbulence may or may not occur. These values are used in this study as criteria to differentiate between turbulence and no turbulence.

4. ANALYSIS OF THE DATA

a. Preparation of the data for computer processing. Each selected detailed wind profile with each corresponding rawinsonde was recorded on magnetic tape. One radar/Jimsphere profile and its associated rawinsonde constituted one set of data. Each set was divided into 250-m increments of altitude from 5 to 14 km. The analysis was limited to the 5-to-14 km range of altitude because this range encompasses the jet stream as well as the most reliable detailed wind-profile data.

The initial processing of the data was done on the IBM 360/65 computer in Fortran IV-G computer language. Samples of each type of calculation were hand-checked to insure validity of the program.

b. Selective grouping of the data. Parameters such as wind shear, rms values of turbulence, etc., were computed over variable

layers (250, 500, 1000, and 2000 m) with the top of each layer being at 6, 7, . . ., 14 km. Computations within each layer were grouped and analyzed independently of the other layers. The layers were made to overlap intentionally to permit an investigation of the influence of scale length (layer thickness) on the relationship between turbulence and the computed parameters. The total number of computations varies somewhat for each layer because of missing data.

The data are grouped further by interval of altitude on the basis of observations of CAT (rms-r $\geq$ 0.85 mps), observations of no CAT (rms-r $\leq$ 0.4 mps), layers of thermal stability ($\Delta T/\Delta Z \geq$ -0.004°C/m), layers where Ri is equal to or less than Ri_{crit}, and layers where there are strong vertical wind shears ($\Delta \vec{V}/\Delta Z \geq$ 0.008 sec^{-1} over a layer of 1 km).

c. <u>Computations performed</u>. The components (zonal and meridional) and resultant rms values of turbulence were computed for each selected wind profile over each of the previously mentioned increments of altitude.

Vertical vector wind shears were computed from the wind profiles over the previously noted increments of altitude by the finite difference scheme

$$\frac{\Delta \vec{V}}{\Delta Z} = \frac{[(u_2-u_1)^2 + (v_2-v_1)^2]^{\frac{1}{2}}}{\Delta Z} \tag{4}$$

where u_i and v_i are the zonal and meridional components of the wind vector, respectively, and ΔZ is the increment of altitude. The

vector wind shear has dimensions of sec^{-1}. The change in direction of the vector wind with respect to height was computed as the numerical difference in direction between the upper and the lower wind vectors divided by the increment of altitude between the wind measurements ($\Delta\alpha/\Delta Z$). Positive values denote veering and negative values backing of the wind with height.

The lapse rate of temperature was computed from the rawinsonde data by the finite difference scheme

$$\frac{\Delta T}{\Delta Z} = \frac{T_2 - T_1}{\Delta Z} \tag{5}$$

where T refers to the temperature (°C), the subscripts 1 and 2 denote lower and upper levels, respectively, and ΔZ is the increment of altitude between the temperature measurements.

The Ri was computed for each interval of altitude for each selected sounding using the rawinsonde temperatures and the FPS-16 radar/Jimsphere data. The Ri is given by

$$Ri = \frac{g/\overline{T} \ (\Delta \overline{T}/\Delta Z + \Gamma_d)}{(\Delta \vec{V}/\Delta Z)} \tag{6}$$

where Γ_d is the dry adiabatic lapse rate (-0.00976°C/m), $\overline{T}$ is the mean temperature of the layer, and g is the acceleration of gravity.

The Colson and Panofsky CAT Index (I) was computed over all the increments of altitude for each set of data.

Linear correlation coefficients and linear regression curves

were computed for selected sets of data. The linear relationships were computed for rms-r values versus vector wind shear, difference in the direction of the vector wind with respect to changes in height, lapse rate of temperature, Ri, and the CAT Index. These linear relationships were computed for the data as grouped under the previously mentioned increments of altitude.

The relationships between turbulence observed from selected profiles and general synoptic conditions was investigated to a limited extent.

5. RESULTS

a. Empirical frequencies of CAT. Table 1 summarizes the total number of observations available, and the total number of observations of CAT and no CAT for all the increments of altitude. The percentages of the observations of CAT are in good agreement with climatological averages for the occurrence of CAT (Reiter, op.cit.; Endlich, Mancuso, and Davies, 1966). Reiter found that CAT occurs approximately 5% of flight time. In the current study, CAT (rms $\geq$ 0.85 mps) was observed on approximately 2 to 6% of the total observations depending upon thickness of the layer.

When rms-r was between 0.4 and 0.85 mps, it was assumed that no significant CAT was present. These conditions existed for 38 to 53% of all of the observations, depending on thickness of the layer. It also was found that 45 to 56% of the observations revealed that no CAT was present (rms-r $\leq$ 0.4 mps). These percentages also

Table 1. Frequencies of CAT (rms-r $\geq$ 0.85 mps) and no CAT (rms-r $\leq$ 0.4 mps) as a function of layer thickness for all data.

ΔZ (m)	250	500	1000	2000
Total no. of observations	2023	2096	2117	2116
rms-r $\geq$ 0.85 mps				
No.	118	114	81	43
% of total obs.	5.8	5.4	3.8	2.0
rms-r $\leq$ 0.4 mps				
No.	1124	1061	1016	954
% of total obs.	55.6	50.6	47.9	45.1

depended on the depth of the layer. These results only indicated the existence of turbulence in a defined layer of the atmosphere. Table 1 does not differentiate between season of the year, the altitude of the observation of CAT, or the degree of the intensity of CAT (light, moderate, or severe). However, it was found that there was a definite seasonal tendency. The few large rms-r values observed from wind profiles in the summer months (May through September) occurred with relatively light wind conditions ($\overline{V} \leq 15$ mps) and were associated with relatively unstable lapse rates of temperature ($\Delta T/\Delta Z \leq -0.007°C/m$). Over 80% of all the observations of CAT occurred during the fall and winter months, and were associated with moderate to strong winds aloft ($\overline{V} \geq 40$ mps), stable lapse rates ($\Delta T/\Delta Z \geq -0.004°C/m$), and occurred at altitudes near the tropopause (12 to 14 km).

Table 2 summarizes the frequencies of observations of CAT as
a function of altitude of observation and thickness of the layer.
In excess of 80% of all the observations of CAT, over all of the
defined layers, occurred at altitudes above 10 km. Generally, the
number of observations of CAT increased with an increase in altitude
and decreased with an increase in layer thickness. Previous statis-
tics (Endlich, Mancuso, and Davies, op.cit.) regarding the frequency
of occurrence of CAT with respect to altitude are in good agreement
with the results obtained in this investigation. Endlich, Mancuso,
and Davies found that the frequency of occurrence of CAT increased
with an increase in altitude, and that the peak frequency was as high
as 18% of flight time for altitudes near the jet stream. In Table
2, the results from the present study are in qualitative agreement
with those of Endlich, Mancuso, and Davies. In the present study
the mean height of the maximum wind speed velocity was observed to
be near 13 km for most of the cases where CAT was observed.

b. Relationships between CAT and selected meteorological
parameters. The rms-r versus the vertical wind shear, for the
entire data sample, provided one of the better linear relationships
found in this investigation. Linear regression curves between rms-r
and vertical wind shear are shown in Fig. 3. The slopes of the
curves increase as the depth of the layer decreases. Since an
rms-r value equal to or greater than 0.85 mps defines an observation
of CAT, and an rms-r value less than or equal to 0.4 mps defines
an observation of no CAT, the intersections of these rms-r lines

Table 2. Frequencies of observations of CAT (rms-r ≥ 0.85 mps) as a function of altitude and layer thickness for the 250-m, 500-m, and 1000-m layers.

Top of each layer (km)	ΔZ (m) 250 No. and % of observations of CAT in each layer No.	%	Cumulative percent of observations for 250-m layer	ΔZ (m) 500 No. and % of observations of CAT in each layer No.	%	Cumulative percent of observations for 500-m layer	ΔZ (m) 1000 No. and % of observations of CAT in each layer No.	%	Cumulative percent of observations for 1000-m layer
6	2	0.9	1.7	1	0.4	0.9	2	0.9	2.5
7	4	1.8	4.1	3	1.3	3.5	1	0.4	3.7
8	1	0.4	5.9	0	0.0	3.5	1	0.4	4.9
9	7	3.1	11.9	3	1.3	6.1	2	0.9	7.4
10	7	3.1	17.8	5	2.1	10.5	4	1.7	12.3
11	11	4.9	27.1	10	4.3	19.3	6	2.6	19.8
12	17	7.5	41.5	16	6.8	33.3	11	4.7	33.3
13	29	12.9	66.1	31	13.3	60.8	27	11.5	66.7
14	40	17.8	100.0	45	19.3	100.0	27	11.5	100.0
	118			114			81		
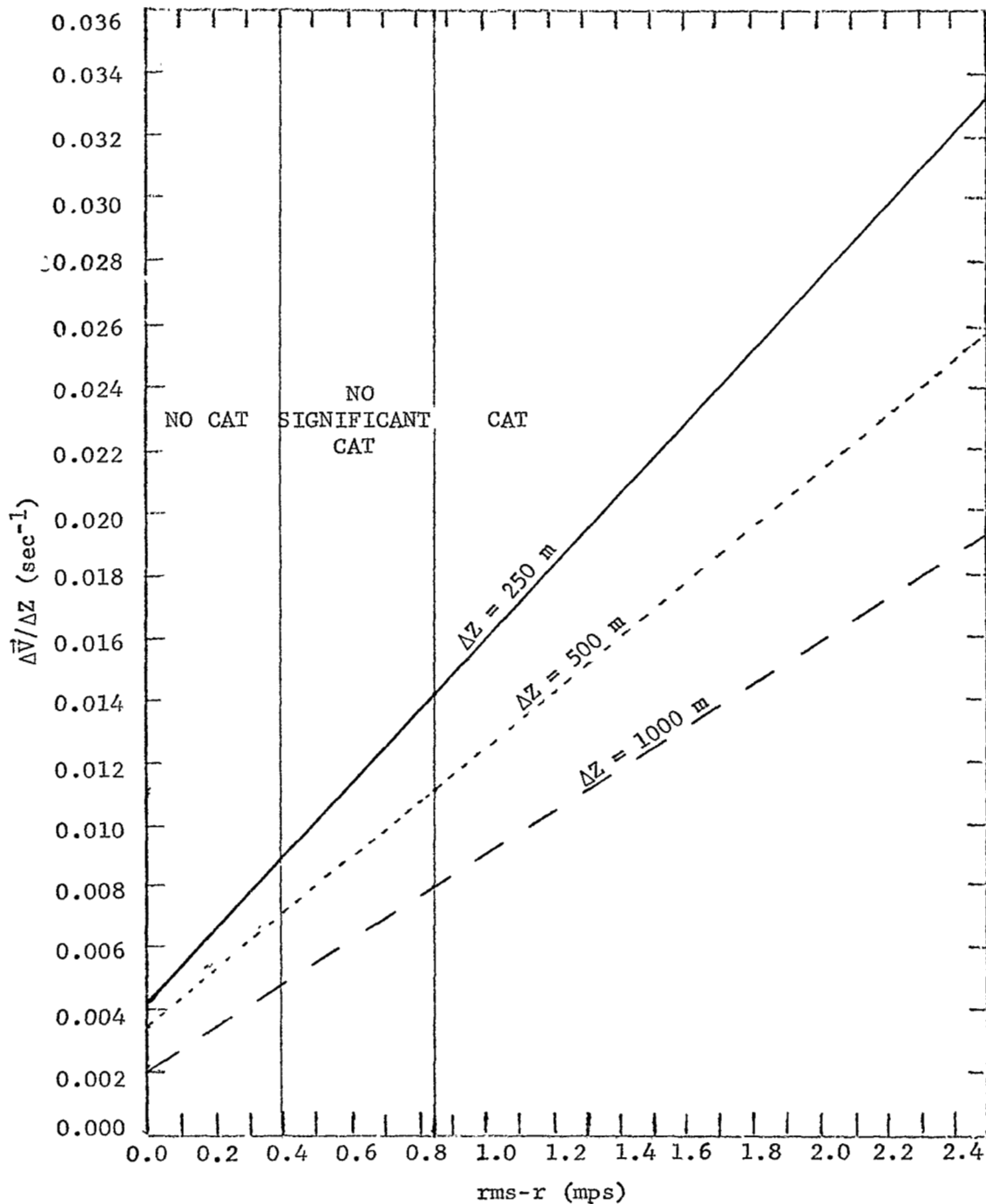
Fig. 3. Linear regression curves for rms-r versus $\Delta\vec{V}/\Delta Z$ over 250-m, 500-m, and 1000-m layers for all data.

with the linear regression curves define "critical" wind shears for CAT and no CAT for the 250-m, 500-m, and 1000-m layers. The magnitude of these "critical" wind shears decreases as the depth of the layer increases.

Table 3 illustrates the frequencies of observations of CAT versus the "critical" wind shears for CAT and no CAT. In the 250-m layer, the "critical" wind shear for CAT was equalled or exceeded in 415 out of 2023 observations (22%), but CAT was observed only 93 times (4.5%), and no CAT was observed 71 times (3.5%). In other words, for observations when the "critical" wind shear was equalled or exceeded, CAT occurred in 22% and no CAT was observed in 17% of these observations. In the 500-m layer CAT occured in 26% and no CAT occurred in 15% of the observations when the wind shear was equal to or greater than the "critical" value. In the 1000-m layer CAT occurred nearly twice as many times as no CAT for observations where the wind shear equalled or exceeded the "critical" value. From a comparison of Tables 1 and 3, it can be seen that over 79% of the observations of CAT for the 250-m and 500-m layers occurred when the "critical" wind shear for each layer was equalled or exceeded, while only 31% of the observations of CAT for the 1000-m layer occurred when the "critical" wind shear for CAT in this layer was equalled or exceeded.

For observations when the "critical" wind shear for no CAT was not exceeded, Table 3 shows that, generally, the observations of CAT increased with an increase in layer thickness, but CAT was

Table 3. The occurrence of CAT and no CAT as functions of the "critical" wind shears shown in Fig. 3.

ΔZ (m)	ΔV/ΔZ "Critical" for CAT	ΔV/ΔZ≥(ΔV/ΔZ) Critical for CAT			ΔV/ΔZ "Critical" for no CAT	ΔV/ΔZ≤(ΔV/ΔZ) Critical for no CAT		
		No. of obs.	No. rms-r ≥0.85 mps	No. rms-r ≤0.4 mps		No. of obs.	No. rms-r ≥0.85 mps	No. rms-r ≤0.4 mps
250	0.014	415	93	71	0.009	922	2	767
500	0.011	375	96	57	0.007	943	2C	681
1000	0.008	333	25	13	0.005	921	18	596

observed only 0.2 to 2% of these observations. It also is seen that the observations of no CAT decreased with an increase in layer thickness when the "critical" wind shear for no CAT was not exceeded. For wind shears less than or equal to the "critical" value for no CAT in each layer, CAT was not observed from 65 to 83% of the observations, depending on the thickness of the layer.

Linear regression curves between rms-r and lapse rate of temperature are shown in Fig. 4. The slopes of these curves decrease as the depth of the layer decreases. As was done in Fig. 3, the intersections of the 0.85 mps and 0.4 mps rms-r lines with the regression curves defines "critical" lapse rates of temperature for CAT and no CAT, respectively. The value of the "critical" lapse rate of temperature for CAT is very nearly the same for all thicknesses of the layers ($\Delta T/\Delta Z = -0.004°C/m$). The "critical" lapse rate of temperature for no CAT decreases (greater instability) as the thickness of the layer increases.

Table 4 shows the frequencies of observations of CAT versus the "critical" lapse rates of temperature for CAT and no CAT. The number of observations when the lapse rate of temperature is equal to or greater than the "critical" value for CAT decreases with an increase in the thickness of the layer. The "critical" lapse rates of temperature were observed in 11 to 16% of the total observations. CAT was observed in 22% (71 out of 318) to 29% (80 out of 276) and no CAT in 4% (9 out of 228) to 26% (83 out of 318) of the observations when the "critical" lapse rate of temperature was exceeded
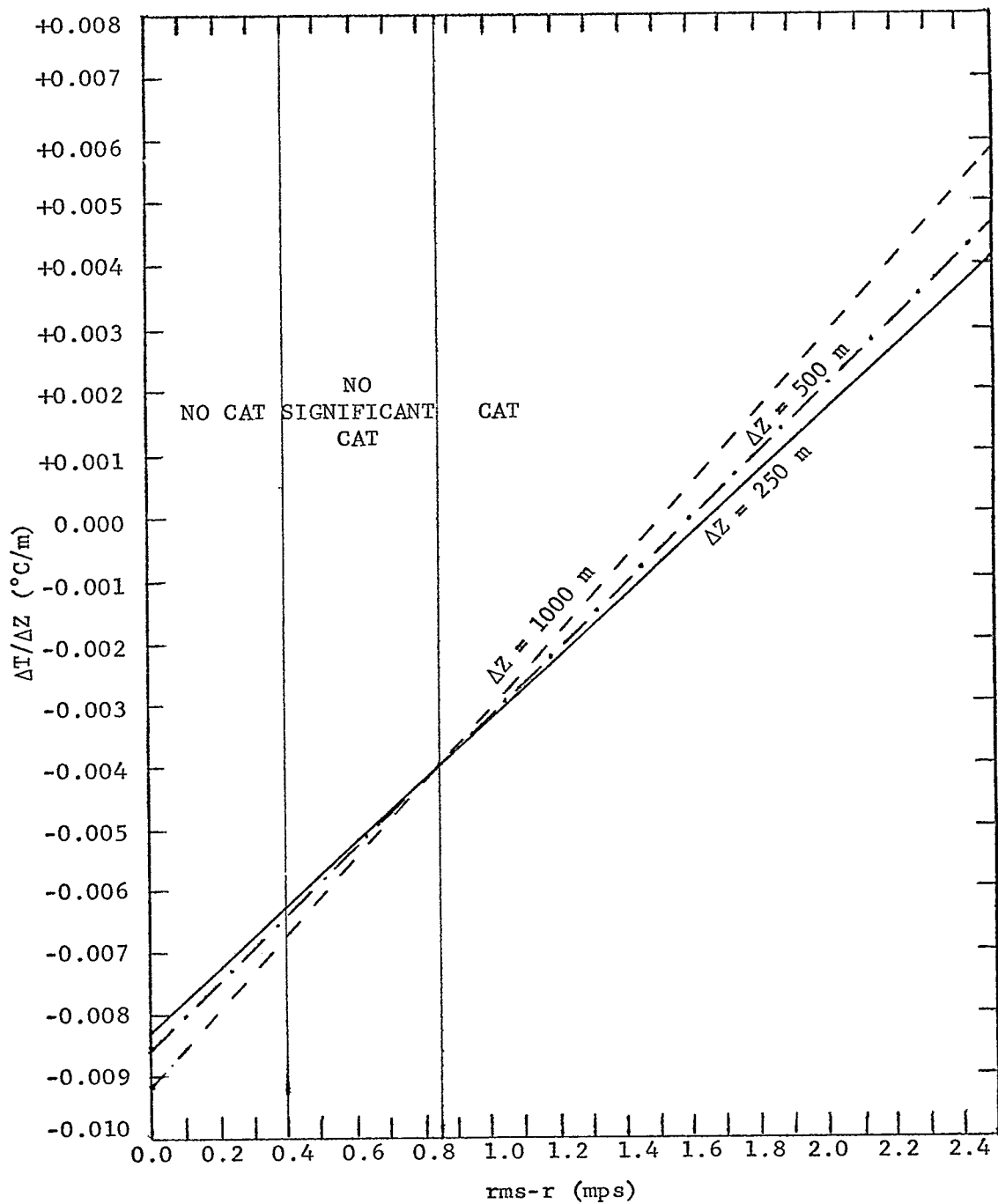
Fig. 4. Linear regression curves for rms-r versus lapse rate of temperature ($\Delta T/\Delta Z$) over the 250-m, 500-m, and 1000-m layers for all data.

Table 4. The observations of CAT and no CAT as a function of the "critical" lapse rates of temperature shown in Fig. 4.

ΔZ (m)	ΔT/ΔZ (°C/m) "Critical" for CAT	ΔT/ΔZ≥(ΔT/ΔZ) Critical for CAT			ΔT/ΔZ (°C/m) "Critical" for no CAT	ΔT/ΔZ≤(ΔT/ΔZ) Critical for no CAT		
		No. of obs.	No. rms-r ≥0.85 mps	No. rms-r ≤0.4 mps		No. of obs.	No. rms-r ≥0.85 mps	No. rms-r ≤0.4 mps
250	-0.004	318	71	83	-0.0062	508	18	319
500	-0.004	276	80	46	-0.0064	615	12	380
1000	-0.004	228	57	9	-0.0067	709	9	456

(more stable). These percentages were dependent on the thickness
of the layer.

For observations when the "critical" lapse rate of temperature
for no CAT was not exceeded (more unstable), Table 4 shows that the
number of observations of unstable layers increases with an increase
in thickness of the layer, and CAT occurs in 1.2% (9 out of 709) to
3.5% (18 out of 503) of these observations depending on the layer
thickness. It also is shown that when the "critical" lapse rate of
temperature for no CAT was not exceeded (more unstable), no CAT was
observed in approximately 62% of these observations for all depths
of the layers.

Tables 5, 6, and 7 summarize the observations of CAT (rms-r $\geq$
0.85 mps) with respect to lapse rates of temperature and vertical
wind shears for the 250-m, 500-m, and 1000-m increments of altitude.
The totals columns from Tables 5, 6, and 7, and the results from
Table 3, indicate that large wind shears are necessary, but not
sufficient, conditions for CAT. It also is apparent, from these
totals columns, that the observations of CAT are strongly dependent
on the thermal stability of the atmosphere ($\Delta T/\Delta Z \geq -0.004°C/m$).
Generally, the observations of CAT increase as the stability increases
for all the increments of altitude. Thus CAT occurs more frequently
in stable layers with large wind shears.

In this investigation, Ri was found to vary considerably with
respect to the height and depth of the layer over which it was
computed. There were increases in Ri values of two to four orders

Table 5. Vertical wind shear versus lapse rate of temperature for observations of CAT (rms-r $\geq$ 0.85 mps) in the 250-m layer.

ΔT/ΔZ (°C/m)	$\Delta\vec{V}/\Delta Z$ (sec^{-1})							
	≥ 0.000 < 0.010	0.010 0.015	0.015 0.020	0.020 0.025	0.025 0.030	0.030 0.035	0.035	Total
< -0.007	1	6	6	1	3	1	0	18
≥ -0.007 < -0.004	1	8	4	4	5	4	3	29
≥ -0.004	0	10	13	12	12	11	13	71
Total	2	24	23	17	20	16	16	118

Table 6. Vertical wind shear versus lapse rate of temperature for observations of CAT (rms-r $\geq$ 0.85 mps) in the 500-m layer.

ΔT/ΔZ (°C/m)	$\Delta\vec{V}/\Delta Z$ (sec^{-1})					Total
	≥ 0.000 < 0.010	0.010 0.015	0.015 0.020	0.020 0.025	0.025	
< -0.007	2	3	2	4	1	12
≥ -0.007 < -0.004	3	9	5	4	1	22
≥ -0.004	13	22	16	17	12	80
Total	18	34	23	25	14	114

Table 7. Vertical wind shear versus lapse rate of temperature for observations of CAT (rms-r $\geq$ 0.85 mps) in the 1000-m layer.

$\Delta T/\Delta Z$ (°C/m)	$\Delta\vec{V}/\Delta Z$ (sec^{-1})					
	$\geq$ 0.000 $<$ 0.003	0.003 0.005	0.005 0.008	0.008 0.012	0.015	Total
$<$ -0.007	4	1	1	1	2	9
$\geq$ -0.007 $<$ -0.004	2	4	5	1	3	15
$\geq$ -0.004	10	18	11	10	8	57
Totals	16	23	17	12	13	81

of magnitude in the same set of data for increasing depths of the layers. These results were in quantitative agreement with the results of Reiter and Lester (op.cit.). The Richardson numbers computed in this investigation were not associated with the frequency of occurrence of CAT in any of the layers.

Table 8 shows the empirical frequencies of CAT and no CAT for values of Ri less than or equal to assumed values of Ri_{crit} for different depths of the layers. The number of observations of CAT decreases with an increase in the increment of altitude; only 5% (2 out of 81) to 16% (19 out of 118) of the observations of CAT were associated with values equal to or less than these values of Ri_{crit}. The percentages of the observations of CAT increased as the depth of the layer decreased. There were 5 to 35 times as many observations of no CAT as there were observations of CAT depending on the

Table 8. Empirical frequencies of CAT and no CAT when $Ri \leq Ri_{crit}$ for assumed values of Ri_{crit} for different depths of layer.

Ri Critical	ΔZ (m)	Number of observations $Ri \leq Ri_{crit}$	Number of observations of CAT when $Ri \leq Ri_{crit}$	Number of observations of no CAT when $Ri \leq Ri_{crit}$
0.25	250	187	19	93
0.50	500	183	14	77
1.00	1000	173	10	62
2.00	2000	197	2	73

thickness of the layer. This would infer, statistically, that no CAT was most likely to be observed for Ri less than or equal to the critical Richardson number. Therefore the Ri was not a good indicator of CAT.

The Colson and Panofsky CAT Index (I) defined by equation (1) and the observations of CAT from the detailed wind profiles produced results that appeared to be in direct contrast with the results of Colson and Panofsky (op.cit.). They obtained increasing positive values of I in association with an increase in the intensity of CAT. The results of the present investigation show that larger values of rms-r were associated with more negative values of I.

The contrast in the results of the two investigations may be due to:

(1) The greater detail of the wind data in the present investigation;

(2)   In the present investigation, observations of CAT were made coincident in time and space with measurements of vertical wind shear and near coincident with measurements of temperature;

(3)   In the present investigation, shallower layers of the atmosphere were considered than those considered by Colson and Panofsky.

However, both studies showed that CAT was associated with large vertical wind shears.

Figure 5 shows the linear regression curves and linear correlation coefficients for lapse rate of temperture versus CAT Index for observations of CAT. The slopes of the curves do not change significantly with increased increments of altitude. However, the linear correlation coefficients increase with an increase in the thickness of the layer. The -0.94 linear correlation in the 1000-m layer was the highest correlation obtained in this investigation. These results indicate that the value of the CAT Index decreases as the lapse rate of temperature becomes more stable for any given layer.

Table 9 summarizes the linear correlation coefficients for rms-r versus each of the selected meteorological parameters as related to layer depth for all data. The correlation of rms-r with vertical wind shear decrease with an increase in the depth of the layer through the 1000-m layer. The correlation between rms-r and the vertical wind shear in the 250-m layer is the largest found for all the correlations computed in Table 9. The correlation
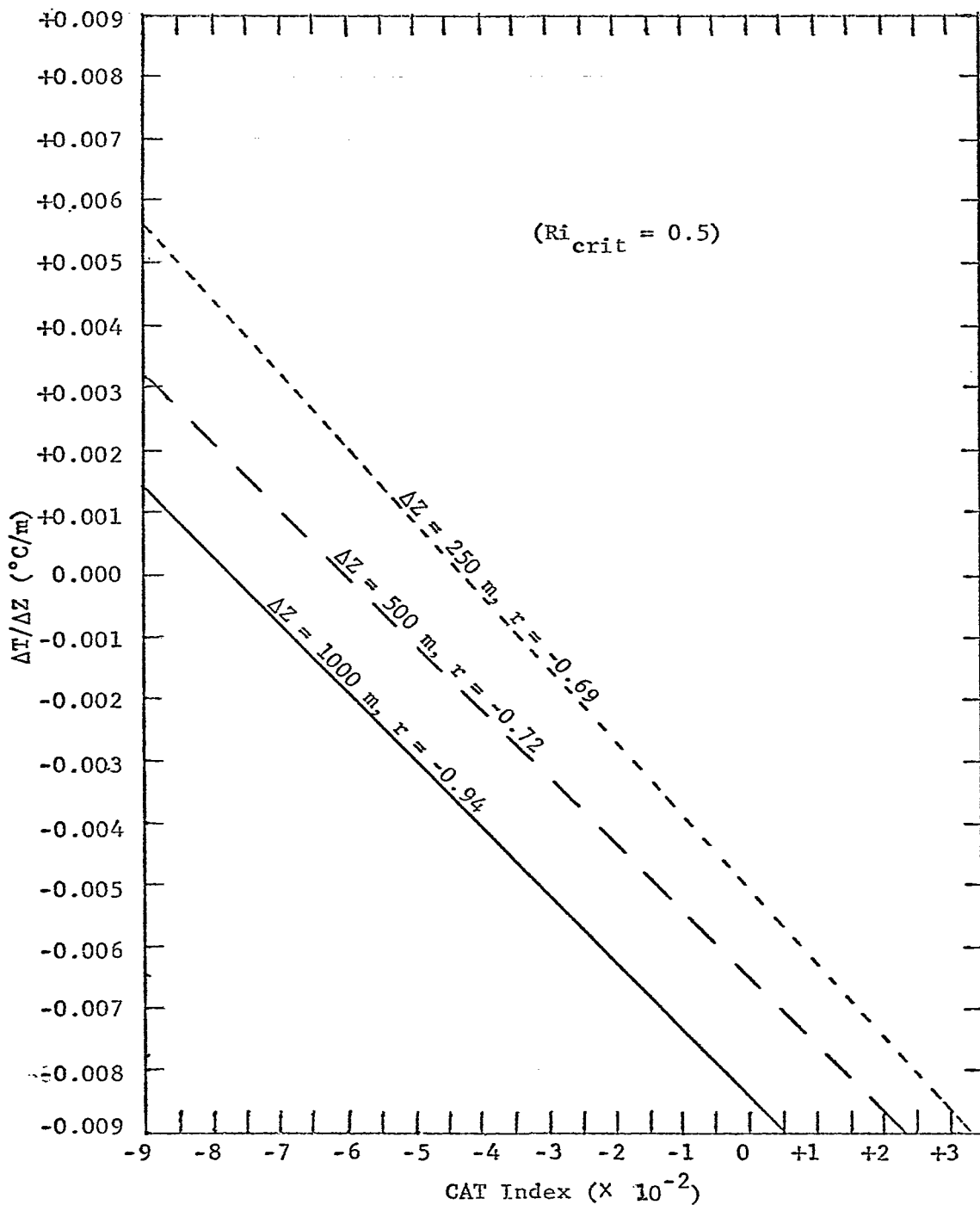
Fig. 5. Linear regression curves and linear correlation coefficients (r) for the CAT Index versus lapse rate of temperature for observations of CAT (rms-r ≳ 0.85 mps) over the 250-m, 500-m, and 1000-m layers.

Table 9. Linear correlation coefficients between rms-r and selected
meteorological parameters as related to depth of layer for
all data.

ΔZ	$\Delta V/\Delta Z$	$\Delta T/\Delta Z$	$\Delta\alpha/\Delta Z$	Ri	I
250 m	0.513	0.129	0.276	0.006	-0.277
500 m	0.403	0.224	0.356	-0.002	-0.286
1000 m	0.375	0.279	0.361	0.003	-0.279
2000 m	0.446	0.016	0.445	-0.001	-0.349

between rms-r and lapse rate of temperature increases as the depth

of the layer increases through 1000 m. The correlation of rms-r

versus the change in direction of the vector wind with respect to

height increases as the depth of the layer increases. The positive

values of the correlation coefficients do not indicate that the wind

veered with respect to an increase in the rms-r. Only the absolute

value of the change in direction was used to compute the correlation

coefficient. Correlations that were attempted using negative values

of $\Delta\alpha/\Delta Z$ (backing), and positive values of $\Delta\alpha/\Delta Z$ (veering) were nil

(r ranges between $\pm$ 0.08). Table 9 shows also that correlations

for rms-r versus Ri were practically nil. There seems to be no

definable relationship whatever between Ri and CAT in this investi-

gation. The CAT Index correlations with rms-r in Table 9 show

almost no change with respect to changes in depth of the layer

through the 1000-m depth. Table 9 shows changes of correlation

coefficients between 2000-m layers and the trend from the other three

depths of the layers. The vertical wind shear, direction change, and CAT Index correlations increase from the values over the 1000-m depth, while the correlation coefficient for lapse rate of temperature shows a large decrease and the Ri shows no significant change. These results imply that stability in deep layers has no pronounced effect on CAT. This could be explained by the existence of shear-gravity waves in thinner layers that would be eliminated when larger layers are considered.

Correlations were computed for observations of CAT (rms-r $\geq$ 0.85 mps) and for observations of no CAT (rms-r $\leq$ 0.4 mps) versus each of the selected meteorological parameters. With the exception of the lapse rate of temperature versus I when turbulence occurred, the results show no significant correlation (r ranges between $\pm$ 0.075).

Figure 6 illustrates the character of the wind-profile data used in this study. CAT was observed in this profile in the 10 to 12 km layer. The rms-r for the 250-m layer, topped at 11 km, was 2.015 mps. The lapse rate of temperature was -0.004°C/m, the vertical wind shear was 0.0285 sec^{-1}, Ri was 1.3, and the CAT Index was -80. In a large number of cases CAT was observed to exist over deeper layers of the atmosphere (1000 m to 2000 m) if there was a noticeable maximum of wind velocity either above or below a stable layer (mostly below). These conditions represent strong wind shear in a stable layer.
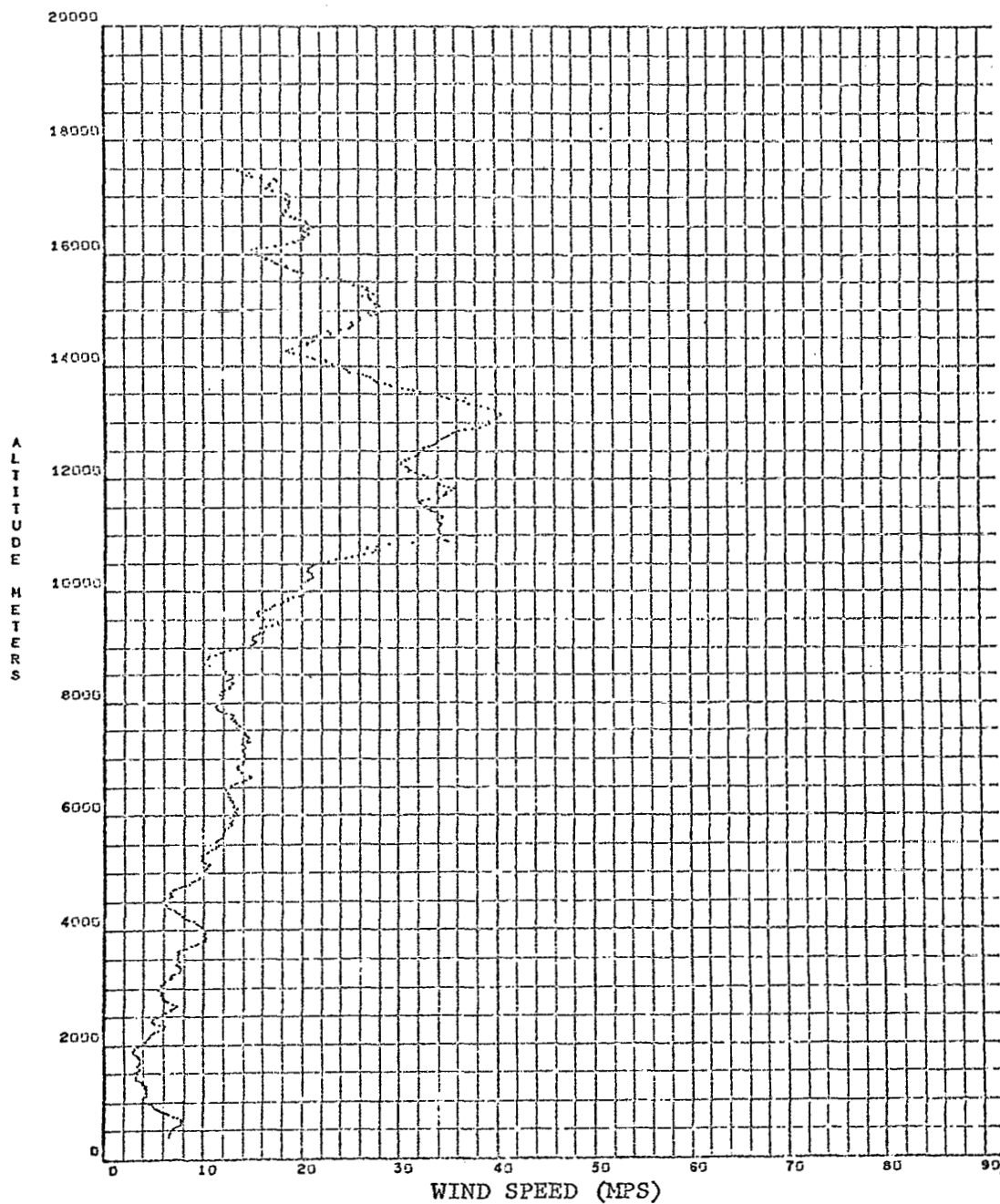
Fig. 6.   Profile of wind speed measured by the FPS-16 radar/
Jimsphere system over Cape Kennedy, Florida.

B-34

6. FORECASTING OF CAT

Rawinsonde measurements tend to provide underestimates of vertical wind shear and lapse rate of temperature. The limitations in the meteorological data provided by this system prevent detailed analysis of CAT from these wind and temperature profiles. Without adequate data, inaccurate analysis results. Unless there is an accurate analysis of data, a good forecast is little more than luck.

The results of this investigation indicate that CAT was observed in thin layers of the atmosphere characterized by large vertical wind shear and stable thermal stratification. Any attempt to forecast CAT must be directed toward identifying the regions that appear favorable for the occurrence of CAT.

The identification of a region where there is CAT is only half of the problem involved in forecasting CAT. There is difficulty in considering a time and space extrapolation of a region of CAT. Does the region of CAT maintain its size, shape, and intensity with respect to changes in time and space? The present investigation cannot hypothesize on answers to this question.

The results presented previously show that in order to forecast CAT, the lapse rate of temperature and vertical wind shear in layers 1000 m and less in depth must be forecast. CAT occurs predominantly in layers with relatively stable lapse rates of temperature and with strong wind shear. Strong wind shear alone is not a sufficient predictor of CAT.

7. CONCLUSIONS AND RECOMMENDATIONS

a. __Conclusions__. The investigation of the data from 252 FPS-16 radar/Jimsphere detailed wind profiles indicated that these data are an excellent source of information on CAT.

Although vertical wind shear showed the highest correlation with the observed rms-r values, many events of CAT (rms-r $\geq$ 0.85 mps) were observed where the "critical" wind shear indicated that no CAT should occur for the different depths of the layers (see Table 3).

In this study, over 80% of the total observations of CAT (rms-r $\geq$ 0.85 mps) were at altitude of 10 km and higher. Over 80% of the total observations of CAT at these altitudes were observed in relatively stable layers ($\Delta T/\Delta Z \geq -0.004°C/m$) and with large wind shears ($\Delta V/\Delta Z \geq 0.008 \sec^{-1}$ over 1 km). Based on the results of this study, the existence of a large wind shear was not a sufficient criterion for the occurrence of CAT.

This study illustrates that the Richardson number is not useful as an indicator of the existence or intensity of CAT. In this same vein, the Colson and Panofsky CAT Index showed remarkable correlation with the lapse rate of temperature for observations of CAT (rms-r $\geq$ 0.85 mps). This was a definite illustration of the possible effect of shear-gravity waves on the occurrence of CAT. This is because the large negative values of the Index come from stable layers with large wind shears.

Data from the upper atmosphere must be coincident in time and space with the occurrence of turbulence in order to reduce the

subjectivity of acutal observations of CAT. Any attempt to establish criteria for the occurrence of CAT must be channeled towards identification of the mesoscale regions of the atmosphere that are favorable for the occurrence of CAT. The current synoptic rawinsonde network does not provide observations of the scale and resolution required to identify all regions favorable for the occurrence of CAT.

Generally, the results of this study support the hypothesis put forth by Kuettner (1952), viz., that unstable shear-gravity waves occur in and near certain regions of maximum wind bands, and that these waves are a prime source of CAT.

b. Recommendations. Further studies of CAT using FPS-16 radar/ Jimsphere wind profiles should be made by analyzing serial profiles made just a few minutes to a few hours apart under conditions suspected to be favorable for the occurrence of CAT.

There should be an attempt to develop an empirical method to compute vertical motion in the upper atmosphere from the detailed wind profiles and associated GMD data. This is an attempt to measure some other meteorological parameter that might be useful in identifying regions of CAT.

An FPS-16 radar/Jimsphere site should be established somewhere in the lee of the Rocky Mountains where there would be a large volume of air traffic for a source of supporting pilot reports of CAT. Past studies of CAT associated with mountain waves could be re-examined using these highly accurate wind data. Most important,

it is in the lee of such mountain ranges that CAT is observed to occur with the highest frequency (up to 18% of flight time).

The development of a method to forecast CAT must consider the effects of vertical motion, advection, convection, radiation, and other parameters on changes in thermal stability of mesoscale regions of the atmosphere. The greatest contribution to this endeavor would come from serial ascents of Jimsphere balloons with an attached instrument package with means of transmitting temperature, humidity, and perhaps some type of accelerometer measurements. An attached accelerometer of some type would help relate rms-r values as a possible indicator of the intensity of CAT from the FPS-16 radar/ Jimsphere wind profiles. Such serial ascents should be made under synoptic conditions that are suspected to be favorable for the existence of CAT. From the current study, such conditions are (1) near a jet stream, (2) layers of thermal stability ($\Delta T/\Delta Z \geq \Delta T/\Delta Z$ "critical" for CAT), and (3) large vertical wind shears ($\Delta V/\Delta Z \geq \Delta V/\Delta Z$ "critical" for CAT).

REFERENCES FOR APPENDIX B

Axford, D. N., 1968: "On the Accuracy of Wind Measurements Using
    an Inertial Platform in an Aircraft and an Example of a Measure-
    ment of the Vertical Mesostructure of the Atmosphere," Journal
    of Applied Meteorology, 7, 645-666.

Clem, L. H., 1957: "Clear Air Turbulence from 25,000 to 45,000 Feet
    over the United States," AWS TR 105-47, Headquarters Air
    Weather Service (MATS), Scott AFB, Illinois, 13 pp.

Colson, D. and H. A. Panofsky, 1965: "An Index of Clear Air
    Turbulence," Quart. J. R. Meteor. Soc., 91, 507-512.

Danielsen, E. F. and R. T. Duquet, 1967: "A Comparison of FPS-16
    and GMD-1 Measurements and Methods for Processing Wind Data,"
    Journal of Applied Meteorology, 6, 824-836.

DeMandel, R. E. and J. R. Scoggins, 1967: "Mesoscale Wave Motions
    as Revealed by Improved Wind Profile Measurements," Journal of
    Applied Meteorology, 6, 617-620.

Eckstrom, Clinton V., 1965: "Theoretical Study and Engineering
    Development of Jimsphere Wind Sensor," Final Report, NASA
    Contract No. NAS8-1158, 78 pp.

Endlich, R. M. and J. W. Davies, 1967: "The Feasibility of
    Measuring Turbulence in the Free Atmosphere from Rising
    Balloons Tracked by FPS-16 Radar," Journal of Applied
    Meteorology, 6, 43-47.

Endlich, R. M. and R. L. Mancuso, 1965: "Objective Analysis and
    Forecasting of Clear Air Turbulence," Final Report, Contract
    Cwb-10871, Stanford Research Institute, Menlo Park,
    California, 56 pp.

Endlich, R. M., R. L. Mancuso, and J. W. Davies, 1966: "Techniques
    for Determining a World Wide Climatology of Turbulence through
    Use of Meteorological Data," AFCRL-66-355, Scientific Report
    1, Contract AF 19 (628)-5173, Stanford Research Institute,
    Menlo Park, California, 62 pp.

Foltz, H. P., 1967: "The Prediction of Clear Air Turbulence,"
    Atmospheric Science Paper No. 106, Department of Atmospheric
    Science, Colorado State University, Fort Collins, 145 pp.

Hardy, K. R. and Hans Ottersten, 1968: "Radar and Aircraft Investigation of Clear-Air-Turbulence," Proceedings of the Third National Conference on Aerospace Meteorology, American Meteorological Society, Boston, 539-546.

Hicks, J. J. and J. K. Angell, 1967: "Radar Observations of Breaking Gravitational Waves in the Visually Clear Atmosphere," Journal of Applied Meteorology, 7, 114-121.

Kuettner, J. P., 1952: "On the Possibility of Soaring on Traveling Waves in the Jet Stream," Aeronaut. Eng. Rev., 11, 1-7.

Lumley, J. L. and H. A. Panofsky, 1964: The Structure of Atmospheric Turbulence, John Wiley and Sons, New York, 239 pp.

Moore, R. L. and T. N. Krishnamurti, 1966: "A Theory of Generation of CAT," Douglas Paper 3801, presented at National Air Meeting on Clear Air Turbulence, February 23, 1966, 20 pp.

Press, H., May T. Meadows, and Ivan Hadlock, 1956: "A Reevaluation of Data on Atmospheric Turbulence and Airplane Gust Loads for Application in Spectral Calculations," Report No. 1272, National Advisory Committee for Aeronautics, 29 pp.

Reiter, E. R., 1963: "Nature and Observation of High Level Turbulence Especially in Clear Air," Technical Paper No. 41, Department of Atmospheric Science, Colorado State University, Fort Collins, 28 pp.

Reiter, E. R. and P. F. Lester, 1967: "The Dependence of the Richardson Number on Scale Length," Atmospheric Science Paper No. 111, Department of Atmospheric Science, Colorado State University, Fort Collins, 39 pp.

Rogers, R. R. and H. A. Camitz, 1965: "Project Baldy - An Investigation of Aerodynamically-Induced Balloon Motions," Final Report, NASA Contract No. NAS8-1140, 80 pp.

Sawyer, J. S., 1961: "Quasi-Periodic Wind Variations with Height in the Lower-Stratosphere," Quart. Journ. Royal Met. Soc., 87, 24-33.

Scoggins, J. R., 1967: "Sphere Behavior and the Measurement of Wind Profiles," NASA TN D-3994, 53 pp.

Susko, Michael and W. W. Vaughan, 1968: "Accuracy of Wind Data Obtained by Tracing Jimsphere Wind Sensors Simultaneously with Two FPS-16 Radars," NASA TMX-53752, George C. Marshall Space Flight Center, Huntsville, Alabama, 48 pp.

Weinstein, A. E., E. R. Reiter and J. R. Scoggins, 1966: "Mesoscale Structure of 11-20 km Winds," Journal of Applied Meteorology, 5, 49-57.